Author/s:
Lee, Hoi Yee

Title:
The dynamics of the B cell response during influenza A virus infection

Date:
2020

Persistent Link:
https://hdl.handle.net/11343/242467

The dynamics of the B cell response during influenza A virus infection

Hoi Yee Lee

ORCID 0000-0002-8510-265X

Submitted in total fulfilment of the requirements of the degree of

Master of Philosophy

May 2020

Department of Microbiology and Immunology

Faculty of Medicine, Dentistry and Health Sciences

The Peter Doherty Institute for Infection and Immunity

The University of Melbourne

ABSTRACT

Although vaccination remains the most effective method of managing influenza epidemics, there is still much that remains to be characterized about humoral immunity against the varying contexts in which influenza infection can occur. With the continuous subversion of humoral immunity by seasonal influenza through antigenic drift and the potential of zoonotic influenza viruses adapting and spreading through human populations through antigenic shift, improving our understanding of B cell immunity against different types of influenza infection could provide important insights into improving management of epidemics and vaccine formulations.

In order to understand B cell responses during influenza infection, the well-characterized C57BL/6 mouse model was used to investigate and compare humoral responses in the context of different influenza infection histories. Markers that identified specific B cell subsets such as germinal centre (GC) B cells and plasmablasts were analysed by flow cytometry paired with influenza virus-specific B cell ELISPOT assays to investigate strain-specific antibody secreting responses within the same experiment. As the surface glycoprotein HA is thought to be the immunodominant response for B cell responses against influenza virus, the prediction is that the greater the antigenic differences between the HA of the first and second infecting strains, the more primary-like the response to the second strain would be.

Primary and homologous secondary B cell responses in the mediastinal lymph node (MLN) and spleen were first characterized using this model to establish baseline responses against influenza virus before heterosubtypic infection was studied through infection of mice with H1N1A/Puerto Rico/8/34 (PR8) virus followed by H3N2 A/Udorn/305/72 (Udorn) virus 7 weeks later. Unexpectedly, a secondary-like plasmablast, GC B cell and Udorn-specific antibody secreting cells was observed during heterosubtypic infection, with earlier and higher magnitude B cell responses. These findings suggested a possible role for cross-subtype T cell memory in modulating B cell responses.

The effect of antigenic drift on the B cell responses during influenza infection was then analysed with the same model. Mice were infected with H3N2 strains isolated between 1972 and 1979, representing different antigenic distance from a virus isolated in 1982 (Ph82). Seven weeks post infection mice were reinfected with Ph82 and the B cell response over the course of infection examined. It was found that infection of strains up to 10 years apart appeared to induce

a secondary-like B cell response in the secondary lymphoid organs when compared to baseline primary and secondary responses against Ph82 virus. Prior infection with any H3N2 strain also resulted in minimal viral replication during the secondary challenge when compared to primary infection groups. However, data from both primary antibody inhibition and HA-specific B cell responses appears to suggest a narrower threshold of recognition, around a maximum of 3 years drift before serum and HA-specific responses cease to bind with other strains.

Taken together, secondary-like B cell responses in both heterosubtypic and drift models of infection and in the case of drift responses, irrespective of reactivity of HA-specific B cells, appear to refute the hypothesis that virus-specific B cell responses would reflect antigenic relatedness between the HA of the infecting strains.

Overall, data from this study identifies the diversity of the overall B cell response against influenza infection in the context of prior exposure to strains of different antigenic properties. Further study into the reactivity of these B cells against different influenza virus components and the role of memory T cells in the observed responses may provide important insights into the nature of host immunity against the ever-shifting target of influenza virus.

DECLARATION

This is to certify that:

i. the thesis comprises only my original work towards the MPhil except where indicated in the Preface,
ii. due acknowledgement has been made in the text to all other material used,
iii. the thesis is fewer than 50,000 words in length, exclusive of figures, tables, maps, bibliographies and appendices.

Hoi Yee Lee

PREFACE

In Chapter 3, the Candidate completed all the experiments in this chapter. Extent of Candidate's contribution: 100%

In Chapter 4, the processing of mouse compartments for flow cytometry and ELISPOT assay shown in Figure was prepared by the Candidate with assistance from Mr Charley Mackenzie-Kludas and Dr Brad Gilbertson. Probes for HA-specific B cells were synthesized and conjugated by Dr Adam Wheatley. Extent of Candidate's contribution: 70%

The work completed in this thesis was supported by the National Health and Medical Research Council (NH-MRC) Program Grant 567122 "Understanding and controlling influenza"

TABLE OF CONTENTS

LIST OF FIGURES

LIST OF TABLES

LIST OF ABBREVIATIONS

ANOVA	Analysis of variance
ASC	Antibody secreting cells
AP	Alkaline phosphatase
B6	C57BL/6
BCIP/NBT	5-bromo-4-chloro-3-indolyl phosphate/nitro blue tetrazolium
BK79	A/Bangkok/79
BM	Bone marrow
BV	Brilliant Violet™
CD	Cluster of differentiation
cRBC	Chicken red blood cells
cRNA	Complementary RNA
DMEM	Dulbecco's modified Eagle medium
DNA	Deoxyribonucleic acid
DPI	Days post-infection
ELISPOT	Enzyme-linked immunospot
FACS	Fluorescence activated cell sorting
GC	Germinal centre
HA	Haemagglutinin
HAU	Haemagglutinating units
HI-FBS	Heat inactivated foetal bovine serum
HPAI	Highly pathogenic avian influenza

HRP	Horse radish peroxidase
IAV	Influenza A virus
IL	Interleukin
ILI?	Influenza-like illness
Ig	Immunoglobulin
LAIV	Live attenuated influenza virus
M1	Matrix protein 1
M2	Matrix protein 2
mAb	Monoclonal antibodies
MDCK	Madin Darby Canine Kidney
MLN	Mediastinal lymph node
mRNA	Messenger RNA
NA	Neuraminidase
NEP	Nuclear export protein
NP	Nucleoprotein
NS1	Non-structural protein 1
PA	Acidic polymerase subunit
PB1	Polymerase basic subunit 1
PB1-F2	Polymerase basic subunit 1 – frame 2
PB2	Polymerase basic subunit 2
PBS	Phosphate buffered saline
PC73	A/Port Chalmers/73
PFU	Plaque forming units
Ph82	A/Philippines/82

PR8	A/Puerto Rico/8/34
QIV	Quadrivalent influenza vaccine
RNA	Ribonucleic acid
RPM	Revolutions per minute
RPMI	Roswell Park Memorial Institute
RT	Room temperature
SA	Streptavidin
TIV	Trivalent influenza vaccine
TV	Trypsin versine
TX77	A/Texas/77
Ud72	A/Udorn/307/72
V_H	Variable heavy-chain domain
Vic75	A/Victoria/75
vRNA	Viral RNA
v/v	volume/volume
WHO	World Health Organization
w/v	weight/volume

CHAPTER 1 – INTRODUCTION

INFLUENZA A VIRUS

Disease pathogenesis

Spread by the respiratory route, influenza A virus typically presents as an acute respiratory illness with cough and nasal congestion coupled with more systemic symptoms of muscle aches, fever and lethargy(1). Although most cases tend to be self-limiting as a upper respiratory tract infection, the very young, elderly or those with underlying illness, such as chronic pulmonary or cardiac conditions, are at increased risk of severe illness and complications such as viral pneumonia or secondary bacterial infection (2). Estimates from the World Health Organization indicate influenza infections cause up to 3-5 million cases of severe respiratory illness and from 290,000 to 650,000 deaths globally each year (3).

Viral structure & replication cycle

Part of the *Orthomyxoviridae* family, influenza A virus manifests as a spherical or filamentous enveloped viral particle containing a negative sense RNA genome consisting of eight single-stranded segments (4) in the form of ribonucleoprotein complexes (vRNPs). Subtypes of influenza A virus are identified by the combination of surface glycoproteins hemagglutinin (HA) and neuraminidase (NA) that they express, with up to 18 HA (H1-H18) and 11 NA (N1-N11) subtypes currently recognized (5). Viruses of H1N1 and H3N2 subtypes currently circulate in human hosts. As illustrated in figure 1.1, the HA, NA and the ion channel M2 are embedded in the lipid envelope of influenza virions. Proportionally, HA consists of approximately 80% of surface proteins, followed by 17% NA with small amounts of M2 (6). Binding tightly beneath the lipid envelope, the matrix protein forms a bridge between the surface glycoproteins and the vRNPs. Each vRNP is comprised of the viral RNA wrapped around the helical nucleoprotein (NP) capsid and is associated with a single polymerase complex, formed by protein subunits PB1, PB2 and PA (7). Small amounts of the nuclear export protein (NEP) can also be found within the virion. A non-structural protein NS1 is encoded by the viral genome and has a role in immune escape.

For a virion to become infectious, the homotrimeric HA glycoprotein must be cleaved from its HA0 precursor form by cellular proteases to generate HA1 and HA2 subunits linked by a single disulphide bond. The HA trimer is made up of a globular head domain (derived from HA1), a stalk

domain (derived largely from HA2), a transmembrane region and a tail region. The globular head contains three receptor binding sites (one per monomer) capable of binding to sialic acid (SA) linked to galactose (Gal) on the host cell receptor (8). The species specificity of influenza strains was found to depend on its preference to bind to host cell receptors containing sialic acid bound to galactose in different linkage conformations. Avian viruses have a preference towards the SAα2,3Gal linkage while human strains show an overall preference to receptors containing the SAα2,6Gal linkage, corresponding with expression of SAα2,3Gal expression in avian intestinal tissue and predominately SAα2,6Gal expression in the human upper respiratory tract where influenza initially replicates (9-12).

The binding of HA to its receptor induces receptor-mediated endocytosis of the virus. The reduced pH within the endosome causes a conformational change in the HA, exposing a hydrophobic fusion region at the N-terminus of HA2 which embeds in the endosomal membrane, bringing the viral and endosomal membranes in contact, resulting in their fusion and the creation of a fusion pore. In addition, this acidic environment opens the M2 proton-selective ion channel, allowing protons to enter the viral core and free vRNPs from the M1 protein. This enables vRNPs to enter into the cell cytoplasm through the fusion pore. Nuclear localization signals on the NP allow the vRNPs to bind cellular nuclear import proteins and enter the nucleus for synthesis of viral messenger RNA (mRNA) for translation into viral proteins and replication of genomic viral RNA (vRNA).

Up until 2001, it was known that these 8 strands encoded 10 viral proteins. However, since the discovery of PB1-F2 in a +1 reading frame shift of the PB1 gene (13), additional proteins such as PA-X, PB1-N40 amongst others have been discovered with many more potential proteins flagged by computation analyses of the influenza genome in open reading frames (14). Adapted from (15), the RNA segments of influenza A virus and a list of major viral products with known functions are shown in table 1.1.

Translated from viral mRNA by host cell apparatus, HA, NA and M2 contain signals that enable them to be trafficked towards the cell membrane for viral assembly. At the cell membrane surface, all eight vRNA segments must be present for a virion to form a fully infectious particle. Evidence shows that these vRNP segments are arranged in an organized manner and may utilize specific mechanisms to ensure all eight gene segments are packaged during assembly of virions (16, 17).

Once the virion is assembled, viral budding and release from the plasma membrane occurs. To prevent the rebinding of HA to the sialic acid receptors of the already infected cell, the tetrameric

surface glycoprotein neuraminidase (NA) on budding virions cleaves terminal sialic acid residues from receptors in the region of budding and from the nascent glycoproteins themselves to prevent aggregation of virions and help virion release. NA may also play a role in infection of cells by breaking down secreted decoy receptors in the respiratory tract to allow the virus to access the respiratory epithelial cells (18).

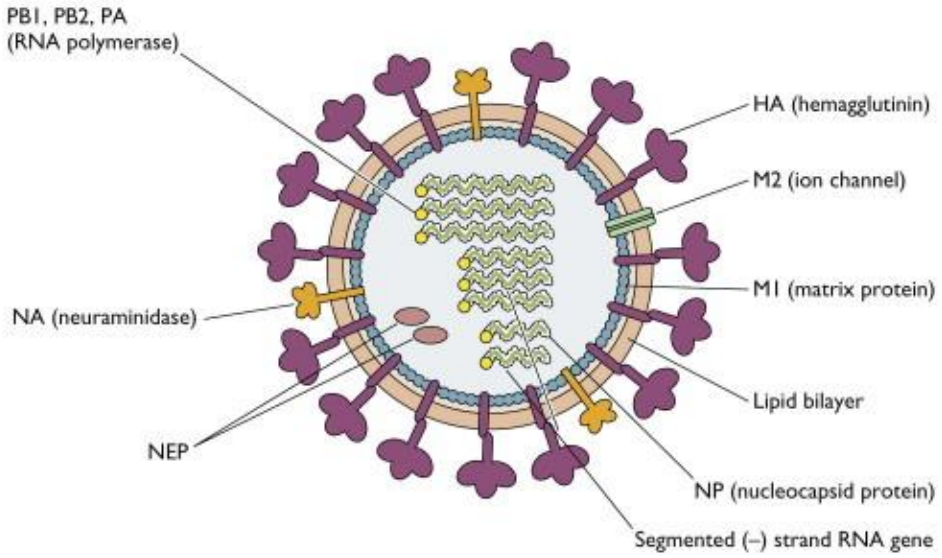

Figure 1.1. Structure of influenza virus.

Structural components of the influenza virus virion, with hemagglutinin (HA) and neuraminidase (NA) embedded on the lipid bilayer with the M2 ion channel. Matrix protein M1 encapsidates and anchors 8 viral RNPs which consist of negative sense, single-stranded RNA surrounded by nucleoprotein (NP) and some nuclear export protein (NEP) with the RNA polymerase complex (PB1, PB2 & PA). Schematic from (19).

Table 1.1. Influenza genome segments and some of their protein products

RNA Segment	Protein product	Known functions
1	PB2	Part of the polymerase complex. Binds to cap of host mRNA to prime viral mRNA transcription.
2	PB1	Part of the polymerase subunit. Catalytic subunit, elongates viral mRNA, cRNA and vRNA.
	PB1-F2	Non-structural. Plays role in pro-inflammatory responses, cell death and viral replication.
3	PA	Part of the polymerase subunit. Contains the endonuclease active site to allow for 'cap snatching' from host mRNA to allow transcription of viral mRNA (20).
4	HA (Hemagglutinin)	Surface glycoprotein. Enables viral entry by binding to sialic acid receptors on cell surface and releases viral RNPs through a pH-dependent conformation change within host endosomes to cause membrane fusion.
5	NP (Nucleoprotein)	Internal protein. vRNA encapsidation and synthesis.
6	NA (Neuraminidase)	Surface glycoprotein. Viral release through the cleavage of sialic acid upon exit of host cell.
7	M1 (Matrix 1)	Internal protein. Maintains virion structure by connecting viral envelope with the nucleocapsid and regulates ribonucleoprotein (RNP) nuclear import.
	M2	Surface protein. Ion channel that allows H^+ from the endosome to enter virion to allow viral RNP uncoating.
8	NS1	Non-structural protein. Evasion of host immunity by inhibiting antiviral responses and regulating expression of viral and host genes (21).
	NS2/NEP (Nuclear export protein)	Nuclear export protein. Exports RNP complex from the nucleus, regulation of viral transcription and recruitment of host ATPase to aid release of virions (22).

Evolution of Influenza Virus

Due to a lack of proof reading by its viral RNA polymerase, influenza virus has a high mutation rate during replication. However, the rates of accumulation of mutations between gene segments vary. For example, the HA segment has been found to have the highest rate of nucleotide changes, while segments relating to the viral polymerase were found to have lower rates of substitutions, likely due to higher constraints on amino acid changes for the maintenance of function. Furthermore, although M, NS and NA gene segments were found to have similar rates as the HA gene, HA was found to have the highest rate of nonsynonymous substitutions, likely indicative of its role in immune evasion by antigenic drift (23).

Antigenic Drift

Antigenic drift describes a process of mutation and selection of HA and NA genes as the virus infects populations over time. Point mutations due to error prone viral polymerase may result in amino acid changes in the antigenic sites of the surface glycoproteins that are selected for within the viral population as they reduce recognition by pre-existing neutralizing antibody responses (24, 25). This enables continued replication of these mutant strains, which can be preferentially spread to further individuals, eventually dominating within a population (26). A hallmark of antigenic drift in human influenza A viruses is the observation that rather than many drifted variants co-existing and evolving in parallel, newly drifted strains tend to 'replace' older strains, with the H3N2 subtype appearing to evolve more rapidly than H1N1 strains (27).

These attributes of antigenic drift have informed the major policies of vaccination formulation against influenza. Vaccine strains are re-evaluated twice a year (to cover each hemisphere's winter influenza season) based on recommendations by the WHO Global Influenza Surveillance and Response System (GISRS). New vaccines are made for each season based on antigenically relevant strains of human influenza A subtypes H1N1 and H3N2, forecast to be the archetypical strain of the emerging lineage, and one or two prevalent strains of influenza B virus (3).

Interestingly, Smith *et al.* (28) showed that continuous genetic evolution of strains did not equate to continuous drift. To visualize the complex relationship between viral strains and antigenic drift over time, the authors constructed a two-dimensional plot or 'antigenic map' whose relative distances between strains corresponded to the HI titres of antisera against each strain when reacted

against all other strains, as shown in figure 1.2. Although it is known that the globular domain of the HA acquires a mean of 1.5 substitutions a year, most commonly in antigenic sites (29), their analyses indicated that antigenic drift seemed to be staggered and punctuated, with new antigenic distinct 'clusters' appearing every 3 to 8 years (30). Furthermore, of the over 50 substitutions and decades of evolution, it has been shown that the antigenic differences between strain clusters that aided escape from antibody responses were largely determined by key single amino acid substitutions near the receptor binding pocket, with supporting mutations to maintain function and viral fitness (31). New variant strains were considered to show significant drift from another when four or more amino acid mutations on a minimum of two epitopes were found on the HA1 protein (32).

Similarly, Russell *et al.* (30) found that although H3N2 isolates seemed distributed across the globe heterogeneously, trends in antigenic drift on a global scale are homogenous, suggesting that strains circulate globally rather than evolving within small areas. Newer, antigenically 'advanced' strains were observed to occur 6-9 months earlier in East-South East Asian countries than other regions, and were shown through phylogenetic analyses to seed other regions as the epidemic migrated with the season. However, such trends seem to be exclusive to H3N2 strains, as more recent studies have found global circulation trends in H1N1 displayed some co-circulation of lineages before coalescing in East-South East Asia as with H3N2 strains (33).

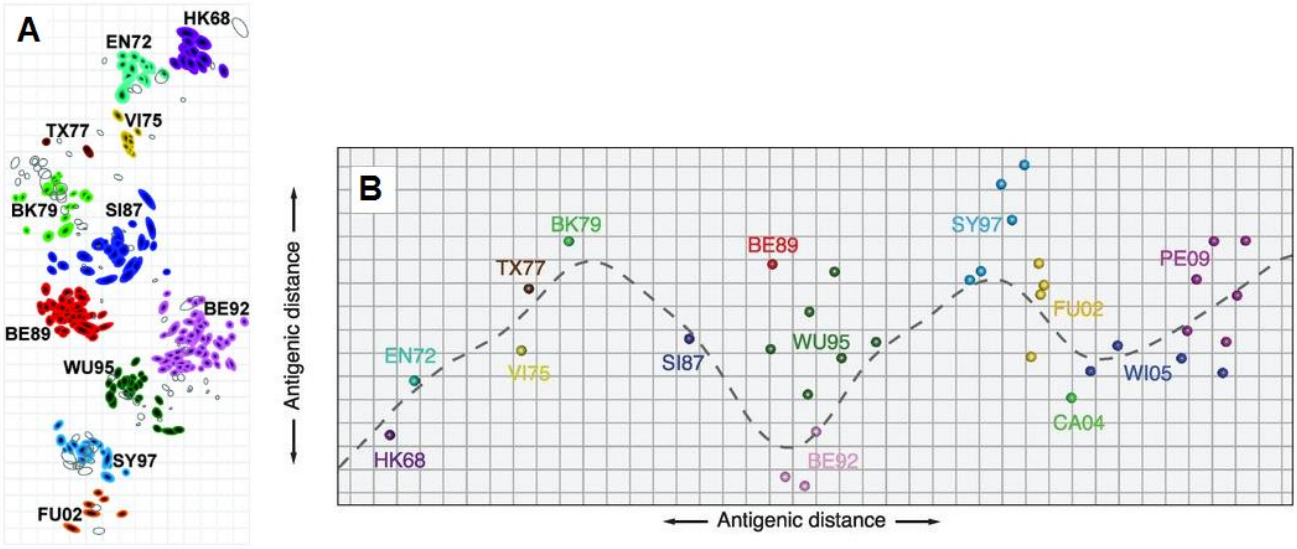

Figure 1.2. Map of major antigenic clusters and drift of H3N2 strains.

A shows the two dimensional antigenic map from (28) of H3N2 influenza A virus clusters from 1968 to 2002. The relative positions of virus strains (coloured) and ferret antisera (uncoloured) are shown plotted on a 2D plane such that the distance between a strain and an antisera directly corresponds to the HI titre in log2. **B** shows a similar plot of the strains from 1968 to 2009 with a dashed line to indicate chronological order; adapted from (34)

Antigenic Shift

Complicating matters further, influenza viruses of subtypes that circulate in avian reservoirs can enter the human population and become endemic, effectively replacing older human subtypes. These emergent strains express antigenically novel HA, and sometimes NA, to which most of the human population would have no prior immunity. Known as antigenic shift, this is thought to be driven in most instances by the reassortment of gene segments from human and zoonotic strains of influenza virus upon coinfection of a host's cell (35). The pig has been implicated as an intermediate in this process as it has receptors for both avian and human viruses in its upper respiratory tract (36).

Due to the lack of immunity in the general population, influenza viruses that have undergone antigenic shift have been responsible for pandemics including the 1918 H1N1 'Spanish flu', the 1957 H2N2 'Asian flu', 1968 'Hong Kong' and more recently, the H1N1 'Swine flu' in 2009. Current strains

of seasonal influenza A viruses are drifted variants of the most recent H3N2 and H1N1 pandemics, (37).

IMMUNE RESPONSES AGAINST INFLUENZA

The mouse model of influenza infection

While in vitro studies can provide valuable information about virological properties and some evaluation of immune mediators, in vivo models remain the most valuable tool for research into immunological responses against influenza virus infection. Studies of immune responses against influenza in mammalian models are most commonly conducted in mice (*mus musculus*) but also used are ferrets (*mustela putorius furo*), guinea pigs (*cavia porcellus*) and pigs (*sus scrofa*).

Key advantages to studies of influenza in the mouse model includes availability of inbred lineages, cost effectiveness of animal husbandry, ability to genetically modify mouse strains as well as the availability of reagents (38). While it would not be expected that murine responses would align perfectly with human responses, this mammalian model is particularly well-characterized and thus provides a reliable basis to study various aspects of the immune response against influenza virus.

However, the limitations of using a murine model to study influenza infection must also be considered. One such limitation is the limited susceptibility to influenza infection. A contributing factor is the presence of only SAα2,3Gal receptors in the respiratory tracts of mice. While avian influenza viruses and early H3N2 strains retain tropism for avian-associated SAα2,3Gal receptors, human influenza viruses have evolved towards a preference for the SAα2,6Gal receptor more commonly found in human respiratory tracts. As a result, later human influenza viruses that are not mouse adapted do not replicate well in mice. H1N1 viruses do not grow naturally in mice (39). Exceptions include pdmH1N109 and laboratory H1N1 strains such as PR8, which have been altered through continuous passage in eggs to express only avian receptor specificity.

Role of innate immunity in influenza infection

The innate immune response is the first line of defence during the initial period of infection by influenza virus. Such responses involve the pathways leading to the release of cytokines, chemokines and the antiviral molecules interferon α/β (IFNα/β) as well as recruitment of innate cells including macrophages, neutrophils, NK cells and dendritic cells (40). Initial detection and response against viral infection is mediated through recognition of viral pathogen associated molecular patterns (PAMPs) by

epithelial and phagocytic cells through pattern recognition receptors (PRRs). Against influenza virus, these PRRs include toll-like receptors such as TLR7 and TLR3 and RIG-like receptors such as RIG-I. These detect different features of the viral RNA and promote downstream responses leading to the transcription and production of the type I interferons (IFNs, which include IFN α and β) amongst other inflammatory signals (41, 42). NOD-like receptors such NLRP3 are also associated with the innate response against influenza virus via detection of various aspects of influenza virus including ssRNA, proton flux and the virulence protein PB1-F2. Activation of NLRP3 results in formation of the inflammasome complex and release of pro-inflammatory cytokines IL-1β and IL-18 (43, 44).

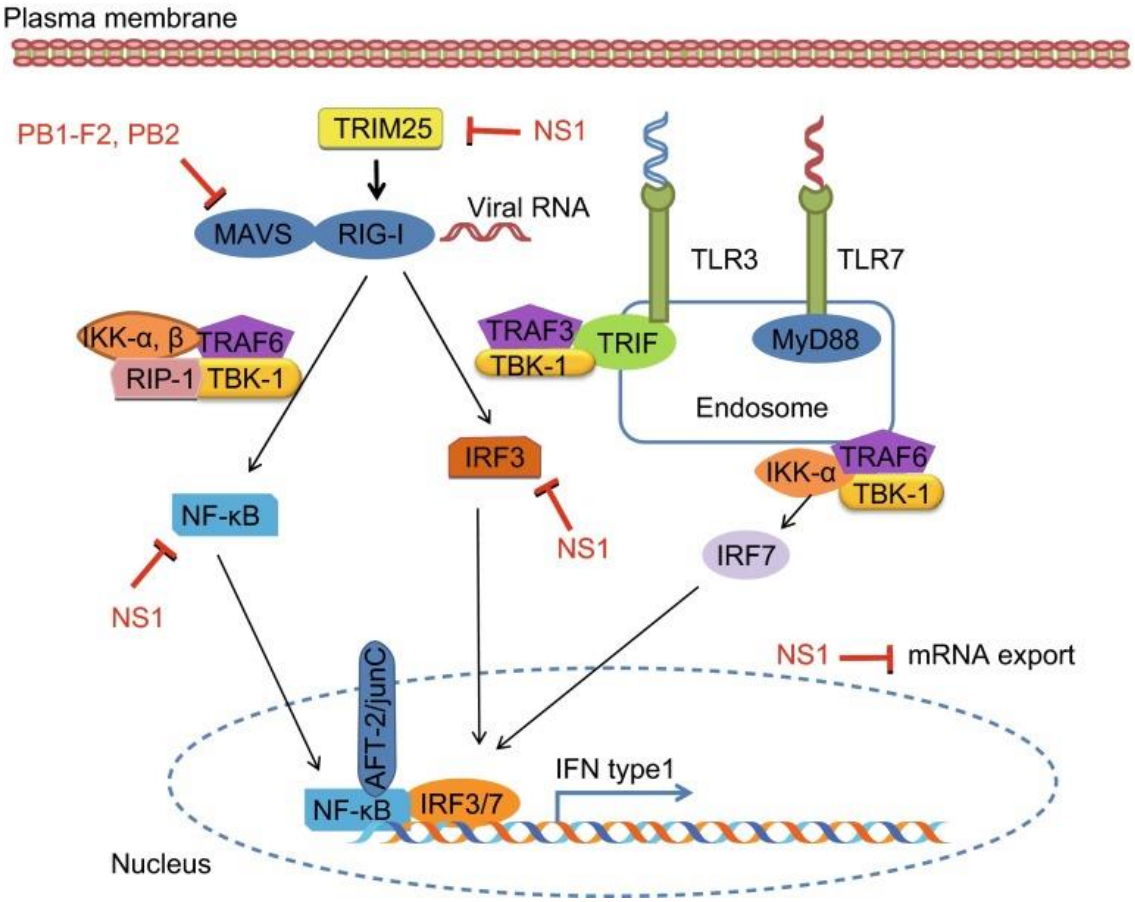

Figure 1.3. Activation of host innate pathways by influenza A virus components.

Obtained from (44), figure shows various activation pathways within a host cell upon detection of influenza virus components such as NS1, PB1-F2 or PB2 leading to the activation of NF-kB to initiate the transcription of type I IFN in response to viral infection.

Amongst the milieu of cytokines and chemokines released during influenza infection, release of chemotactic signal CCL2 by infected epithelial cells is associated with the recruitment and activation of alveolar macrophages and monocytes. Activated macrophages release proinflammatory cytokines such as IL-6 and TNF-α, phagocytose infected cells and virus particles and aid in the regulation of adaptive immunity (45). However, in some cases, alveolar macrophages have also been associated with excessive inflammation and immunopathology during influenza infection (46).

Natural killer (NK) cells also play an important role in the control of influenza infection through lysis of infected cells either through direct binding to HA on virus-infected cells or through binding of antibodies by CD16 receptors through a process known as antibody-dependent cell cytotoxicity (ADCC) (47, 48).

Bridging the innate and the adaptive response are the dendritic cells (DCs), which aid in the activation of adaptive immunity through antigen presentation. Through mechanisms of phagocytosis, direct infection and cross presentation, dendritic cells can present viral peptides through both MHC class I and class II, thus activating both $CD8^+$ cytotoxic and $CD4^+$ helper T cells against the viral infection (45, 49).

Role of adaptive immunity during influenza infection

In comparison to the immediate, non-specific response against pathogens, the adaptive immune response is honed against specific antigens of a pathogen such as influenza virus but takes some time over the course of infection to become activated and perform its effector functions. Typically, these responses are categorized into the cellular and humoral arms of the adaptive immune response.

Cellular Immunity

The cellular arm of the adaptive immune response is primarily directed by cytotoxic ($CD8^+$) T cells and T helper ($CD4^+$) cells.

Activated by DC antigen presentation, cell-to-cell signalling and cytokines, $CD8^+$ T cells play a vital role through the control of viral spread. Cytotoxic T cells recognize virus-infected cells by the interaction of their T cell receptors with specific viral peptides presented by MHC class I molecules on the infected cell surface. This interaction triggers release of perforin and granzyme to initiate death of the infected cell and of anti-viral and pro-inflammatory cytokines (50). With regards to influenza infection, $CD8^+$ T cells tend to recognise epitopes of highly conserved internal components of

influenza virus such as NP, M1, NS1 and PB1 (51, 52) in addition to the variable surface glycoproteins. These targets on the internal proteins are highly advantageous as they are less likely to undergo mutation to escape immune recognition compared to the surface glycoproteins, allowing for memory cytotoxic T cells to cross-react with various influenza strains and even different subtypes (53).

$CD4^+$ helper T cells, on the other hand, act as directors of the response against influenza infection. Upon presentation of peptides on MHC class II molecules and co-stimulatory signalling by antigen presenting cells, $CD4^+$ T cells become activated and during influenza infection, are most likely to differentiate into Th1 or Th2 cells based on the cytokine microenvironment (54). In turn, T helper cells aid in honing the response against influenza infection through release of cytokines and cellular interactions with other adaptive cells. Th1 cells primarily release IFN-γ and IL-2 and are largely responsible in promoting cytotoxic T cell responses and establishing $CD8^+$ T cell memory, while Th2 cells release IL-4, IL-5 and IL-13. Both aid in B cell activation and differentiation, likely developing into T follicular helper (Tfh) cells with appropriate B cell signalling (55, 56).

Humoral Immunity

The humoral arm of the adaptive immune response against influenza virus is mainly directed by the different subsets of B cells. During influenza infection, B cells with surface immunoglobulin (Ig) receptors that can directly recognize the surface antigens of the virus will undergo activation, resulting in cellular signals that allow differentiation to occur through transcriptional changes within the cell(57).

While HA is thought to be the immunodominant with regards to antibody responses, lower proportions of antibodies to other viral components including the NA and NP are also mounted in infected individuals (58, 59). Neutralizing antibodies against the HA in particular are largely directed against discrete antigenic sites located around the receptor binding pocket of the hemagglutinin and these antibodies sterically prevent viral entry into host cells. The levels of such HA-specific antibodies, detected in a hemagglutination-inhibition assay, have been shown to correlate with protection (31, 60). In addition to this, antibodies to HA are also capable of eliminating the infected cell either by antibody plus complement-mediated lysis or by antibody-dependent cellular cytotoxicity (ADCC). Further studies have also shown that antibodies directed against M2 and NP, and particularly NA, are also capable of limiting infection, reducing disease severity (58, 61-63).

Antibody isotypes observed following influenza infection include IgM, IgA and IgG(64). Virus-specific IgM has largely been associated with initial non-class switched responses, but a study by

Skountzou *et al.* suggests a longer-lived role in the protection against influenza, especially in conjunction with the complement network to aid in viral neutralization (65). Secretory IgA antibodies, on the other hand, are transported to the mucosal surfaces of the respiratory tract and enable protection of the epithelial cells of the airways, both extracellularly and intracellularly, as well as prevention of viral transmission (66-68). Influenza-specific IgG has been shown to be the dominant antibody and is associated with long-term protection against specific strains (69). B cells expressing IgG have been shown to have higher proliferative capacity and are more likely to differentiate into plasma cells compared to IgM (70).

B CELL RESPONSE AGAINST INFLUENZA VIRUS

B cell activation during infection

During infection, B cells may differentiate into various effector cells to help control and clear the invading pathogen. Upon activation, T-dependent B cells migrate to the germinal centre (GC) to interact with T follicular helper (Tfh) cells to undergo isotype switching, affinity maturation and differentiation. These intermediary B cells are known as germinal centre B cells and continue differentiation into either plasmablasts or memory B cells. The fully differentiated form of plasmablasts, plasma cells, act as the major producers of antibodies during an infection. Memory B cells act as sentinels which become reactivated by interaction with their cognate antigen to respond to reinfection more rapidly and at a higher magnitude.

During infection, the process of B cell activation begins with activation signals through cross-linking of B cell receptors with antigen. In the plasma cell differentiation pathway, early expression of the transcriptional repressor Blimp-1 in extrafollicular B cells will commit a portion of B cells to a short-lived plasma cell fate, repressing affinity maturation and isotype switching. These unswitched, non-affinity matured plasmablasts, ie. antibody-producing cells that have yet to differentiate to a complete plasma cell phenotype, and short-lived plasma cells allow an early antibody response against the ongoing infection (71).

In comparison, the T-dependent B cell response takes around 5-7 days to develop and is promoted by contact with and cytokine signalling from CD4+ T follicular helper cells. These signals are required for class switching and migration into germinal centres (72). During a respiratory infection such as influenza virus, the main sites for germinal centre reactions include the draining mediastinal lymph nodes (MLN) and the mucosal-associated lymphoid tissue (MALT) (68). The structure and

signalling environment of GCs subsequently promotes affinity maturation and differentiation of GC B cells into memory and plasma cells later during infection to aid clearance of infection through high affinity IgG and IgA antibodies (73-75).

While the majority of antibody-secreting cells undergo apoptosis after infection, a small proportion migrate to the bone marrow, where they become long-lived plasma cells (LLPC), constitutively releasing antibody against their cognate antigen to aid in prevention of reinfection by the same viral strain in the recovered host (76). An example of the longevity of these responses was shown in a study of donors born on or before 1915 where all participants within this age range displayed seroreactivity against 1918 pandemic influenza virus and 7 of 8 donors retained circulating antigen-specific memory B cells against the virus for up to 10 decades (77).

In addition to the highly specific B cell responses, a subset of B cells known as ($CD5^{+}$) B-1 cells also play an important role in the humoral response against influenza infection. B-1 cells exhibit innate-like properties, secreting polyactive IgM antibodies without antigen stimulation. These constitutively present ‘natural’ IgM antibodies act as an early defence against infection and have similar effector functions as IgM produced by B cells with receptors specific to one epitope. In addition, studies have shown that both natural and induced IgM responses must be present for effective induction of the class-switched IgG response (78).

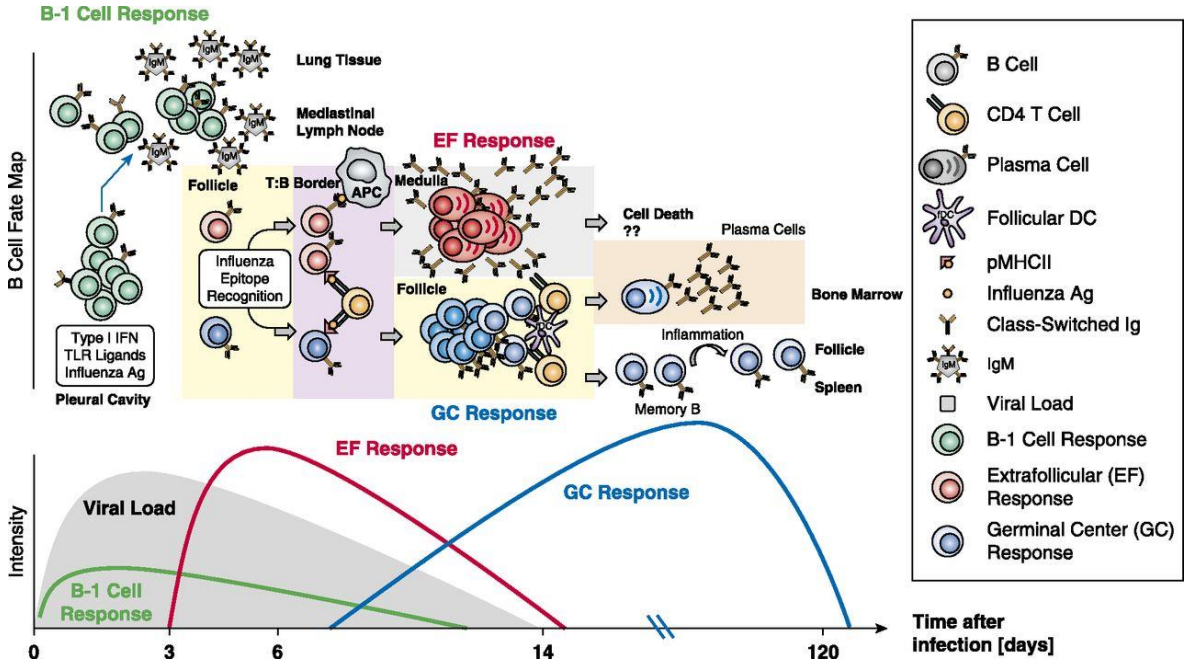

Figure 1.4. The kinetics of B cell responses during the course of influenza infection

T-independent and T-dependent B cell responses during viral infection. Obtained from (79), figure shows the timing and differentiation pathways of the T-independent B-1 responses and the T-dependent early follicular (EF) response and germinal centre (GC) B cell responses over the course of viral infection.

Antibody responses against influenza virus

The antibody response against influenza seems to be highlighted by clear hierarchies of immunodominance. Altman *et al.* (29) have shown that approximately two thirds of the antibody produced after immunisation with inactivated influenza virus is directed to the HA, although this may differ in response to infection. Of the antibodies against HA, responses to the well-defined major antigenic sites dominate over other less well recognised determinants elsewhere on the molecule. Seminal studies from the 1980s showed that circulating seasonal H3N2 and H1N1 strains contained five major antigenic sites in the hemagglutinin head around the receptor binding site (RBS) (A to E in H3N2 and Ca1, Ca1, Cb, Sa and Sb in H1N1) (80, 81). The production of these neutralizing antibodies has been shown to correlate with protective immunity and currently, the inactivated detergent-disrupted influenza vaccine relies on the production of this antibody response to prevent infection and/or lessen its severity. More recently, studies have been able to further map the immunodominance hierarchy

between these sites in both H1N1 (82) and H3N2 (83). However, this protective response in turn promotes selective pressure for influenza A viral strains to undergo antigenic drift in these sites.

Although theoretically advantageous, antibodies against more conserved sites such as the stem or receptor binding site (RBS) of the HA appear in lesser frequencies, likely as they are much less accessible in comparison to the major antigenic sites (84, 85). Furthermore, such responses may also be affected by competition for T cell help when B cells of differing specificities draw from the similar antigen-MHC II complex requiring the same pool of specific CD4+ T cells for stimulation (86).

A further break down of the immunodominance of antibody responses against influenza virus proteins was provided by Altman *et al* (87) and summarized in Figure 1.4. Through examination of mouse (and lamprey) antibodies against influenza A virus, it was found that approximately 80% of antibody responses were directed to the HA and mostly against the antigenic sites on the globular head upon immunization of inactivated virus. While neutralising anti-HA responses contribute predominately contribute to the antibody response (29), responses against other components of influenza virus may also play a role in control and prevention, especially against heterosubtypic infections. The relative ability of responses against specific influenza virus components to inhibit influenza infection was shown in a study by Epstein *et al* (88) where mice were immunized with recombinant vaccinia viruses expressing one of the influenza virus proteins before challenged with PR8 influenza virus. It was found that only mice immunized with recombinant viruses expressing either HA or NA showed significant protection and that this protection was not T cell dependent through MHC class I-deficient mice depleted of $CD4^+$ T cells.

While antibodies against NA are not generally considered neutralizing, induction of anti-NA antibodies showed a reduction in viral titres over time, likely limiting infection through the inhibition of viral exit of an infected cell (45, 89, 90). NA antibody responses may also confer cross reactivity in viruses with the same NA but differing HAs, given the partial protection conferred by the transfer of sera from mice challenged with a virus containing human N1 into naïve mice during avian N1 virus challenge. Cross reactivity of human sera with avian N1 strains was also demonstrated in the same study (91). Furthermore, when H3N2 viruses replaced previously circulating H2N2 strains after the 1968 pandemic, higher anti-N2 antibody titres were found to be associated with a reduction in influenza-related symptoms and lower levels of virus shedding (92). Similarly, a notable decrease in infection and disease was shown in those with pre-existing anti-N2 antibodies during the 1968 outbreak when a community in Michigan was exposed to H3N2 virus for the first time (58). This is further

corroborated by a recent study which showed that immunization with a formulation containing N1 was able to aid in protection of heterologous infection of a mismatched N1 (93). While – as a surface glycoprotein – NA undergoes antigenic drift and actually acquires substitutions at a more rapid rate than HA, it has been found that the timing of drift in the NA does not necessarily align with drift in the HA of a viral strain (94). Thus, anti-NA antibodies may be useful as a means of reducing disease and transmission in the context of antigenic drift in the immunodominant HA (95).

As an internal protein, NP presents an important antigen for T cell responses. Anti-NP antibodies have also been investigated as a potential means towards a universal vaccine given the high conservation of NP sequence between all influenza A strains. Anti-NP antibodies have been shown to be capable of limiting viral replication, including during heterosubtypic infection, and protecting against lethal challenges of influenza (61, 96). Further studies have shown that anti-NP IgG promotes viral clearance through cellular immunity and FcR-related innate responses (97).

Found on the viral membrane in low concentrations, antibodies against the M2 protein have drawn attention due to the highly conserved nature of M2 as well as the capacity for anti-M2 antibodies to reduce viral titres and protect against lethal infection (63, 98). As M2 is found on infected cells at low concentrations, low levels of antibodies against M2 can be found during natural infection(99).

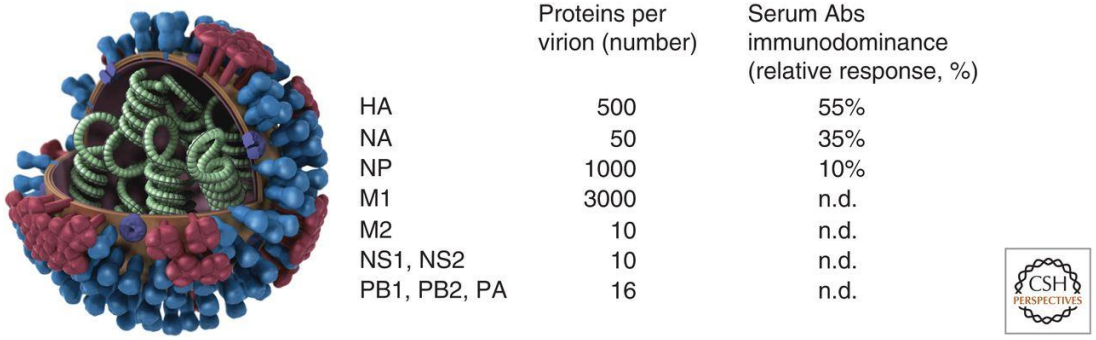

Figure 1.5. **Immunodominance of serum antibody responses against influenza A virus.**

Immunodominance of serum antibody responses against influenza A virus. Figure from (59) summarising data from two studies which examined the abundance of viral proteins in influenza virions (100) and mouse serum antibodies were measured after immunization with inactivated influenza A virus (87). n.d., not determined.

Vaccination against influenza A virus

Through prevention and reduction of illness, vaccination remains the most effective means of controlling the spread of influenza (3). As the induction of robust antibody responses against well-matched strains has been shown neutralize viruses, the primary aim of influenza vaccines is to induce strain-specific antibodies against target strains in recipients that effectively inhibits the virus (101).

Current vaccine types are predominantly based on inactivated virus (IIV) but live attenuated virus (LAIV) vaccines are also available. Vaccines contain HA and NA antigens from circulating strains of human H1N1, H3N2 and one or two prevalent influenza B strains (102). Attenuated influenza vaccines were previously recommended in young children based on promising clinical trials, but more recent studies have painted a less favourable picture of the efficacy of LAIV (103, 104), leading to the US Advisory Committee on Immunization Practices to recommend it not be used in the 2017-2018 influenza seasons (105). Since the 1970's, the inactivated virus vaccines have been formulated through amplification of the virus in embryonated eggs followed by purification by sucrose gradient centrifugation, chemical inactivation and "splitting" into its components using detergents (106). For H3N2 strains, chosen strains undergo reassortment with the egg-adapted A/Puerto Rico/8/1934 (H1N1) strain while being selected for the H3N2 HA and NA components to ensure a high yield during amplification. Mass production of vaccines takes at least 6 months (107) and thus review of selected strains must take place well before the influenza season begins in either hemisphere – February for the northern hemisphere and September for the southern hemisphere (101, 102).

Given the prolonged timeframe of vaccine production, strains selected are predictions of the antigenically dominate strains for the upcoming influenza epidemic seasons. Although the WHO committee makes recommendations on the best available evidence, strain mismatches have occurred in several instances, resulting in substantially reduced vaccine effectiveness (VE) (106). In the Northern Hemisphere during the influenza season of 2014-2015, VE was as low as 23% as a result of a mismatch of the antigenic characteristics of H3N2 vaccine component A/Texas/50/2012 and the predominately circulating A/Switzerland/9715293/2013-like strains. Furthermore, evidence has arisen suggesting that egg-associated adaptations may also affect the antigenic properties of chosen viruses. Since the 2014-2015 season, H3N2 strains acquired a mutation that added a glycosylation site on the HA. However, the 2016-2017 egg-adapted H3N2 vaccine strain was observed to show a reversion in this mutation. Individuals vaccinated with this egg-adapted strain were shown to have minimal increases in response to the circulating target strain post-vaccination in stark contrast to the participants that received a

vaccine with a recombinant H3 antigen possessing the glycosylation site who showed a four-fold increase in antibody responses to the circulating strain (108).

While vaccines remain the best method of protection against influenza spread and infection, further studies into antigenic drift and the nature of the B cell response against drifted strains would further inform strain recommendations and help maximize the effectiveness of future vaccines.

THE IMPACT OF ANTIGENIC DRIFT ON B CELL RESPONSES AGAINST INFLUENZA VIRUS

Currently, the effectiveness of the annually updated vaccine is reliant on the selection of strains that are antigenically similar to upcoming circulating strains. While a perfect strain match would play a strong role in ensuring a robust VE, further studies have delved deeper to investigate the relationship between repeated exposure to antigenically drifted strains and the B cell response against them.

In adults, strong evidence exists that influenza vaccinations largely promote the recall of affinity matured IgG memory B cell responses over naïve B cell responses (109, 110). This has been shown to be a result of the acquisition of immunity against influenza strains circulating during childhood, with the quantity of IgG and IgA influenza-specific memory B cells in peripheral blood increasing from 0.5-month-old children to 5 years of age before reaching a plateau (110). Although influenza infection can induce lifelong immunity against the exposed strain (77), the antibody titres against vaccinated strains appear to decline to about half over the course of around 2 years in adults (111).

But the properties of pre-existing B cell memory against prior influenza strains in the context of antigenic drift has been and remains a topic of some debate. One of the most discussed subjects is the phenomena of ‘original antigenic sin’, whereby the antibody response to the first strain of influenza a host is exposed to becomes the most predominate response against influenza despite exposures to newer, antigenic drifted strains.

Evidence supporting this phenomenon dates back to studies over half a century ago by Francis (112) and Davenport (113), where it was shown that human infection of drifted influenza strains produced a strong antibody response specific for strains encountered in the individual’s childhood while responses against the infecting drifted strain was diminished. It was postulated that these highly

responsive memory B cells against previous strains would respond and as a result produce large quantities of antibodies with low affinity to recent antigenically drifted strains. This response may also inhibit the naïve B cell pool's capacity to recognize the antigenically drifted strain because of memory B cell-induced antibodies competing naïve B cells for antigenic sites, thereby inhibiting their activation.

This is also corroborated by another study (114) showing that individuals that received the IIV from the previous year and had appreciable hemagglutinin inhibition (HI) titres against the vaccine strain, responded with lower levels of IgA antibody secreting cells (ASCs) in peripheral blood and lower titres of sera antibody inhibition against the newer vaccine strains. A more recent study (115) found similar results, showing that individuals who were not vaccinated in the last 3 seasons showed substantially larger vaccine-specific IgG^+ plasmablast responses than those who were vaccinated recently and this was similarly reflected in their HI titres. Furthermore, Andrews *et al.* (116) showed that higher pre-existing serum antibodies were correlated with a more strain-specific response to the HA head upon vaccination against the 2009 pandemic H1N1 while plasmablasts from individuals with lower titres were associated with a more cross-reactive response against the HA stalk, in line with the general hypothesis of prior responses hindering more diverse, potentially cross-reactive responses.

In the last decade, this idea has been further elaborated on with the concept of 'antigenic seniority', defined as the idea of primary infection – usually in childhood – having the highest priority in responses with subsequent infecting strains taking a lower stepwise priority in the immune response against drifting strains. This was first shown in a study investigating antibody titres in sera of individuals from Guangdong, China (117) where it was shown that individuals had the highest titres against strains circulating when they were around 7 years old while antibody titres mounted against strains following this initial exposure declined steady with time and antigenic difference. Further modelling of this data appeared to suggest this each exposure to virus or vaccine strains appeared to shape the immune response against subsequent infections or vaccinating strains, in contrast to the theory of original antigenic sin which focused only upon the initial strain hosts were exposed to in childhood (118, 119).

Other studies (109, 120) have shown an opposing perspective, painting a more complex picture of the nature of memory B cell responses against influenza in the presence of antigenic drift. Notably, Wrammert *et al.* (109) showed that the reactivity of human antibodies and their underlying B cells were shown to bind a new influenza strain with equal or greater affinity despite the drifted strain being very

antigenically similar to the previously experienced strain, contesting the idea that prior B cell responses against an older strain might outcompete for antigenic sites during exposure to a newer infection where similar sites may be most likely to be recognised.

Furthermore, data from Fonville *et al.* (34) suggests that although the overall antibody and memory B cell responses against influenza is highly influenced by the exposure of circulating strains during childhood, an individual's distinct 'antibody landscape' will shift to produce high affinity antibodies to the most recent strain upon infection. This occurs despite the tendency for pre-existing antibody titres towards strains circulating during the individual's childhood to predominate during periods of no immunological challenge. Although titres of these more recent antibodies will decay in the years post exposure to a new challenging strain, the host's overall 'landscape' against strains are altered by the infection.

In addition to this, infection with an antigenically diverse H3N2 influenza virus resulted in an increased level of neutralizing antibody against both the infecting and previously encountered strains, a phenomenon coined 'back-boosting' in the paper. This was further reported and supported by a recent study (121) that showed that the plasmablast and B cell responses against vaccination of more antigenically distant strains were more robust than strains of more similar antigenic properties to those that the host had pre-existing immunity against. Taken with the negative correlation of high pre-existing sera-based inhibition and the production of both plasmablasts and memory B cells, this phenomenon was suggested to be the result of masking of viral epitopes by way of binding by pre-existing host antibodies. Both conclude that vaccination of more antigenically diverse strains of influenza are more likely to provide a robust and protective B cell response against both recent and prior strains.

This new wealth of data on the effect of antigenic drift on antibody responses against influenza has many implications for vaccination, however a distinction must be made between the immunological implications of infection versus vaccination. This can be seen in a study by Kim *et al.* (122), where it was shown that immune responses against A/Fort Monmouth/1/47 (FM1) vaccination was far more efficacious in mice with a history of prior infection with the antigenically related virus PR8 compared to those immunized with PR8. This was reflected not only in increased levels of the antibody responses against PR8 and FM1, but also in the levels of plasmablasts, PR8-specific and FM1-specific ASCs as well as the increased breadth of hemagglutinin inhibition of other H1N1 viruses, suggesting that the

immune responses induced by infection have long-arching implications for the continued immunity against drifting strains.

Much discussion of vaccine-induced B cell against influenza has arisen because of various seasons of lowered vaccine effectiveness, especially with regards to H3N2, but this is not a new debate. As early as 1999, a computational analysis by Smith *et al.* (123) examined the effect of antigenic distance between past and present vaccine strains and epidemic strains in an attempt to reconcile conflicting data on whether repeated vaccinations proved effective or hindering. The model proposed a hypothesis that antigenic distance between past and present vaccination and epidemic strains would all affect the cross-reactivity and stimulation of B cell pools that could react and protect against the epidemic strain. Ultimately, this model predicted that successive vaccination of antigenically similar strains would be less effective against epidemic strains, especially epidemic strains that are more antigenically advanced. In this case termed 'negative interference', restimulation of B cells against the epitopes from prior vaccine is more likely interfering with stimulation of B cells by epitopes in the present vaccine strain that may also be present in the epidemic strain. In addition to its predictive strength of prior seemingly conflicting studies on repeated vaccinations (124, 125), a more recent study examining the effect of vaccination of 3 seasons during 2010-2015 also appeared to show evidence in support of this hypothesis (126). When present and prior vaccination strains were more antigenically distinct, little to no negative effect on vaccine effectiveness (VE) was observed as in the 2010-2011 season. Conversely, the more antigenically similar vaccine strains during the 2014-2015 season and a more antigenically distinct epidemic strain appeared to have a significant negative impact on VE.

However, given that not all 'antigenic sin'-like responses are hindering (127), conflicting data and the potential effect of adjuvants in improving the diversification of the vaccine response (128), antigenic distance between vaccine strains may be another factor in the myriad of variables that determine vaccine effectiveness against influenza A strains.

The nature of the humoral response against the continuously drifting strains of influenza remains a complex and nuanced process. With its relevance to continued protection and immunity against influenza through vaccination, the nature and balance of naïve and memory B cell responses in the context of antigenic drift and protection against future infection remains a vital subject of study and investigation.

SCOPE AND AIMS OF THIS PROJECT

Many studies have furthered our understanding of the effect of antigenic drift on the B cell response against influenza virus in humans in recent times. Although the most relevant 'model', human participants often have a varied and unknown infection history with influenza viruses, complicating the study of prior immunity in the context of an infection with a drifted influenza strain.

In comparison, animal models such as ferrets and mice allow for exposure to influenza viruses or antigens to be carefully controlled to study the relevant responses with a known immune history. As such, studies like that of O'Donnell *et al.* (129), have used animal models to examine the antibody responses against viruses in cases of antigenic drift.

Yet, while there is a large wealth of data regarding the specificity and dynamics of the antibody responses against influenza, the kinetics of B cells and their subsets which are responsible for the production of these antibodies are less well studied. At the time of writing, it remains unknown whether the immunodominance hierarchy of influenza-specific antibodies also reflects the immunodominant responses in influenza-specific B cells. However, given the immunodominance of HA-specific antibody responses against influenza (87, 88), at the beginning of this study we hypothesised that the dynamics and specificity of the recall of B cell responses during secondary infection against influenza virus would reflect the antigenic relatedness between the first and second infecting strains.

This project aims to use the C57BL/6 mouse model to investigate the naïve and memory B cell responses against paired strains of influenza virus with varying degrees of antigenic distance during primary and secondary infection. Chapter 3 established a model to characterize the kinetics of the primary, secondary and heterologous B cell response against influenza virus by B cell ELISPOT and flow cytometry. In particular, a protocol was established wherein various types of immune histories could be examined in a singular experiment. In Chapter 4, the model established in Chapter 3 was used to examine the effect of antigenic drift on B cell kinetics, where mice infected with paired strains of varying antigenic distance were compared to mice with expected primary and secondary responses.

Specific aims include:

1. To characterise the kinetics of the B cell response during the course of primary and secondary influenza virus infection in the C567BL/6 mouse model.
2. To examine the effect of antigenic shift on B cell kinetics during infection of H3N2 influenza virus with prior exposure to a H1N1 virus.

3. To examine the effect of antigenic drift on B cell responses during infection of paired H3N2 strains of varying antigenic distance.

CHAPTER 2 – MATERIALS AND METHODS

CELL CULTURE MEDIA

RF_{10}: Roswell Park Memorial Institute (RPMI)-1640 medium without L-Glutamine (Media Preparation Unit [MPU], The University of Melbourne [UoM]) with supplements of 10% volume/volume (v/v) heat-inactivated (56˚C, 30 min) foetal bovine serum (HI-FBS; Gibco, Grand Island, New York, USA), 25 IU/mL penicillin (Gibco), 25 µg/mL streptomycin (Gibco), 24µg/mL gentamicin (Pfizer, Bentley, WA, Australia), 2 mM glutamine (Sigma, St. Louis, MO, USA) and 2mM sodium pyruvate (BDH chemicals, Poole, Dorset, England).

RPMI+anti: RPMI-1640 medium without L-Glutamine supplemented with 25 IU/ml penicillin, 25 µg/mL streptomycin, 24 µg/mL gentamicin, 2 mM glutamine and 2 mM sodium pyruvate.

L-15 medium (2x): Lebovitz's L-15 medium with L-Glutamine (Gibco) dissolved into pyrogen-free Baxter water (pH 6.8; Baxter Healthcare Pty. Ltd., NSW, Australia) with supplemented 25 IU/mL penicillin, 25 ug/mL streptomycin, 0.4 mM HEPES buffer (Gibco) and 0.028% weight/volume (w/v) sodium hydrogen carbonate (NAHCO3; Sigma) in HANKS (Media Preparation Unit; MPU).

Agarose overlay medium: 0.9% (w/v) Type I agarose (Sigma) with TPCK treated trypsin (Worthington Biochemicals, Lakewood, New Jersey, USA) in L-15 medium.

Egg infection medium: Phosphate buffered saline (PBS; MPU) with 120 µg/mL gentamicin.

B cell medium: RF_{10} media additionally supplemented with 0.1 mM of 2-mercaptoethanol (CalBioChem, San Diego, California, USA).

All media was filtered through a 0.45µm membrane filter (Millipore, Billeria, Massachusetts, USA) and stored at 4˚C prior to use.

BUFFERS AND SOLUTIONS

PBS: 137 mM sodium chloride (NaCl), 10 mM sodium hydrogen phosphate (Na_2HPO_4), 2.7 mM potassium chloride (KCl) and 1.47 mM potassium dihydrogen phosphate (KH_2PO_4) in MilliQ water (pH 7.4; MPU).

Trypsin versine (TV): Earle's balanced salt solution, 0.05% (v/v) trypsin and 0.02% (w/v) versine (MPU).

Lysis buffer: 0.5 M Tris (Chem-Supply, Gillman, South Australia, Australia), 0.6 M potassium chloride (KCl; Chem-Supply) and 0.5% (v/v) Triton-X (United States Biochemical, Cleveland, Ohio, USA) in double distilled water adjusted to a pH of 7.8.

PBSN$_3$: Phosphate-buffered saline solution (PBS; MPU) containing 0.1% (weight/volume [w/v]) sodium azide (Sigma Aldritch).

PBST: PBS (MPU) with 0.05% (w/v) Tween-20 (LabChem, Auckland, New Zealand).

BSA$_{10}$PBS: PBS (MPU) containing 10% (w/v) bovine serum albumin (BSA; Sigma Aldrich)

BSA$_5$PBST: PBS (MPU) with 5% (w/v) BSA and 0.05% (w/v) Tween-20.

Fluorescence-activated cell sorting (FACS) buffer: PBS (MPU) with 10% (w/v) BSA and 0.02% (v/v) sodium azide.

VIRUSES

Influenza virus strains A/Puerto Rico/8/34 (PR8; H1N1) and A/Udorn/307/72 (Udorn; H3N2) were used in this study as well as vaccine seed viruses containing the HA and NA of either A/Port Chalmers/1/73 (PC73; H3N2), A/Victoria/3/75 (Vic75; H3N2), A/Texas/1/77 (TX77; H3N2), A/Bangkok/1/79 (BK79; H3N2) or A/Philippines/2/82 (Ph82; H3N2) on a PR8 background (all other genes from PR8). The PR8 virus is mouse adapted. Udorn is a human isolate while the viruses reassorted with PR8 have surface glycoproteins from viruses that were human isolates. The Ph82 virus has been mouse adapted by selection for resistance to inhibitors in mouse lung (130).

Viruses were propagated by inoculation of 10 day old embryonated chicken eggs (Seqirus, Parkville, Victoria, Australia) before incubating at 35°C for 48 hours. Eggs were then placed at 4°C overnight before allantoic fluid was harvested and clarified by centrifugation at 1000 g for 5 minutes at 4°C. Aliquots were then stored at -80°C. Infectious viral titres (plaque forming units [PFU] / mL) and HA titres were determined by plaque assay and HA assays respectively prior to use.

CELL LINES

Madin Darby Canine Kidney (MDCK) cells: MDCK cells were cultured in 75 cm^2 tissue culture flasks (TC75; Corning Inc., New York, USA) with RF$_{10}$ culture media. When cell monolayers reached confluence, cells were passaged by removing media and washing with PBS before adding 2.5 mL of TV at 37°C until cells detached from the flask. RF$_{10}$ was added to the solution before cells were

pelleted at 400 *g* for 5 minutes by centrifugation and resuspended in warmed RF_{10} and seeded into a new TC75 flask.

VIRUS PURIFICATION FROM ALLANTOIC FLUID

To detect B cells specific for viral strains without the presence of egg proteins by B cell enzyme-linked immunospot (ELISPOT) assay, viruses were purified from frozen allantoic fluid stocks of A/Udorn/1972 (H3N2) and A/Philippines/1982 (H3N2) amplified in embryonated chicken eggs. Polyethylene glycol (PEG) 6000 (Sigma Aldrich) was added to the thawed allantoic fluid stocks to make a solution of 8% w/v while stirring. Once the PEG was dissolved, the solution was centrifuged at 9000 rpm at 4°C for 30 min on the Beckman Avanti J-E centrifuge using the JLA16.250 rotor. The pellet was then resuspended in $PBSN_3$ with an underlay of 5% w/v sucrose in $PBSN_3$ and centrifuged at 25,000 rpm at 4°C for 1.5 h in the Beckman Ultracentrifuge XL-90 with the sw28 rotor at maximum acceleration and deceleration.

The resuspended pellet was then layered over a 35 mL linear sucrose gradient consisting of 15 to 80% (w/w) sucrose in $PBSN_3$ and centrifuged at 25,000 rpm for 2.5 hours with maximum acceleration and no deceleration. The visible band of virus within the gradient was then harvested, resuspended and centrifuged to dilute out the sucrose before the purified virus pellet was resuspended in 1mL $PBSN_3$.

The resultant product was measured for protein content by the Bradford assay and HA titre by hemagglutination assay.

BRADFORD PROTEIN ESTIMATE ASSAY

Purified viral stocks were quantified for protein content by Bradford Protein Estimation prior to use in the B cell ELISPOT assay. Standards containing various concentrations of BSA up to 1 mg/mL in distilled H_2O were prepared prior to measurement. Samples were diluted 1:2, 1:5 and 1:10 to ensure a reading within the range of detection of the assay. 20 µL of diluted samples and standards were then added to plastic cuvettes (Sarstedt, Nümbrecht, Germany) before 1 mL of 1x BioRad Protein Assay dye was added to each cuvette and read using a BioPhotometer (Eppendorf, Hamburg, Germany) at 595nm.

Optical density of the standards was used to plot a standard curve which in turn enabled protein concentrations of samples to be calculated using the formula of the curve.

HAEMAGGLUTINATION ASSAY

A hemagglutination assay was performed to determine the hemagglutinating units (HAU) of viruses. Viruses were serially diluted in PBS (MPU) across 96-well round-bottom plates at 25 µL total volume. An overlay of 25 µL of 1% chicken red blood cells (cRBCs; Sequirus) was added and allowed to incubate at room temperature for 30 min before scoring for agglutination.

HAU titres (HAU/mL) were calculated using the following formula: HAU/mL = 40 x dilution factor x 2^{n-1}, where n is the end point well containing 1 HAU.

HAEMAGGLUTINATION INHIBITION ASSAY

Hemagglutination inhibition (HI) assays were performed to determine the titre of mouse serum antibodies that prevented hemagglutination of chicken red blood cells by the haemagglutinin of influenza virus strains. Mouse sera were treated with receptor destroying enzyme (RDE; Sigma Aldrich) overnight at 37°C before being neutralized by 0.72% (w/v) sodium citrate yielding a final serum dilution of 1:10.

Viral stocks were assayed by HA to determine 4HAU prior to the HI assay. RDE-treated serum samples (25 µL total volume) were serially diluted in 96-well round-bottom plates and an equivalent volume of virus (4 HAU) was added to all wells and gently resuspended before incubating at RT for 30 min. 25 µL of 1% cRBCs were then added before incubating for another 30 min at RT. Plates were then scored for haemagglutination, with inhibition titres recorded as the reciprocal of the highest dilution of sera required to completely inhibit haemagglutination.

PLAQUE ASSAY

To determine infectious viral titres in samples of virus or lung homogenates, plaque assays were performed using MDCK cells. MDCK cells were seeded in 6-well tissue culture (TC6; Costar, Wugiang, Jiangsu Province, China) plates in RF_{10} and incubated overnight at 37°C and 5% CO_2. Media was aspirated from confluent MDCK monolayers and washed with RPMI+anti. Samples containing virus were serially diluted in RPMI+anti before 135 µL was added to the cell monolayers and incubated for 45 min at 37°C with 5% CO_2. An overlay of 3 mL of agarose overlay medium was then added and incubated at 37°C with 5% CO_2 for 72 h. Distinct plaques produced by cytopathic effects (CPE) as a result of MDCK cell infection were then counted.

The infectious viral titre per mL of each sample was then calculated by averaging the mean number of plaques multiplied by the dilution factor of the sample with the assumption that each plaque represents initial infection of a single cell by a single infectious virion.

MOUSE INFECTION

For all mouse influenza infections, 8-10-week-old female C57BL/6 mice were lightly anesthetized by isoflurane (Veterinary Companies of Australia Pty Ltd, Kings Park, NSW, Australia) inhalation (2 L/min). 50 µL of virus diluted in RPMI (Gibco) was delivered to the external nares to establish a total respiratory tract infection. Mice were monitored for overt clinical signs and/or body weights depending on the virulence of influenza virus strain as outlined in the ethics up to 10 days post infection, then twice a week upon recovery. At predetermined timepoints specified in the experimental models, mice were culled by CO_2 asphyxiation.

MOUSE ORGAN HARVEST AND PROCESSING

Harvesting and processing peripheral blood by heart puncture

To harvest peripheral blood, an incision below the ribcage of asphyxiated animals was made and extended upwards to the chin to expose and cut into the pleura. The heart was then punctured to allow peripheral blood to bleed into the pleural cavity and extracted using a 3mL syringe into a heparinised tube for analysis of cell content or a 1.5 mL Eppendorf tube for collection of serum.

For cellular analyses, red blood cells were lysed by adding samples to 7.5 mL of distilled water (dH_2O) for 10-15 s before 2.5 mL of saline solution (3.6% w/v NaCl in dH_2O) was quickly added to restore an isotonic environment for the cells to prevent lysis. Samples were then centrifuged at 2200 rpm for 7 min, washed with 10 mL PBS and kept on ice until ready for further processing.

To harvest serum from whole blood, samples were left overnight to settle and clot at 4°C. The samples were then centrifuged at 2000 *g* for 10 min at 4°C before serum was pipetted into a clean 1.5 mL Eppendorf tube. This process was then repeated to ensure all red blood cells were removed from serum samples before sera were labelled and stored in -20°C until use.

Processing of lung tissue

Lung tissue was dissected after blood was harvested and stored at -80°C until ready for processing. To quantify viral loads in tissue samples by plaque assay, lungs were thawed and homogenized in 1 mL RPMI+anti. Samples were then clarified by centrifugation for 5 min at 1000 *g* to pellet tissue debris before 3x 200 µL aliquots of supernatant were stored in -80°C until ready for virus quantification by plaque assay.

Processing of spleen and mediastinal lymph nodes

Spleen and mediastinal lymph nodes were removed and collected in separate tubes containing 1mL of PBS. To make single cell suspensions, the organs were pressed through a 70 µm sieve (BD Falcon, Franklin Lakes, NJ, USA) and resuspended in 3 mL PBS for spleen and 1 mL for MLN.

Collection of bone marrow

Bone marrow was obtained from the femur and tibia of mice by dissection of bone and shaving off the epiphysis on either side of bone. PBS was passed through the marrow using a 19G needle fitted to a 1mL syringe until all marrow was obtained and placed on ice until ready for further processing.

Red blood cell depletion for single cell suspensions of spleen, MLN and bone marrow samples

Single cell suspensions of spleen, MLN and bone marrow were centrifuged at 600 *g* for 3 min. Supernatant was discarded and cells were resuspended in 1 mL tris-buffered ammonium chloride (pH 7.2; ATC) warmed to 37°C for 3 min at RT to allow for RBC lysis before being diluted in 9 mL PBS. Samples – including peripheral blood – were then centrifuged for 3 min at 600 *g* and resuspended in PBS – 1 mL for MLN, BM and blood and 3 mL for spleen.

Samples were then aliquoted for further processing in various assays including quantification of cell numbers using a coulter counter (Beckman Coulter), determination of the number of virus-specific antibody secreting cells by the enzyme-linked immunospot (ELISPOT) assay and analysis of cellular phenotypes by flow cytometry.

ENZYME LINKED IMMUNOSPOT (ELISPOT) ASSAY

The ELISPOT assay was utilized to quantify the number of virus-specific antibody secreting cells in influenza-infected mouse samples. Briefly, 96-well 0.45um surfactant-free mixed cellulose ester membrane filter plates (Merck Millipore, Darmstadt, Germany) were pre-coated with purified whole

influenza virus at 5 µg/mL in $PBSN_3$ and stored in 4°C overnight. Plates were then washed and blocked with $BSA_{10}PBS$ for at least 1 h RT.

After quantification of cell counts, MLN and splenic samples were centrifuged at 600 *g* for 3 min and resuspended in B cell media to attain a concentration of 10^6 cells/mL for MLN and 10^7 cells/mL for spleen samples. Blocked plates were washed 3 times with PBST before 100 µL of MLN or splenic sample was added – 10^5 and 10^6 cells respectively – to the plates in duplicate and serially diluted across the wells in B cell media. An additional 100 µL of B cell media containing 10U of recombinant IL-2 was added before plates were incubated overnight at 37°C with 5% CO_2.

Plates were then washed twice in dH_2O and twice with PBST before incubation with pooled goat anti-mouse IgA, IgG2c, IgG3 or IgM at 1:1000 dilution (Southern Biotech) for 2 h at RT. Plates were then washed (4x PBST, 1x PBS) and 100 µL of substrate solution made with 1 BCIP/NBT tablet (Sigma Aldrich) per 10 mL dH_2O was added to the wells. After 30 min incubation at RT, plates were washed with dH_2O 3 times and allowed to dry.

Once dry, plates were counted using a dissecting stereo microscope. Each spot represents a single virus-specific ASC and hence the number of virus-specific ASC per million cells could be derived from the total cells in each sample and the dilution of each sample well.

ANALYSIS OF B CELL RESPONSE KINETICS BY FLOW CYTOMETRY

To investigate the phenotype of cells in single cell suspensions of MLN, spleen, peripheral blood and BM, samples were first processed and RBC depleted as described. Samples were aliquoted into round-bottom 96-well plates and centrifuged at 600 *g* for 3 min before being resuspended in 1:50 dilution of CD16/CD32 (BD Pharmigen) as a FcR block. After 5 min incubation at RT, cells were washed and centrifuged before cells were resuspended in the appropriate cocktail of surface antibodies (see Table 2.1 and Table 2.2) and incubated on ice in the dark for 30 min. For studies involving the analysis of virus HA-specific B cells, probes created from HA sequences of specific influenza strains and modified to be unable to bind to sialic acid were synthesized in processes outlined in *Whittle et al. (131)* and conjugated to fluorophores by Dr. Adam Wheatley of the Kent laboratory (University of Melbourne, Parkville, Australia). Cells were then washed with FACS buffer 3 times, resuspended in 0.1 µg/mL BV510 conjugated to streptavidin (BD Biosciences, cat no. 563261) and incubated on ice in the dark for 30 min. After another 3 washes with FACS buffer, cells were fixed and permeabilized using the BD Cytofix/Cytoperm Fixation/Permeabilization kit (BD Biosciences) as per manufacturer instructions.

Cells were then incubated in the intracellular stain cocktail as detailed in Table 2.1 for 30 min on ice in the dark. Samples were then washed with 1xPerm/Wash buffer (BD Biosciences) and FACS buffer before being resuspended in FACS buffer and stored in mini FACS tubes overnight at 4°C.

Samples were then analysed by flow cytometry on the BD LSRFortessa (BD Biosciences) and subsequent data was analysed using FlowJo version 10.5.2 (TreeStar). Any values of 0 were set to the limit of detection – a single cell detected in total MLN, BM and was equivalent to 10 total cells.

Table 2.1. Antibody cocktails for flow cytometry

Cocktail Type	Antibody	Concentration (µg/mL)	Manufacturer
Surface stain	CD38-BV421	0.2	BD Biosciences
	Live/Dead-Aqua	1:800	Life Technologies
	MHC class II-BV605	0.2	BD Biosciences
	B220-BV711	0.2	BD Biosciences
	IgD-BV786	0.2	BD Biosciences
	CD19-APC	0.1	BD Biosciences
	GL7-PerCPCy5.5	1	BioLegend
	CD138-PE	0.5	BD Biosciences
	CD3-Biotin	0.25	eBiosciences
	CD5-Biotin	0.25	BD Biosciences
	F480-Biotin	2.5	BioLegend
	CD11c-Biotin	2.5	BD Biosciences
	Gr1-Biotin	0.5	BD Biosciences
Intracellular stain	IgA-FITC	2.5	BD Biosciences
	IgG1-FITC	0.25	BioLegend
	IgG2c-FITC	1.25	Southern Biotech
	IgG3-FITC	1.25	Southern Biotech
	IgM-PECy7	1	eBiosciences

STATISTICAL ANALYSIS

For comparisons of a single group over a period of time, data was analysed by a repeated measure one-way analysis of variance (ANOVA). For comparisons of multiple groups over a period of time, data was analysed by two-way analysis of variance (ANOVA) with Tukey's multiple comparisons tests. For comparisons between two groups at one time point, data was analysed by the Mann-Whitney test or the Student's t-test. Statistical significance was demonstrated by a P value of <0.05. All data analysis was conducted with GraphPad Prism version 7.0 (GraphPad Software Inc., La Jolla, CA, USA).

CHAPTER 3 – THE KINETICS OF THE B CELL RESPONSE DURING INFLUENZA A VIRUS INFECTION

INTRODUCTION

The T-dependent B cell response is an integral component of host immunity against influenza virus infection, aiding in viral clearance and recovery during the course of infection and protection against subsequent infections by similar strains. Although much of the focus has been towards antibody production and its role in the prevention of infection, a broad picture of B cell responses during influenza infection has been elucidated through various studies. During influenza infection, B cell responses are found to be most prominent in the mediastinal lymph node, the draining lymph node of the lungs, and to a lesser degree, the spleen (79). Numbers of follicular GC B cells – identified by GL7 expression and low levels of CD38 expression – in the lymph nodes have been shown to be a predictor of serum antibody responses, suggesting that these GC B cells are the progenitors to antibody secreting cells once fully differentiated (82). In terms of kinetics, BALB/c mice were shown to display a peak level of response at around 15 dpi for GC B cells while plasmablasts, identified by marker CD138, peaked at around 10 dpi in the MLN during primary PR8 infection (132). In comparison, initial antibody-secreting cell responses in humans have been shown to peak in peripheral blood at 7 days post-vaccination and post-infection (109, 133, 134).

As mentioned previously, responses seen post-vaccination in influenza-experienced adults also suggest that a majority of influenza-specific antibody secreting cells originate from memory B cells due to the high level of mutations seen in their V_H genes which codes for the variable antigen binding portion of the antibody (109). A study by Sze *et al.* using a mouse model, in comparison, suggests that long lived plasma cells in the spleen are derived from both affinity matured germinal centre B cells and extrafollicular B cells that have not undergone somatic hypermutation as evidenced from the proportion of cells containing mutations in their variable regions (135). This suggested that a greater breadth of B cells may play roles in secondary and recall responses than previously expected.

With zoonotic influenza infection and the ever-impending risk of a pandemic in the case of antigenic shift, cross-reactive B cell immunity has been a topic of much interest in the field of influenza research. As naturally occurring cross-reactive antibodies against multiple influenza subtypes are

uncommon (136, 137), it is thought that minimal secondary responses occur during so called heterosubtypic infection, which is infection of a host with prior experience of infection by influenza virus of another subtype. However, analysis of IgG^+ memory B cells from healthy donors post vaccination showed clones reactive with a panel of recombinant baculovirus-expressed influenza HAs from different H3N2 viruses as well as those from other subtypes. This analysis showed that memory B cells cross-reactive against multiple subtypes were relatively abundant and that the serum antibody response may not fully represent the repertoire of B cells (138). It would therefore be of interest to investigate the cross-reactive potential of the B cell response during heterologous influenza infection and the protective capacity of the humoral immune system as a whole in this context in the mouse model.

In this chapter, a comprehensive analysis of the B cell response in the context of primary, secondary and heterosubtypic influenza infection was assessed using the C57BL/6 mouse model. A combination of techniques was used to provide a broader picture of the development of the response during the period of infection. Flow cytometry enabled the assessment of the kinetics of B cell response and its relevant subsets including plasmablasts and GC B cells through specific markers. In addition, enzyme-linked immunospot assay (ELISPOT) was used to identify virus-specific antibody secreting cells by coating plates with the virus of interest.

RESULTS

Primary B cell responses during influenza infection are most prominent in the spleen and mediastinal lymph nodes.

To characterize primary B cell responses during influenza infection in mice, naïve C57BL/6 mice were infected with $10^{4.5}$ pfu A/Udorn/307/72 (H3N2, Ud72), a past seasonal influenza A strain. At 5, 7, 10- and 14-days post infection (dpi), spleen, mediastinal lymph nodes (MLN), bone marrow (BM) and peripheral blood were harvested for analysis by flow cytometry. Markers chosen for this analysis (Table 3.1) enabled the examination of B cells and their subsets, including $B220^{lo}CD138^+$ plasmablasts and $GL7^+CD38^{lo}$ germinal centre (GC) B cells. Further dissection of non-class switched versus class switched responses was also enabled through the inclusion of antibodies identifying specific isotypes of immunoglobulin; IgM for non-class switched and pooled IgG1, IgG2c, IgG3 and IgA for class switched. Gating strategies for each compartment are shown in Supplementary Figure 1. GC B cells

were not included in BM and peripheral blood analyses as germinal centres are structures which form in secondary lymphoid organs such as the spleen or lymph nodes.

Table 3.1. Selection panel for flow cytometric analysis of B cell subsets.

Specific Marker	Aids detection of	Fluorochrome
CD38	Germinal Centre B cells	Brilliant Violet 421
Streptavidin (SA)	Non-B cells & dead cells for exclusion (Live/Dead-Aqua & Dump channel)	Brilliant Violet 510
B220	Pan B cell marker	Brilliant Violet 711
IgD	Non-class switched B cells	Brilliant Violet 786
CD19	Pan B-cell marker	APC
IgA/G1/G2c/G3 (pooled)	Class-switched B cells	FITC
GL7	Germinal centre B cells	PerCP-Cy5.5
CD138	Plasma cells/blasts	PE
IgM	Non-class switched B cells	PE-Cy7
CD3	T cells	Biotin
CD5	B1 cells ('innate-like')	(Dump channel via
F480	Macrophages	SA-BV510)
CD11c	Dendritic cells	
Gr-1	Granulocytes	

As seen in Figure 3.1, the total number of cells in the spleen, blood and BM showed little differences between infected and RPMI control animals, despite some very small but statistically significant differences on day 5 in the BM and 14 in peripheral blood, which did not appear to be biologically significant. Similarly, the total B cell numbers in these tissues showed no overall differences between infected and control mouse groups. For the MLN, an RPMI control was not possible as a comparator because these lymph nodes only become visible and large enough for extraction following infection. However, in contrast to the other tissues, cellular and B cell responses in the MLN peaked at 7 dpi, reproducing the finding of preliminary experiments. Total B cells showed a significant rise ($p<0.01$) in numbers of approximately 2-fold between 5 and 7 dpi, after which the numbers showed a rapid decline by day 10 ($p<0.01$), continuing to day 14 ($p<0.001$). The pattern of

peak and decline was also reflected in MLN cell numbers, with a significant difference noted between days 7 and 14 post infection ($p<0.05$). Given that the MLN is the draining lymph node of the lungs, this is also in line with a rapid expansion of the immune response proximal to the site of infection and contraction once the infection has been cleared.

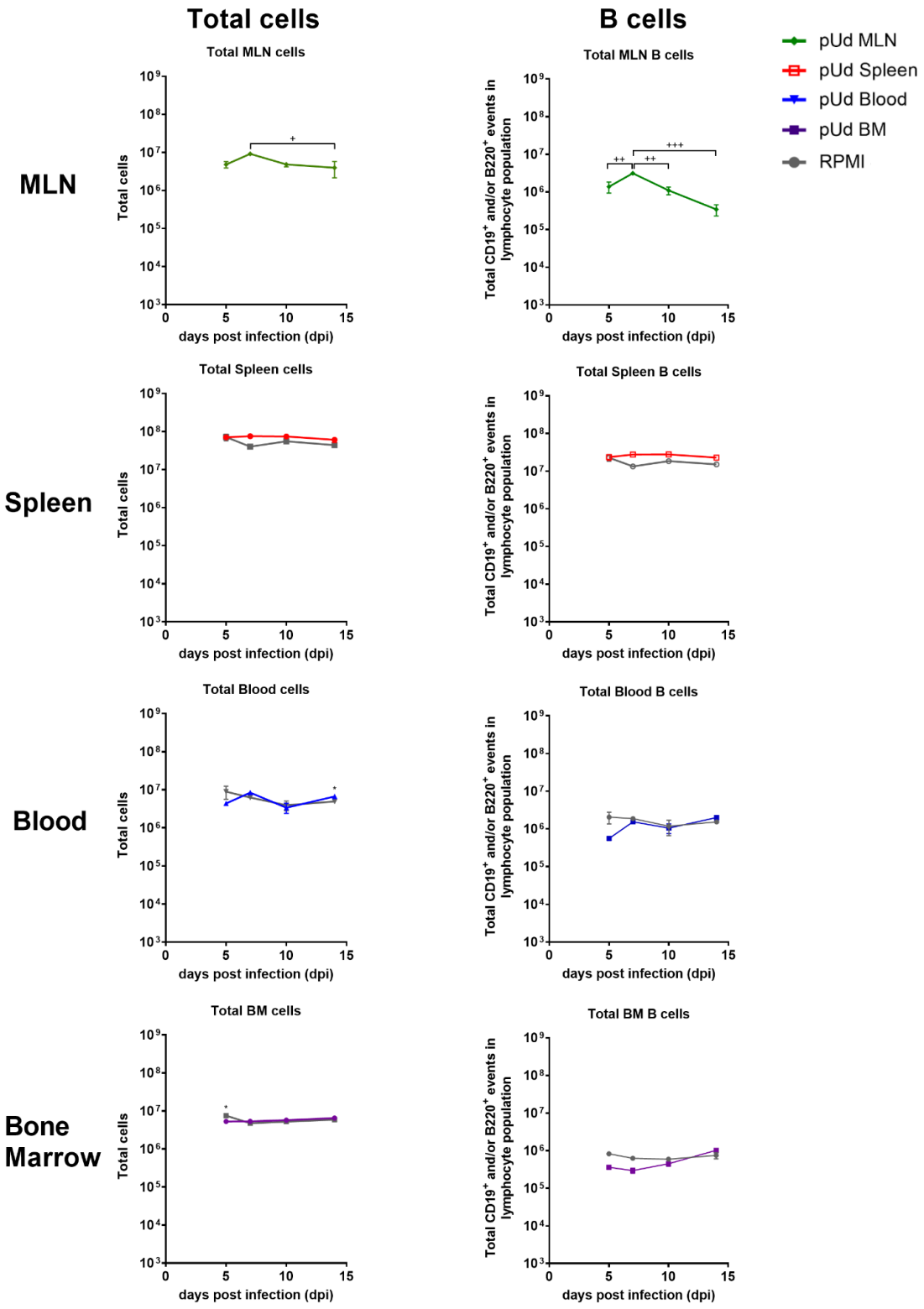

Figure 3.1. Kinetics of B cells in murine compartments during primary IAV infection by flow cytometry.

6-8-week-old C57BL/6 mice (n= 5) were infected with $10^{4.5}$ pfu of Ud72 virus. On days 5, 7, 10 and 14 post infection (dpi), spleen, mediastinal lymph nodes (MLN), bone marrow (BM) and peripheral blood were collected and processed for analysis by flow cytometry. The number of cells in each sample was determined using a Beckman Coulter Counter. Figure shows total cell numbers of lymphocytes and overall $B220^+$ B cells in MLN, spleen, BM and blood. Symbols represent + $p<0.05$, + $p<0.05$, ++ $p<0.01$, +++ $p<0.001$ by one-way ANOVA between time points for MLN with Tukey's multiple comparisons test and * $p<0.05$ represents two-way ANOVA of infected versus RPMI for other samples with Tukey's multiple comparisons test.

Similar to total B cells, MLN plasmablast populations (Figure 3.2) reached a significant peak at 7 dpi ($p<0.0001$), with numbers rising around 100-fold from day 5, while responses in other tissues showed no significant rise after infection compared to controls (ns by two-way ANOVA). Again, this may reflect a more rapid response at the MLN due to its proximity to the site of infection. This is especially pertinent as the primary role of antibody secretion by plasmablasts would be most effective at the site of infection to aid in neutralizing any remaining infectious virus and help resolve infection. Of these plasmablasts from the MLN of infected mice, both IgM^+ and IgA/G^+ subsets reached a significant peak by 7 dpi ($p<0.01$, one-way ANOVA), especially IgA/G^+ plasmablast responses where an approximate 1000-fold increase from 5 to 7 dpi was observed. Furthermore, there are greater numbers of IgA/G^+ than IgM^+ plasmablasts at the peak of the response, suggesting that the class switched plasmablast population appears to play the more prominent role during primary influenza infection.

In the other tissues and blood, no significant rise in IgM^+ plasmablasts was observed in infected compared to control mice. However, IgG/A^+ responses reached a significant peak at 10 dpi in the spleen and blood compared to controls ($p<0.05$), suggestive of later involvement compared to the MLN. Taken together, the data suggest that class-switched IgA/G^+ plasmablast responses appear to predominate over non-class-switched plasmablast responses over the course of infection, especially within the MLN but later in the spleen and peripheral blood as well.

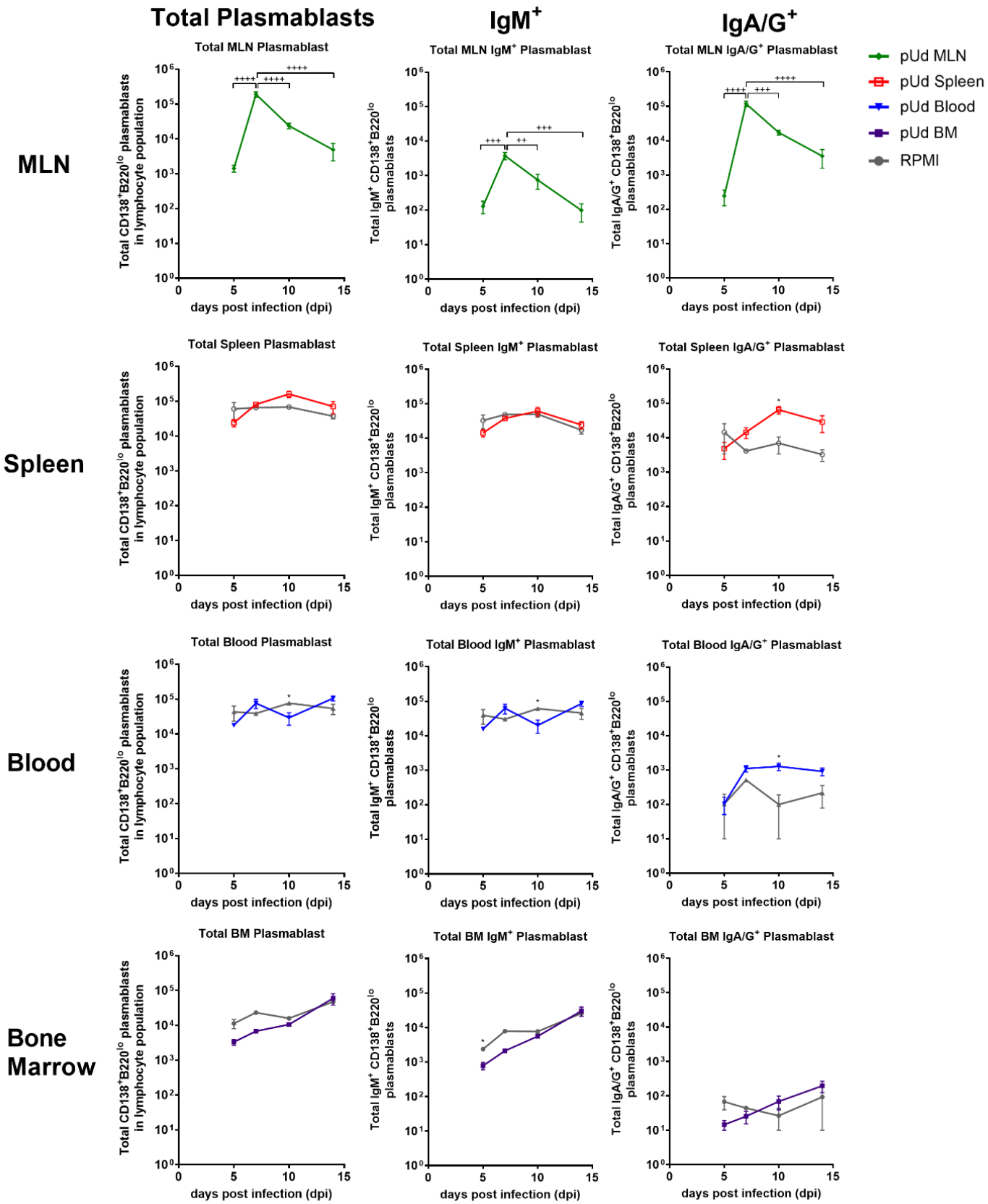
Total Plasmablasts
IgM+
IgA/G+
MLN
Spleen
Blood
Bone Marrow
pUd MLN
pUd Spleen
pUd Blood
pUd BM
RPMI
Total MLN Plasmablast
Total MLN IgM+ Plasmablast
Total MLN IgA/G+ Plasmablast
Total Spleen Plasmablast
Total Spleen IgM+ Plasmablast
Total Spleen IgA/G+ Plasmablast
Total Blood Plasmablast
Total Blood IgM+ Plasmablast
Total Blood IgA/G+ Plasmablast
Total BM Plasmablast
Total BM IgM+ Plasmablast
Total BM IgA/G+ Plasmablast
Total CD138+B220lo plasmablasts in lymphocyte population
Total IgM+ CD138+B220lo plasmablasts
Total IgA/G+ CD138+B220lo plasmablasts
days post infection (dpi)

Figure 3.2. Kinetics of plasmablasts in murine compartments during primary IAV infection by flow cytometry.

6-8-week-old C57BL/6 mice (n= 5) were infected with $10^{4.5}$ pfu of Ud72 virus and processed at appropriate time points as mentioned in Figure 3.1. Figure shows total cell numbers of $CD138^{+}B220^{lo}$ plasmablasts with subsets of IgA/G^{+} versus IgM^{+} intracellular expression. Symbols represent ++ $p<0.01$, +++ $p<0.001$, ++++ $p<0.0001$ by one-way ANOVA and Tukey's multiple comparisons test and * $p<0.05$ for infected versus RPMI by two-way ANOVA and Tukey's multiple comparisons test.

Germinal centre B cell populations continued their expansion beyond 7 dpi (Fig. 3.3). In the MLN these cells reached a peak at around 10 dpi ($p<0.05$), at least a hundred-fold increase from 5 dpi, before declining by 14 dpi. In line with the trend seen in plasmablast responses, GC B cells in the spleen appeared to respond later, approaching a peak around 10-14 dpi in infected mice compared to RPMI control mice ($p<0.05$). These results are suggestive of the expected maturation of B cell responses in germinal centres after the resolution of infection. Like the IgA/G^{+} plasmablast response, the class-switched IgA/G^{+} GC B cell response appeared very similar to the total GC B cell response in kinetics. MLN IgA/G^{+} GC B cell responses peaked at 10 dpi, showing a significant increase compared to prior timepoints and remained high at the 14 dpi time point. In comparison, IgM^{+} GC B cell responses in the MLN show a more significant decline from 10 to 14 dpi ($p<0.01$), which is in line with the isotype switching process expected during maturing GC responses. Splenic IgM^{+} and IgA/G^{+} GC B cell responses from infected mice were significantly above those of control mice at 10 dpi ($p<0.05$) and continued to plateau from 10-14 dpi ($p<0.05$).

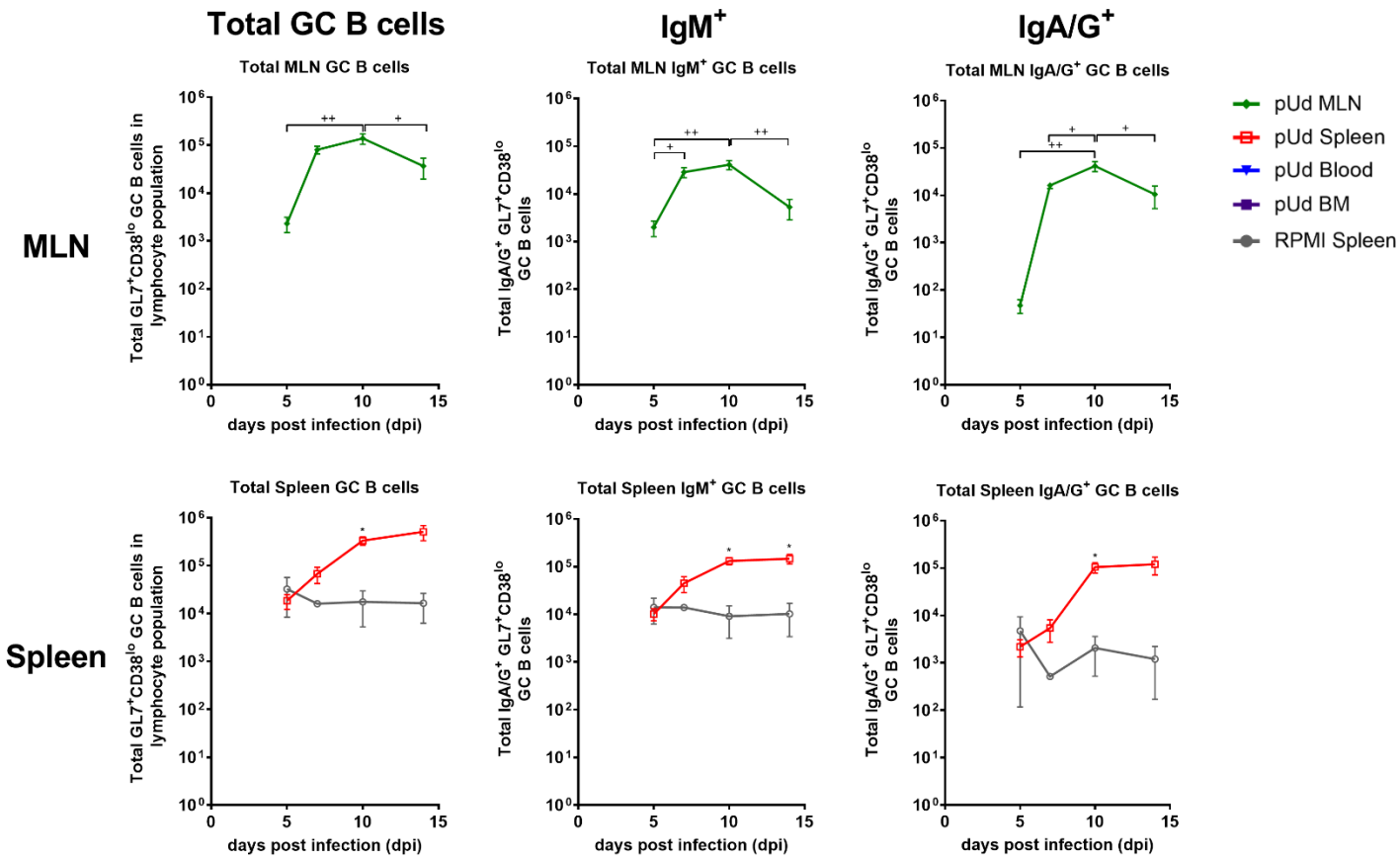

Figure 3.3. Kinetics of GC B cells in murine compartments during primary IAV infection by flow cytometry.

Six to eight-week-old C57BL/6 mice (n= 5) were infected with $10^{4.5}$ pfu of Ud72 virus and processed at appropriate time points as mentioned in Figure 3.1. Figure shows total cell numbers of $GL7^{+}CD38^{lo}$ germinal centre (GC) B cell subsets with subsets of IgA/G^{+} versus IgM^{+} intracellular expression. Symbols represent + $p<0.05$, ++ $p<0.01$ by one-way ANOVA with Tukey's multiple comparisons test and * $p<0.05$ by two-way for infected versus RPMI ANOVA with Tukey's multiple comparisons test.

Analysis of the percentages of IgM^+ compared to IgA/G^+ GC B cells and plasmablasts in the spleen over the course of infection (Figure 3.4) revealed prominent trends between the class-switched and non-class-switched populations. In both plasmablasts and GC B cells, it was found that populations of non-class-switched IgM^+ subsets began at significantly higher proportions than class-switched IgA/G^+ subsets ($p<0.05$ at 5 dpi, $p<0.01$ at 7 dpi for plasmablasts and $p<0.01$ at 5 dpi, $p<0.0001$ at 7 dpi for GC B cells). Populations of IgM^+ subsets in both compartments decreased while class-switched IgA/G^+ subsets increased over the course of infection up to 14 dpi. These data are suggestive of a steady process of class-switching during the process of B cell activation in secondary lymphoid organs as expected in response to primary infection.

Overall, these experiments have successfully characterized the kinetics of the B cell response during primary H3N2 influenza infection. Results indicated that the B cell response appeared most prominent in the MLN at 7 dpi and spleen at 10 dpi, while populations in peripheral blood and BM remained at baseline. This experiment has also provided insights into the timing and kinetics of plasmablast and GC B cell responses in the different organs as well as the kinetics of class switching. Together, these data provide insight into overall B cell activation over the course of primary influenza virus infection.

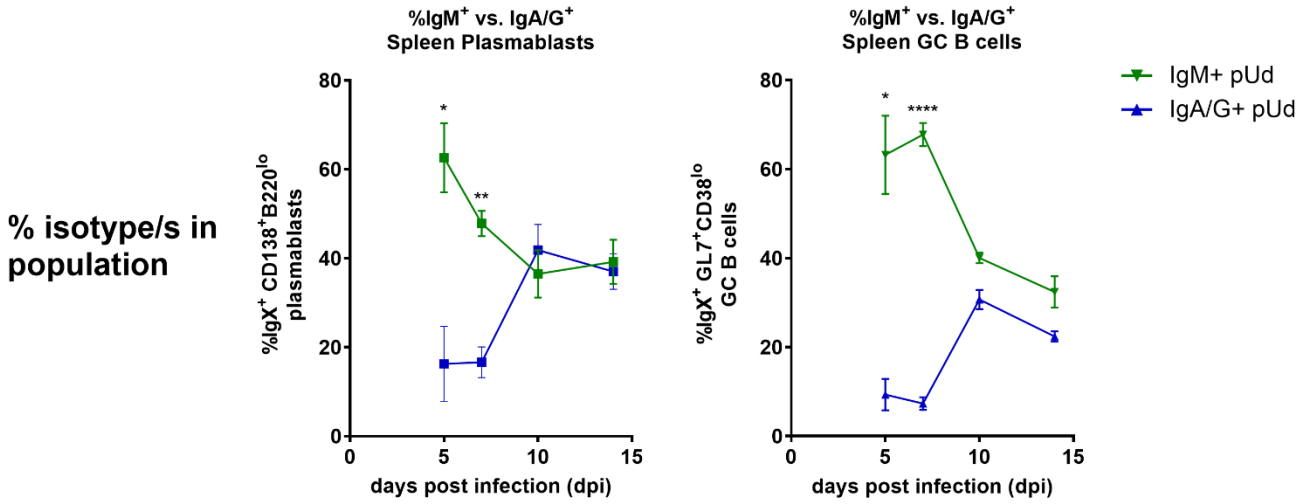

Figure 3.4. Percentages of IgM+ versus IgA/G+ plasmablasts and GC B cells in murine compartments during primary IAV infection by flow cytometry.

6-8-week-old C57BL/6 mice (n= 5) were infected with $10^{4.5}$ pfu of Ud72 virus and processed at appropriate time points as mentioned in Figure 3.1. Figure shows the percentage of these isotypes within subset populations of the spleen. Symbols represent * $p<0.05$, ** $p<0.01$, **** $p<0.0001$ by two-way ANOVA with Sidak's multiple comparisons test.

While flow cytometric analysis of B cell populations can inform overall trends on the expansion of cells, it does not discriminate between virus-specific and non-specific proliferation. To investigate the virus-specific primary B cell response against influenza infection, the enzyme-linked immunospot (ELISPOT) assay was utilized to detect influenza-specific antibody-secreting cells (ASCs). MLN and splenic B cell compartments specific for Ud72 virus were examined in mice during the course of infection with $10^{4.5}$ pfu Ud72 (Figure 3.5). Separate analyses for IgM^+ and pooled IgG/A^+ virus-specific antibody secreting cell numbers were conducted to examine the degree of class switching occurring in each compartment.

The results are plotted here as absolute numbers (Fig. 3.5 A and B) and as a frequency within the organ (Fig. 3.5 C and D). While the totals of both IgM^+ and pooled IgA/G^+ Ud72-specific ASC responses in the MLN and spleen appeared to peak at 7 dpi, only IgA/G^+ MLN responses showed a statistically significant elevation at that time point ($p<0.0001$ versus 5 dpi) due to the spread of responses in the spleen. The total splenic IgG/A^+ ASC responses in infected mice showed a small but significant rise at 14 dpi compared to control spleen ($p<0.05$). Although the greatest increase in absolute numbers of class switched B cells occurred in the spleen (Fig. 3.5 B), the largest proportional increase was observed in the MLN (Fig. 3.5 D). Of note, the peak of the Ud72-specific ASC response in terms of both numbers and frequency was day 7 for both MLN and spleen – this is in agreement with the peak response for plasmablasts (of which ASCs are a subset) in the MLN as detected by flow cytometry but is earlier than the peak detected by flow cytometry in the spleen. Thus, while the kinetics of overall numbers of primary B cell responses appear to vary depending on compartment, the more virus-specific responses in MLN and spleen seem to peak within a similar time frame.

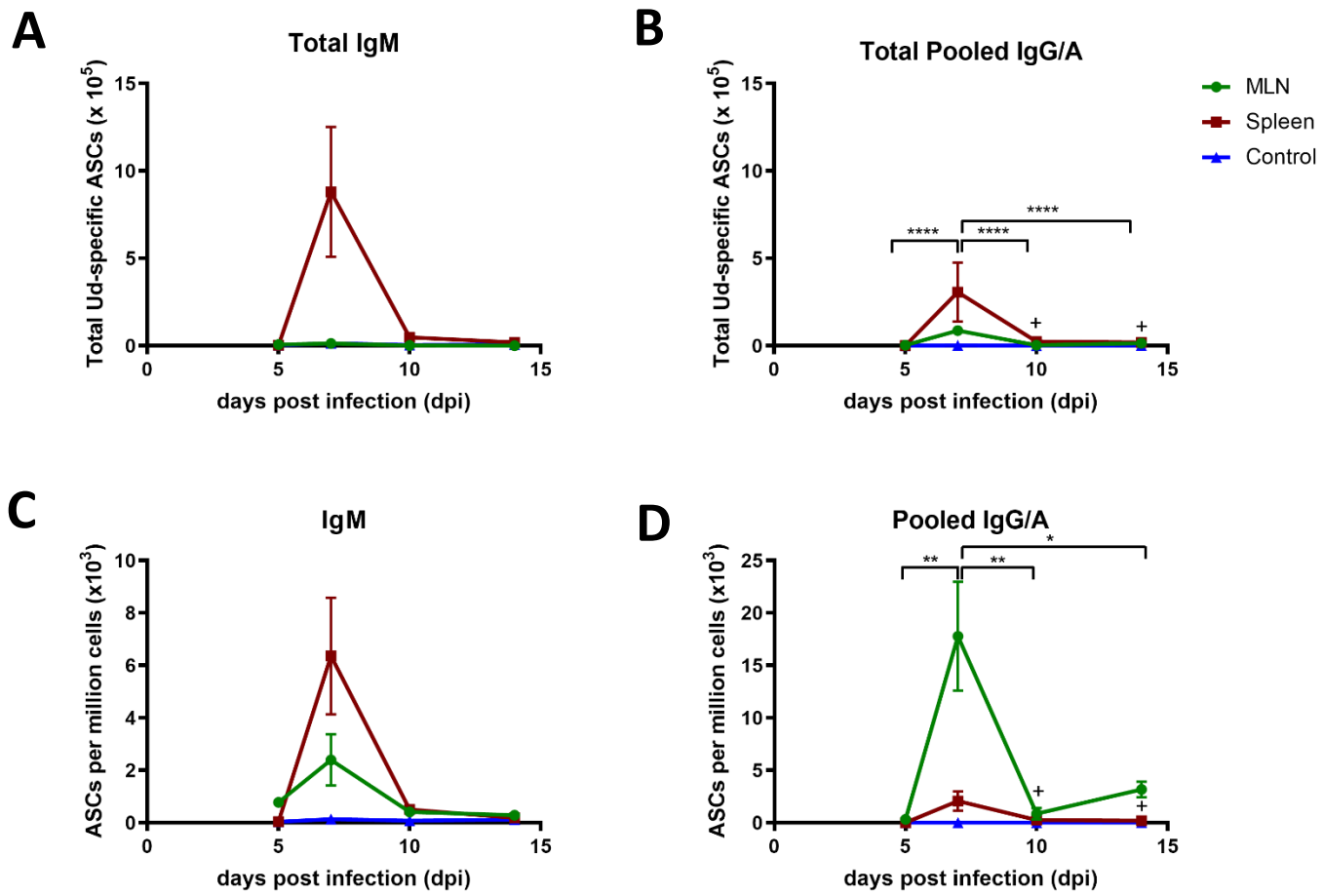

Figure 3.5. Kinetics of the IgM+ and pooled IgG/A+ antibody secreting response (ASC) to primary H3N2 Ud72 infection by ELISPOT assay.

8-week-old female C57BL/6 mice (n=4) were infected with $10^{4.5}$ pfu of Ud72 (H3N2) or RPMI as a control. Spleen and MLN were collected on days 5, 7, 10 and 14 post infection and processed into single cell suspensions. Cells were then quantified using a Beckman Coulter Counter before 10^6 spleen cells and 10^5 MLN cells were added to plates coated overnight with lysed purified Ud72 virus. Samples were serially diluted across the wells, left overnight in media with IL-2 before being washed off. Alkaline phosphatase-conjugated antibodies were used to bind anti-mouse IgM or pooled IgA/G respectively to detect cells which secreted Ud72-specific antibodies to develop into precipitating 'spots'. Each spot is representative of a single antibody secreting cell. The numbers of A) total IgM^+ and B) total pooled IgA/G^+ as well as the proportion per million cells for C) IgM^+ and D) pooled IgA/G^+ responses in each compartment are shown. Control group represents the number of Ud72-specific ASCs in the spleen of mock RPMI infected mice. Symbols represent

*p<0.05, **p<0.01, ***p<0.001, ****p<0.0001 by one-way ANOVA with Tukey's multiple comparisons and +p<0.01 for spleen vs. control by one-way ANOVA.

Ud HA-specific B cell subsets represent a small proportion of total virus-specific responses during primary Ud infection.

To further investigate the specificity of the B cell response against Ud infection, specialised Ud HA probes with a mutation on the receptor binding site (RBS) to prevent sialic acid binding were used in flow cytometry to analyse the HA-specific response against primary Ud infection. MLN and spleen from mice were infected with $10^{4.5}$ pfu of Ud at 7 and 14 dpi were harvested and processed for analysis as shown in Figure 3.6.

Ud HA-specific plasmablasts and GC B cells represented a relatively small proportion of the total plasmablast and GC B cell populations respectively. Ud HA^+ plasmablasts in the MLN were only about one hundredth rising to one tenth of the overall plasmablasts ($p<0.05$ for 7 and 14 dpi, total vs. HA^+ plasmablasts). Similarly, total plasmablast populations in the spleen were found to be at least 30-fold higher than the HA^+ population at 7 and 14 dpi as well as in the control. However, statistical significance was only noted between total and HA^+ populations at 14 dpi ($p<0.0001$) likely as a result of the variability between samples. As plasmablasts lose the capacity to bind to its specific antigen during differentiation into plasma cells (139), this may contribute to the relatively small populations of HA-specific cells in this subset.

However, this would not explain the results seen in the GC B cell population where cells would be expected to retain expression of its surface Ig to bind its cognate antigen. While populations of HA^+ GC B cells in the MLN appeared to be small at 7 dpi in proportion to the total population ($p<0.01$), representing only about 1%, the total number of HA^+ GC B cells appear to make up about 10% of the overall GC B cell population in the MLN by day 14. This may be suggestive of the continued affinity maturation and proliferation of antigen specific B cells occurring at the draining lymph node of the site of infection. In comparison, Ud HA^+ GC B cells in the spleen uniformly represented less than 5% of the overall GC B cell population at both 7 and 14 dpi as well as the RPMI control (denoted as day 0), showing significant differences with the overall total GC population ($p<0.05$ for all groups, total population vs. HA^+ population).

As seen in the results from Figure 3.5, the Ud-specific ASC response by ELISPOT appears to be relatively uniform at 14 dpi, with the exception of the IgA/G$^+$ ASC response in the MLN which was seen to be somewhat elevated at 14 dpi. This is reflected by the higher magnitudes of this subset in comparison with IgM$^+$ ASC in the MLN ($p<0.05$).

As plasmablasts and its terminally differentiated counterparts plasma cells are the main producers of antibodies, antigen secreting cell populations would be expected to correlate with their numbers. In accordance with this, total combined populations of IgM$^+$ and IgA/G$^+$ virus-specific ASC populations make up a proportion of total plasmablasts (around 20%), while total Ud HA-specific plasmablasts in turn make a proportion of virus-specific ASCs as would be expected (around 35% for MLN, 10% for spleen). It is notable that the Ud HA$^+$ makes up a relatively small population of virus-specific cells when compared to Ud-specific ASCs, suggesting that despite the reported immunodominance of HA-specific antibody, HA-specific B cells still make up a small proportion of all virus-specific antibody secreting cells. This suggests that the virus-specific B cell response may be far more diverse than expected and that HA$^+$ B cells may readily release more antibodies against its antigen despite its relatively small numbers even in the pool of virus-specific B cells.

While this method of analysing the virus HA-specific response was highly informative, these virus HA-specific probes only became available near the end of the experimental period of this thesis. Viral HAs of strains used in later chapters (notably Ph82) were tested but not shown due to their inability to detect virus HA-specific cells even after extensive troubleshooting.

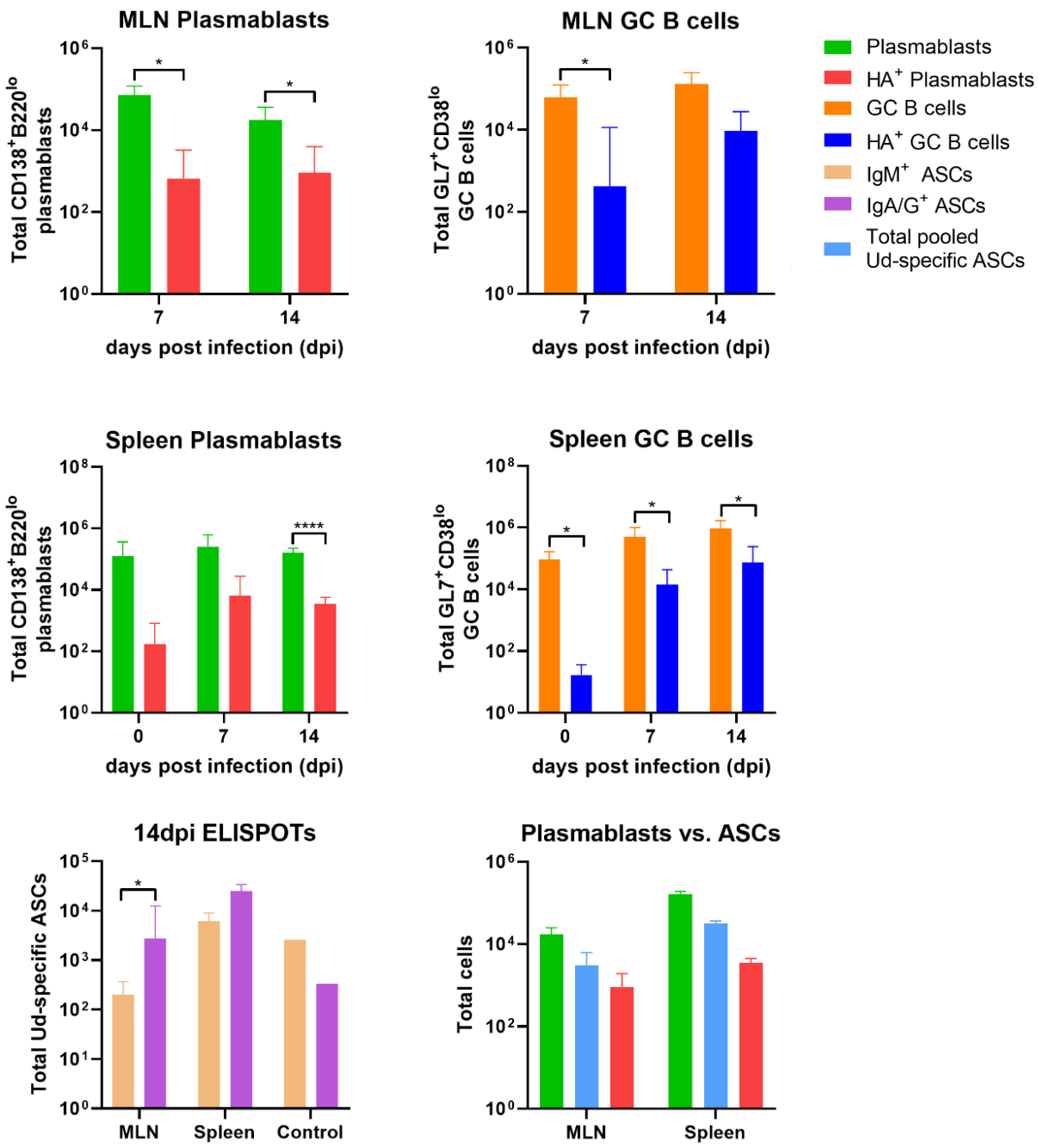

Figure 3.6. Total Ud HA-specific plasmablasts and germinal centre B cells in murine compartments during secondary IAV infection.

6-8-week-old C57BL/6 mice (n= 3-4) were infected with $10^{4.5}$ pfu of Ud72 virus 6-8 weeks post initial infection. On days 7 and 14 post infection (dpi) of the second dose, spleen, and MLN were collected and processed for analysis by flow cytometry. The number of cells in each sample was determined

using a Beckman Coulter Counter. At 14dpi, samples were also processed for Ud virus-specific ASCs using a B cell ELISPOT assay. Figure shows total numbers of overall and Ud HA-specific $CD138^{+}B220^{lo}$ plasmablasts and $GL7^{+}CD38^{lo}$ germinal centre (GC) B cells by flow cytometry as well as total Ud-specific ASCs at 14dpi by ELISPOT. Control mice were given RPMI as mock infections and analysed at the same time points as the infected groups before spleen data was pooled and displayed at 0dpi or control on the x-axis of resultant graphs. Symbols represent *$p<0.05$, ***$p<0.001$ by two-way ANOVA.

Reinfection with an identical strain of influenza virus induces an earlier response in MLN and spleen as expected of a secondary B cell response.

To further examine the kinetics and magnitude of B cell responses against influenza virus, B6 mice were infected with 100 pfu of Ud72 and then challenged with 10^5 pfu Ud72 virus 7 weeks later as a model of secondary homologous infection. A larger dose of virus was used for the secondary infection to avoid its rapid neutralization by antibodies raised in response to the primary infection. MLN, spleen, BM and peripheral blood were harvested on days 3, 5, 7 and 10 post-infection to be processed and analysed by flow cytometry with the gating scheme as shown in Figure 3.7A.

As shown in Figure 3.7 B-D, total B cell, plasmablast and GC B cell responses in the MLN in this secondary model peaked on day 5, two days earlier than that seen in the primary responses (Fig. 3.1-3). By day 7, all MLN B cell populations had significantly declined. Interestingly, in the spleen, B cell subsets appeared to show a ‘double peak’ pattern previously not shown in primary responses. This may be indicative of an initial activation of the Ud72-specific memory B cell population in the spleen at 3 dpi. The subsequent slight drop in numbers may represent recruitment of these activated cells into the MLN by 5 dpi in parallel with additional expansion of cells in the spleen that peak at 7 dpi. Analysis of additional animals is needed to confirm the significance of the double peak pattern. The rise of overall B cells from 3 to 5 dpi in the blood ($p<0.05$) and a significant decrease from 5 to 7 dpi in plasmablasts ($p<0.01$) may be indicative of patterns of B cell and plasma cell recruitment during the course of infection.

It should be noted that, although the number of total B cells is markedly higher in the spleen than the MLN, it can be seen that GC B cells in the MLN outnumber even those seen in the spleen at 5 dpi despite their relative organ sizes. This further supports that the major site of activation is located in

the MLN as the draining lymph node of the lung where the infection is taking place. Overall, these results confirm that secondary B cell responses against Ud72 influenza virus respond earlier to reinfection than primary infection, with an initial peak in the draining lymph node by day 5 after infection that may correspond to the recall of memory B cells.

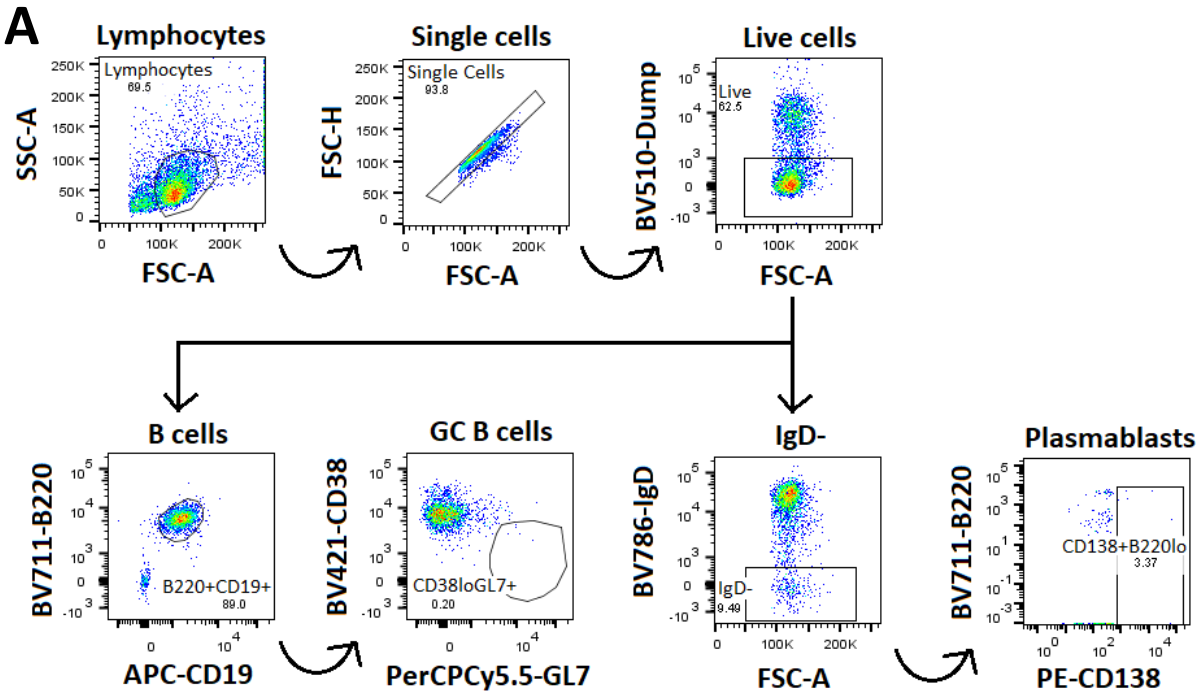

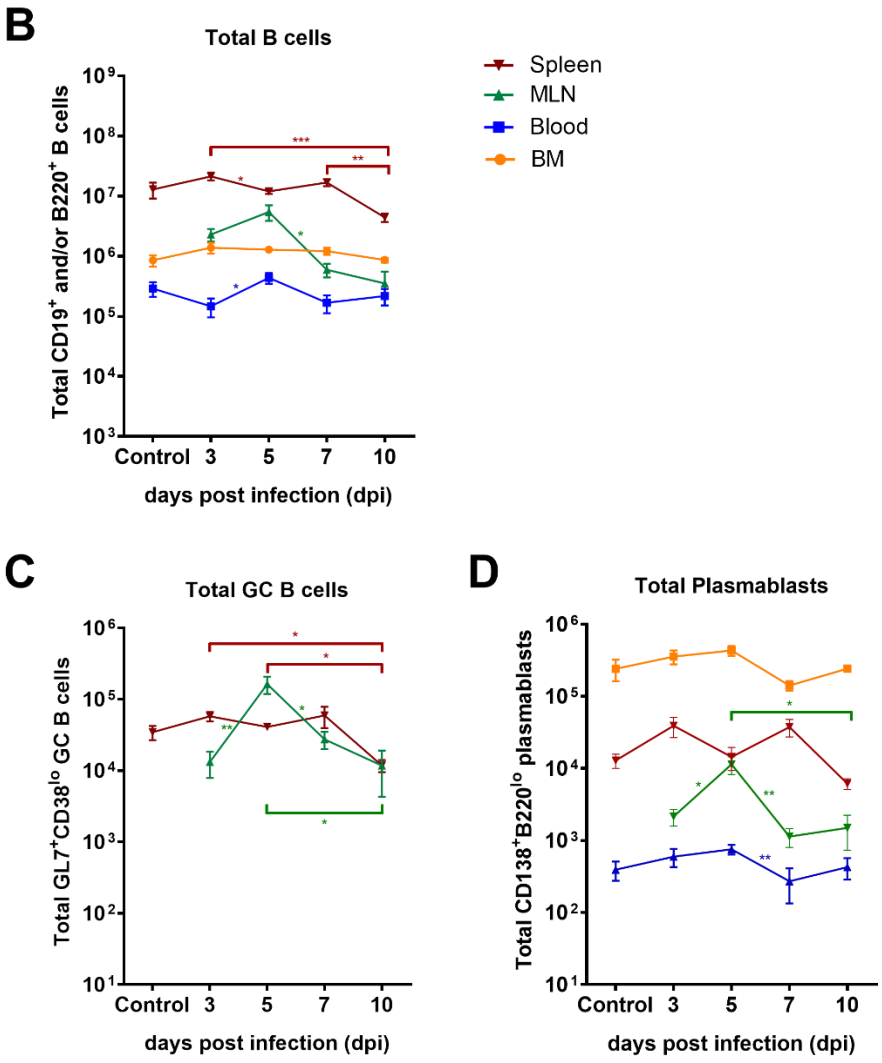

Figure 3.7. Kinetics of total B cells, plasmablasts and germinal centre B cells in murine compartments during secondary IAV infection.

6-8-week-old C57BL/6 mice (n= 5) were infected with 100 pfu of Ud72 virus, and re-infected with 10^5 pfu of Ud72 virus 6-8 weeks post initial infection. On days 3, 5, 7 and 10 post infection (dpi) of the second dose, spleen, MLN, BM, and peripheral blood were collected and processed for analysis by flow cytometry. The number of cells in each sample was determined using a Beckman Coulter Counter. A) the gating scheme for cellular events B) total numbers of overall $CD19^+B220^+$ B cells, C) $GL7^+CD38^{lo}$ germinal centre (GC) B cells and D) $CD138^+B220^{lo}$ plasmablasts are shown. Control mice were given RPMI as mock infections and analysed at the same time points as the infected groups before data was pooled and displayed as 'control' on the x-axis of resultant graphs. Symbols represent *p<0.05, **p<0.01, ***p<0.001 by one-way AVOVA.

In a model of antigenic shift, infection of H3N2 Ud72 in the context of prior exposure to H1N1 PR8 induces early secondary-like B cell responses.

Characterization of both primary and secondary B cell response kinetics enabled the further examination of B cell responses in the varied contexts of influenza infection. Especially pertinent is the scenario of antigenic shift where a virus of a novel subtype, bearing a completely distinct HA and sometimes also NA, is introduced to the human population. To model the effect of antigenic shift on the B cell response against influenza infection and compare the kinetics and magnitude of the responses to those obtained in primary or secondary influenza infection, BL6 mice were infected with 10^5 pfu Ud72 (H3N2) virus after prior infection with either 30 pfu PR8 (H1N1), 100 pfu Ud72 or media alone as a control (Figure 3.8). This experimental design simulates secondary infection with a homologous virus to which B cells are already primed, and with a heterologous subtype virus that is not expected to have substantial antibody cross-reactivity to the surface antigens.

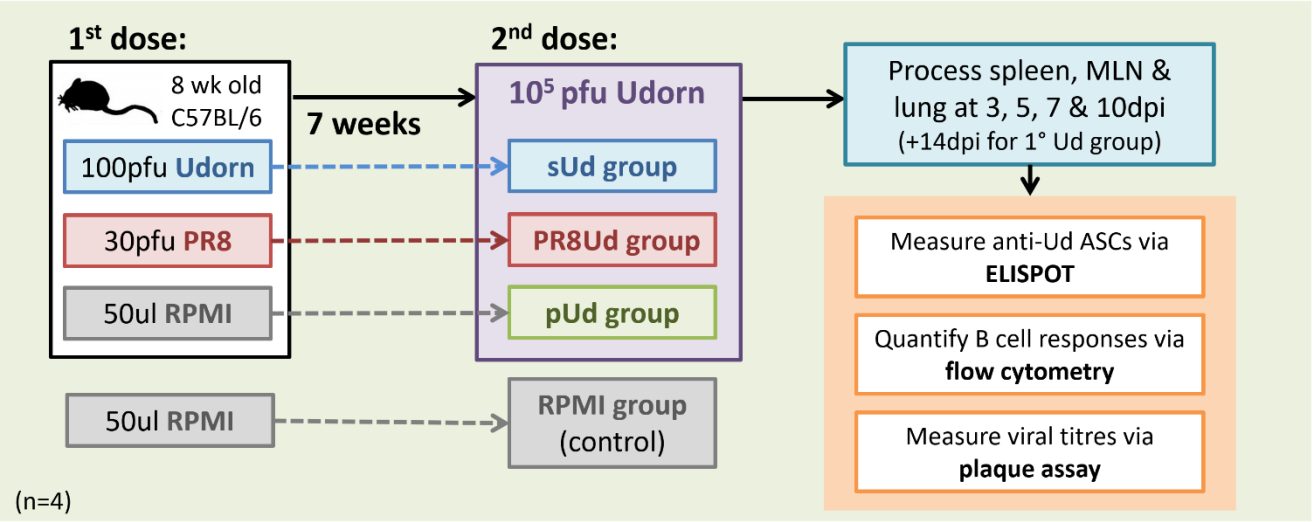

Figure 3.8. Experimental protocol to investigate the kinetics of the B cell and Ud72-specific ASC response during H3N2 Ud72 infection in mice with prior exposure to H1N1 PR8 infection.

C57BL/6 mice (n=4) were infected according to the schedule shown. On days 3, 5, 7 and 10 post Ud72 infection (dpi), spleen and MLN were collected and processed for analysis by flow cytometry and ELISPOT. The number of cells in each sample was determined using a Beckman Coulter Counter.

The total MLN lymphocyte and B cell numbers were found not to vary substantially between infected groups (Figure 3.9), suggesting that overall numbers of B cells are relativity similar during influenza infection – whether primary, homologous secondary or heterosubtypic secondary. Similarly, total B cell subset population in the spleen of all groups appears to be relatively similar to those seen in the RPMI group, likely due to the large relative population of B cells in the lymphoid organ. Although significant differences were observed in splenic B cell populations, it is noted that no groups were significantly different from the control RPMI mice which suggests that all responses were still within baseline. The only exception appears to be the primary responders (pUd) which appear to have a marginally lower proportion of B cells compared to RPMI control at 10 dpi, which may be indicative of recruitment to germinal centres and/or the site of infection.

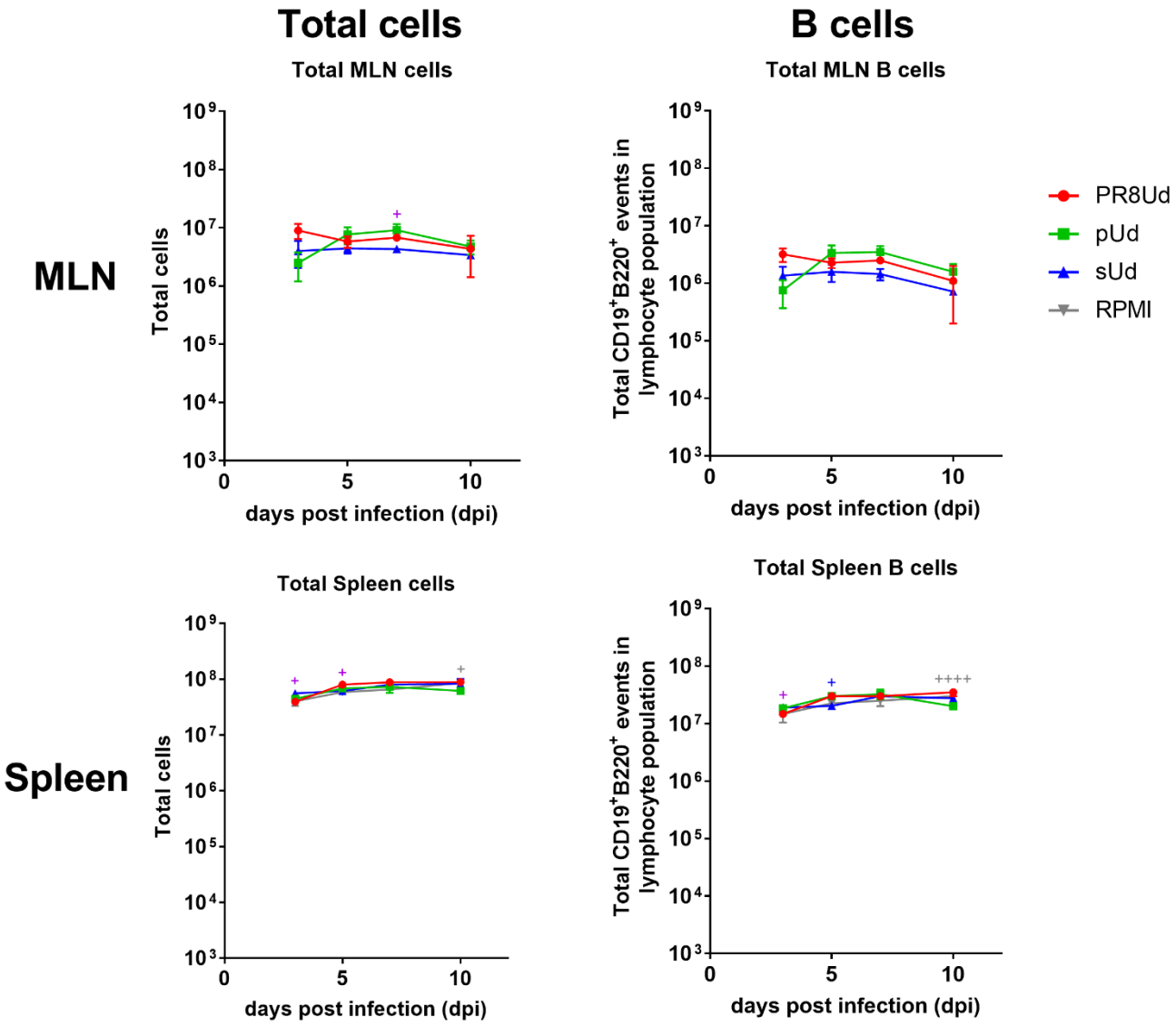

Figure 3.9. Kinetics of the B cell response during H3N2 Ud72 infection in mice with prior exposure to H1N1 PR8 infection.

C57BL/6 mice (n=4) were infected and processed according to the schedule shown in Fig. 3.8. Figure shows total numbers of cells and overall $CD19^+B220^+$ B cells. Symbols above timepoints indicative of statistical significance by Mann Whitney test (* symbols) or two-way ANOVA (+ symbols). Number of symbols indicative of level of significance: * $p<0.05$, ** $p<0.01$, *** $p<0.001$, **** $p<0.0001$. Colours represent the comparisons made – colours conforming to the key represent pUd compared to the group with the same colour in the key and purple represents comparisons between sUd and PR8Ud.

In agreement with the data shown in primary models, the MLN plasmablast responses in the pUd group rose sharply to a peak on day 7 post infection (Figure 3.10). This contrasts with the pattern observed for both secondary Ud72 infection (sUd) and heterosubtypic infection (PR8Ud) where the responses on day 3 appeared greater than for the primary response and rose steeply (by at least 10-fold) at day 5 then more gradually to day 7, subsequently declining at a similar rate to the pUd group once the infection has been cleared. Although this experiment did not have enough power to show a statistically significant difference in these two patterns by two-way ANOVA, analysis of day 3 and day 5 responses in isolation using a Mann-Whitney test revealed a significant increase in the PR8Ud group over the pUd group on both days ($p<0.05$), indicative of an earlier and potentially more secondary-like response in mice with prior heterosubtypic infection. The sUd group, despite having a similar pattern to the PR8Ud was not different to the pUd at early timepoints which could be a reflection of the difference in antigen stimulus compared to the PR8Ud group. It is likely that a substantial amount of the challenge virus in the sUd group was neutralized by antibody raised in the primary infection. This is less likely to have occurred in the group previously infected with PR8 which is antigenically dissimilar to the challenge virus. Of interest is the observation that, even at the peak of the secondary response, the number of PR8Ud plasmablasts was no greater than in the primary response. Similar to prior experiments, IgA/G^+ plasmablast responses in the MLN were found to match the trends and kinetics seen in overall populations, including significant increases of the subset in PR8Ud compared to pUd ($p<0.05$) in the earlier time points of 3 and 5 dpi by Mann-Whitney test. The similar magnitudes of IgA/G^+ compared to overall plasmablast responses later during infection suggests a predominately class-switched plasmablast response as the B cell response matures over the course of the infection.

The similar kinetics also suggests that timing of class switching corresponds closely with overall expansion of plasmablasts in the MLN.

In comparison, minimal differences between groups were found for plasmablasts in the spleen. No statistical differences were noted in overall plasmablast populations by Mann-Whitney or two-way ANOVA tests, likely due to the spleen being distal from the site of infection. Class-switched IgA/G$^+$ plasmablasts were found to significantly increase in pUd populations as compared to the sUd and RPMI groups by two-way ANOVA at 10 dpi ($p<0.05$), however, suggestive of the development of class-switch responses expected near the post-infection resolution.

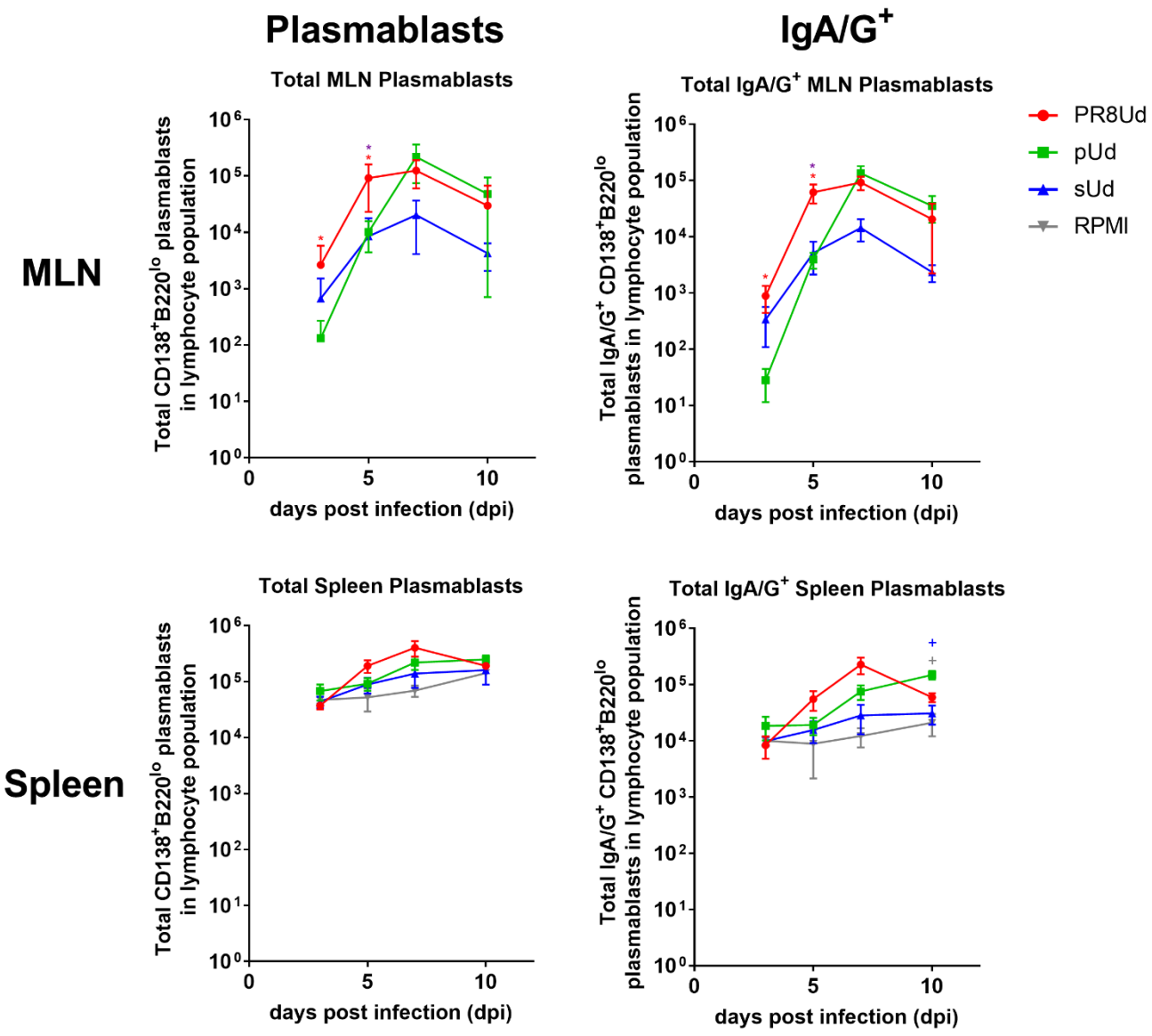

Figure 3.10. Kinetics of the plasmablast response during H3N2 Ud72 infection in mice with prior exposure to H1N1 PR8 infection.

C57BL/6 mice (n=4) were infected and processed according to the schedule shown in Fig. 3.8. Figure shows total numbers of $CD19^+$ $B220^{lo}$ plasmablasts and IgA/G^+ plasmablasts. Symbols above timepoints indicative of statistical significance by Mann Whitney test (* symbols) or two-way ANOVA (+ symbols). Number of symbols indicative of level of significance: * $p<0.05$, ** $p<0.01$, *** $p<0.001$, **** $p<0.0001$. Colours represent the comparisons made – colours conforming to the key represent pUd compared to the group with the same colour in the key and purple represents comparisons between sUd and PR8Ud.

While general patterns in MLN and splenic GC B cells (Figure 3.11) show similarities to those seen in plasmablasts, statistical analysis indicated that the PR8Ud group showed elevated levels of overall GC B cells compared to sUd at 7 dpi ($p<0.01$, two-way ANOVA). Using Mann-Whitney tests, it was shown that both sUd and PR8Ud were significantly elevated at 3 dpi compared to pUd ($p<0.05$), suggestive of an initial secondary-like response. This is in line with the trends in magnitudes seen in overall B cell and plasmablast responses and suggests that prior exposure to influenza infection may allow for a higher magnitude GC response at early time points in the secondary response. As noted in MLN plasmablasts, IgA/G^+ subsets within the population appear to follow trends seen in the GC B cells, with PR8Ud and sUd significantly elevated responses compared to pUd at 3 dpi ($p<0.05$, Mann-Whitney test) suggestive of an initially secondary-like response before becoming more primary-like at later timepoints as shown by the significant increase compared to sUd by two-way ANOVA at 7 dpi ($p<0.05$).

In comparison, splenic GC B cell responses between groups were found to be similar in response apart from a significant elevation in the pUd group compared to sUd and RPMI at 10 dpi ($p<0.05$). While the GC B cell response in the spleen seems unchanged from baseline, results suggest that mice exposed to Ud for the first time as a primary infection have elevated levels of GC B cells, likely as a result of developing germinal centre reactions near the resolution of infection as expected. This trend can be seen more prominently in the IgA/G^+ subset of GC B cells where populations of class-switched GC B cells are from the pUd group significantly lower than sUd initially at 3 dpi ($p<0.05$, Mann-Whitney & two-way ANOVA) but gradually rise at least one log-fold by 10 dpi and is significantly higher than sUd by two-way ANOVA at this time point ($p<0.05$). Interestingly, it was also

found that initial IgA/G$^+$ GC B cell numbers at 3 dpi were elevated in the sUd group compared to the RPMI control group ($p<0.05$, two-way ANOVA), suggestive of pre-existing class-switched B cells as expected in a secondary response. Similarly, numbers of IgA/G$^+$ GC B cells were found to be significantly higher than control at 7 dpi for PR8Ud ($p<0.05$, two-way ANOVA) which may reflect an elevated response due to some pre-existing memory combined with increased stimulation due to differences in B cell antigens as a result of heterologous infection.

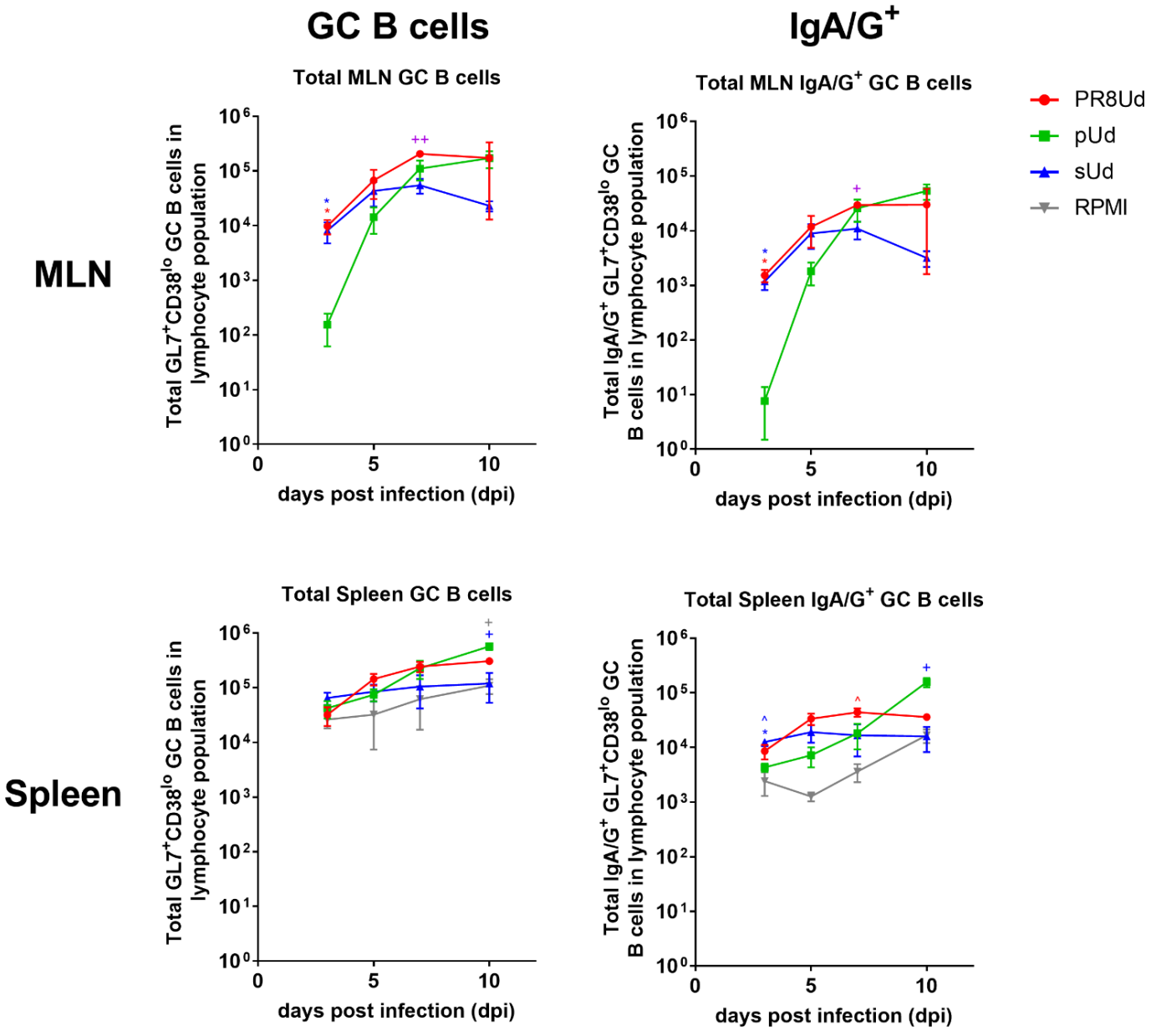

Figure 3.11. Kinetics of the GC B cell response during H3N2 Ud72 infection in mice with prior exposure to H1N1 PR8 infection.

C57BL/6 mice (n=4) were infected and processed according to the schedule shown in Fig. 3.8. Figure shows total numbers of $GL7^{+}CD38^{lo}$ germinal centre (GC) B cells and IgA/G^{+} GC B cells. Symbols above timepoints indicative of statistical significance by Mann Whitney test (* symbols) or two-way ANOVA (+ symbols). Number of symbols indicative of level of significance: * $p<0.05$, ** $p<0.01$, *** $p<0.001$, **** $p<0.0001$. Colours represent the comparisons made – colours conforming to the key represent pUd compared to the group with the same colour in the key and purple represents comparisons between sUd and PR8Ud. The ^ symbol was used to indicate comparisons with RPMI with the group of the same colour by two-way ANOVA.

These results were similarly reflected in the trends of the ELISPOT assays evaluating Ud72-specific antibody secreting cells as seen in Figure 3.12. In the MLN, it was found that the PR8Ud group showed significant differences with sUd at both early timepoints of 3 and 5dpi ($p<0.05$, Mann Whitney) as well as later at 7 dpi ($p<0.001$, two-way ANOVA). While some secondary-like kinetics are occurring in the PR8Ud responses, virus-specific antibody secreting cell responses in the context of prior infection of influenza with a differing subtype still shows aspects of responding in a primary-like fashion with regards to an initial non-class switched virus-specific B cell response. However, results from the pooled IgA/G^{+} ASC response in the MLN also indicates that the PR8Ud group has a marked elevation in class switched responses early during the infection at 5 dpi compared to both sUd and pUd ($p<0.05$, Mann Whitney). This appears to suggest that exposure to a different subtype prior to infection puts the PR8Ud in a unique situation where class-switched responses are enhanced during infection. It is likely that greater antigen stimulus than with sUd due to an inability to completely neutralize the virus, together with pre-existing cross-reactive T cell immunity, may contribute to this enhancement. While trends in IgM^{+} ASC responses in the spleen suggest that PR8Ud responses appear to peak at 7 dpi as pUd does, no statistical significances between any groups were found and suggests a minimal response no different from baseline in all groups. In addition, splenic IgA/G^{+} ASC responses showed an early elevated PR8Ud response at 5 dpi compared to pUd ($p<0.05$, Mann-Whitney test), which suggests a potentially more secondary-like response early during infection as observed in flow cytometry. Also similar to responses seen in class-switched plasmablasts and GC B cells, pUd responses appeared to significantly elevate by 10 dpi compared to RPMI and sUd ($p<0.01$, two-way ANOVA) which may be indicative of maturing GC responses and its resultant class-switched, differentiated populations.

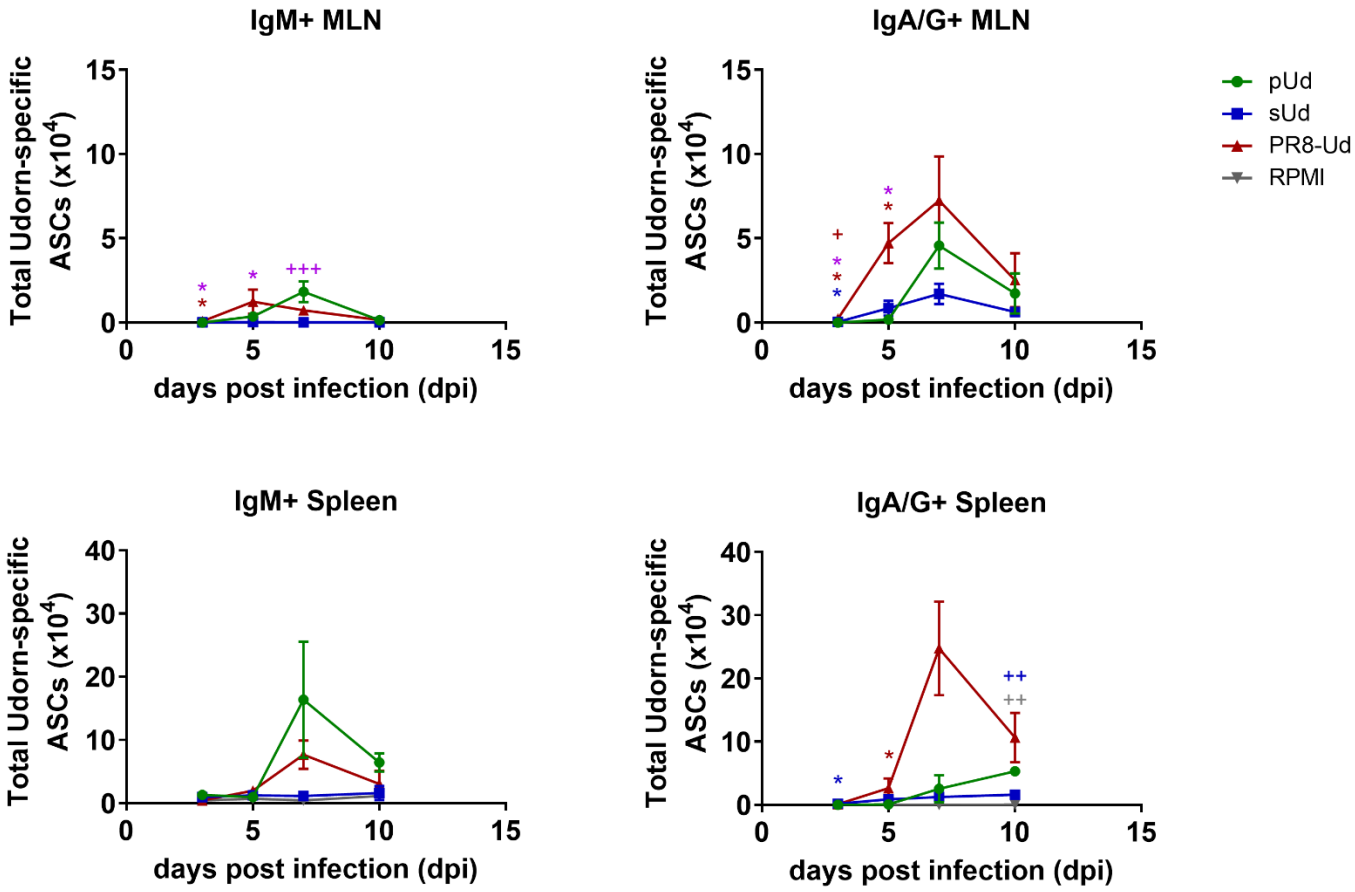

Figure 3.12. Kinetics of the Ud-specific ASC response during H3N2 Ud72 infection in mice with prior exposure to H1N1 PR8 infection.

C57BL/6 mice (n=4) were infected and processed according to the schedule shown in Fig. 3.8. ELISPOT assay was used to determine the number of IgM^+ and pooled IgA/G^+ Ud72-specific antibody secreting cells in the MLN and spleen. Symbols above timepoints indicative of statistical significance by Mann Whitney test (* symbols) or two-way ANOVA (+ symbols). Number of symbols indicative of level of significance: * $p<0.05$, ** $p<0.01$, *** $p<0.001$, **** $p<0.0001$. Colours represent the comparisons made – colours conforming to the key represent pUd compared to the group with the same colour in the key and purple represents comparisons between sUd and PR8Ud.

Examination of viral loads in the lungs from the influenza infected mice after Ud72 infection (Figure 3.13 A) shows that mice from the pUd group had the highest initial titres in their lungs at around 10^6 pfu/mL which cleared around days 7-10 while the PR8Ud group appeared to be a log-fold lower in titre at 3 dpi ($p<0.05$, two-way ANOVA) before titres quickly dropped and cleared by 7 dpi. In comparison, mice with prior exposure to Ud72 had no detectable viral titres and were significantly lower in titre compared to pUd and PR8Ud at 3 dpi ($p<0.001$). Although Ud72 is capable of replicating to high titres in the lung as seen in the pUd group, which still showed significantly higher titres compared to sUd and PR8Ud at 5 dpi ($p<0.001$), the humoral and cellular memory induced by Ud72 in the initial infection likely provided protection to the sUd group and prevented the secondary Ud72 infection from becoming established. This provides validation of the proposal that the lower magnitude of B cell responses in sUd compared to PR8Ud groups, including differences seen at 5 dpi between these groups ($p<0.05$) was due to neutralization of the challenge virus with a resulting decrease in antigen stimulus for the secondary B cell responses. In addition, some level of cross-protection against Ud72 by prior exposure to heterosubtypic PR8 virus that allowed mice to more rapidly clear the infection was likely contributed to by CD8 T cells or cross-reactive helper CD4 T cells (140, 141).

Mice were also monitored over the course of the primary and secondary infections for body weight and clinical signs. As viral doses were low and sublethal, mice showed minimal clinical signs over the course of primary infection (Figure 3.13 B). Animals infected with a small dose of the mouse-adapted strain PR8 lost a maximum of 10% of their body weight as expected but recovered to their initial starting weight within 14 days. Loss of body weight for groups infected with the high dose of 10^5 pfu Ud72 correlated with prior exposure history. Mice exposed to influenza virus for the first time (pUd) lost the most weight, followed by a moderate weight loss in mice previously infected with a different subtype (PR8Ud) while mice previously exposed to Ud72 showed virtually no loss in body weight. As a surrogate for disease severity, the weight loss data appeared to align perfectly with the observed viral titres, with prominent weight loss and highest viral titres seen in the pUd group, followed by moderate weight loss combined with lower titres of infection in the PR8Ud group and finally no weight loss and undetectable viral titres in the sUd group. This also aligns with the expected quality of immunological memory against Ud72 from each group, with sUd fully protected from reinfection of Ud72, PR8Ud likely having some level of protection against influenza virus and finally, no prior memory in pUd mice.

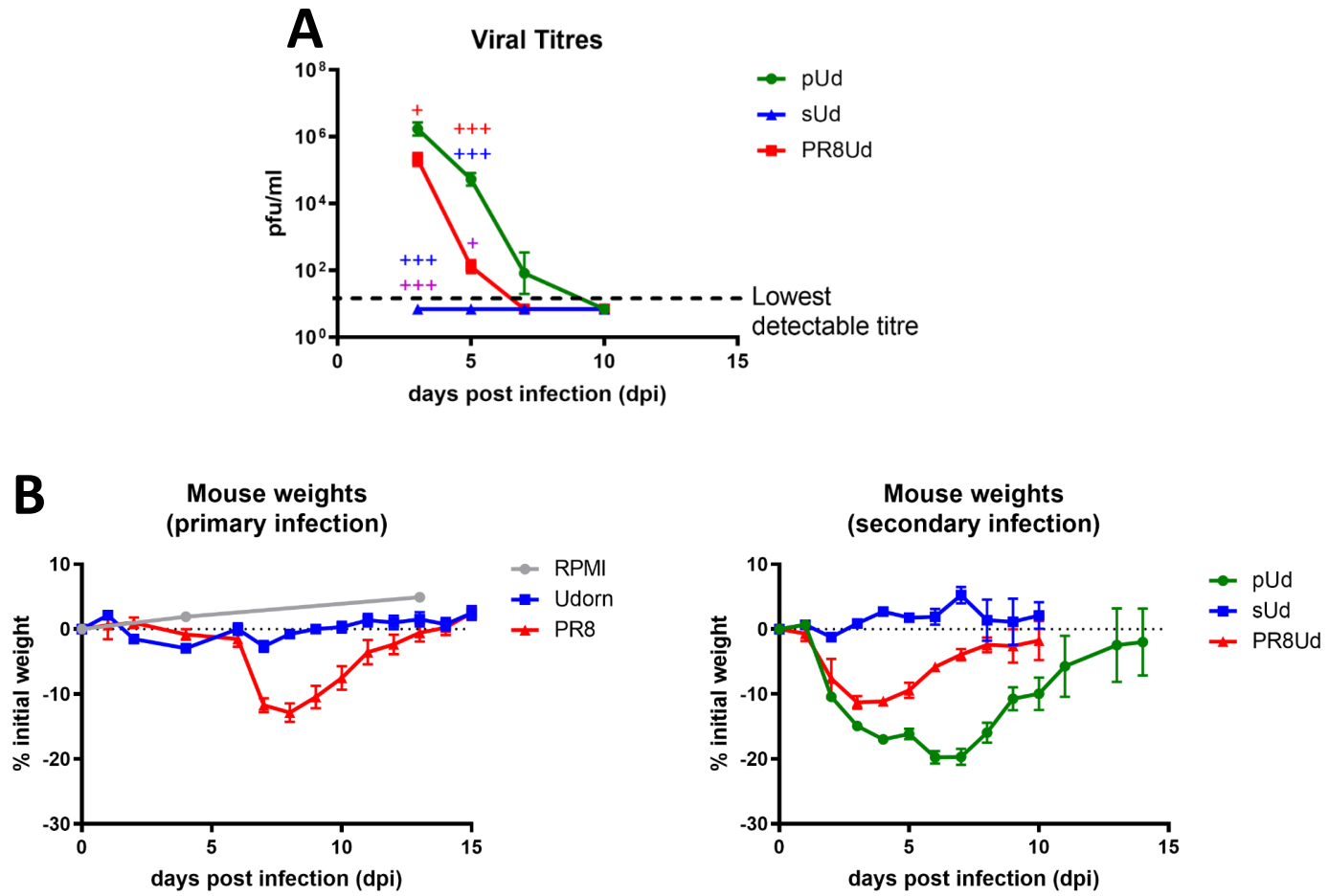

Figure 3.13. Viral replication and weight loss during H3N2 Ud72 infection in mice with prior exposure to H1N1 PR8 infection.

C57BL/6 mice (n=4) were infected and processed according to the schedule shown in Fig. 3.8. Figure shows A) Infectious viral titres were determined by plaque assay of homogenized lungs and B) body weight of mice infected with primary (low dose) and secondary (high dose) influenza viruses. Symbols above timepoints indicative of statistical significance by two-way ANOVA (+ symbols). Number of symbols indicative of level of significance: * $p<0.05$, ** $p<0.01$, *** $p<0.001$, **** $p<0.0001$. Colours represent the comparisons made – colours conforming to the key represent pUd compared to the group with the same colour in the key and purple represents comparisons between sUd and PR8Ud.

Sera raised against PR8 is unable to neutralize Ud72 virus.

To confirm that the enhanced viral clearing responses we observed with prior exposure of Ud72-infected mice to PR8 virus is unlikely to be due to classical neutralizing antibodies, BL6 mice were infected with 30 pfu of PR8 or $10^{4.5}$ pfu Ud72 and blood was obtained 7 weeks post infection by heart puncture for processing and extraction of sera. Sera was then assessed for inhibition of H3N2 Ud72 and H1N1 PR8 viruses by hemagglutination inhibition (HI) assay, indicative of antibodies capable of blocking attachment to sialic acid receptors. As shown in Table 3.2, sera raised against H3N2 Ud72 was able to successfully inhibit Ud72 virus but not H1N1 PR8 virus, while likewise, sera raised against H1N1 PR8 was able to inhibit PR8 virus but not Ud72. Sera from mock RPMI infected mice were unable to inhibit Ud72 or PR8 virus as expected. In line with the current literature, sera raised against Ud72 or PR8 show minimal inhibition of viruses outside of the infected subtype likely due to the large differences in antigenic properties. Such results suggest that the earlier and higher magnitude responses seen in mice infected with Ud72 after prior PR8 infection are likely not influenced by pre-existing HI antibodies although the role of cross-reactive antibodies that function by other mechanisms (such as antibody-dependent cellular cytotoxicity) cannot be ruled out.

Table 3.2. Average & standard deviation of hemagglutination inhibition (HI) titres of mouse sera raised against H3N2 Ud72 and H1N1 PR8 viruses.

Virus	PR8	Ud72
Ud72/72	<10[a]	288 ± 72
H1N1 PR8	280 ± 80	<10
RPMI (control)	<10	<10

[a]Detection limit of the assay was 10 HI units.

Given that HA is known to be the immunodominant antigen against influenza for B cell responses, it was unexpected for B cell responses against H3N2 Ud to respond in a secondary-like manner in mice with prior exposure to the H1N1 virus PR8 in the experiment described from figures 3.8-13. While flow cytometry data informs of populations of differing subsets, it should

be noted that a prominent proportion do not appear to be virus-specific (as seen from results from Figures 3.6), which suggests that the secondary-like response may be in part a result of the stimulatory environment due to infection. Furthermore, data from Figure 3.6 also suggested that the HA-specific response against influenza then only makes up less than 30% of the virus-specific B cell response. Hence it may be possible that a large proportion of these boosted secondary-like responses seen in Ud-infected mice with prior infection of PR8 may be the result of recognition of other antigenic sites of the influenza virus by B cells or T cells such as internal proteins or more conserved sites of the NA surface glycoprotein. While HA-specific responses are known to be most prevalent in mammalian responses and most efficiently prevent infection (82), results from this chapter appear to suggest that the specificity of the B cell responses against influenza may be much broader than first thought which, in turn, appears to have a profound effect on the ability of the adaptive immunity to respond to the same virus with differing surface antigens.

CHAPTER 4 – THE EFFECT OF ANTIGENIC DISTANCE ON B CELL RESPONSES DURING SECONDARY INFLUENZA INFECTION

INTRODUCTION

While characterizing the primary, secondary and heterologous responses against influenza aids in the understanding of how B cell immunity is developed against the virus, most immunocompetent adult humans have pre-existing immunity to some strain of influenza A as a result of previous infection or vaccination during their lifetime (109). While some component of a secondary response would be expected in these individuals, the effect of ongoing antigenic drift complicates the expected response against infection with newer strains.

As previously discussed, various models to explain the effect of antigenic drift on B cell responses against influenza have been proposed. These models, which include original antigenic sin and antigenic seniority, are often based on observations of human antibody responses against influenza. Over the course of decades of research, it has become clear that the short-term and long-term responses against influenza strains as well as the immune responses against vaccination versus infection play important roles in how the B cell and antibody responses develop.

The humoral response against influenza has been plotted in various studies (34, 142) as an "antibody landscape" representing antibody reactivity of a current antiserum against a spectrum of prior drifting strains that is shaped according to whether an individual is exposed to various strains over their lifetime. In the short-term, Fonville *et al*'s study showed that individuals raise the highest antibody titres against the current infecting strain compared to other drifted strains of the same subtype in the case of infection, but that serum inhibition of prior strains is also boosted, termed 'back-boosting'. In the long term, these titres decline over the years leading to the observation of 'antigenic seniority', whereby sera from individuals show the highest titres against strains exposed during childhood followed by the next chronological strain and so on as a hierarchy (117). Ongoing exposure to various influenza strains undergoing antigenic drift has

been clearly shown to have a profound effect on the antibody landscape of hosts, reflecting the underlying B cells that produce these responses.

To further study the effect of antigenic similarities on the antibody response against influenza, O'Donnell *et al.* (129) infected ferrets with strains of H1N1 from different decades before challenging with the more recent but immunologically distinct 2009 pandemic H1N1. This experiment examined the effects of varying degrees of antigenic distance between the first infecting virus and the challenge strain, the HA of which had previously been shown to be similar in its antigenic sites to the pandemic 1918 strain (143). It was found that with the exception of an antigenically similar swine-origin virus, ferrets showed less protection against the 2009 pandemic strain the closer the H1N1 priming virus was to 2009 chronologically. This was similarly reflected in the antibody reactivity of the ferret's serum against each strain, where only sera from ferrets primed with early H1N1 viruses showed some level of neutralization of the 2009 pandemic strain. Hence later strains that had undergone antigenic drift over the last 90 or so years became more antigenically distant from the emerging pandemic virus. This correlated with observations during the 2009 pandemic, where infections and hospitalizations occurred in children and young adults but were less than expected in older adults, likely due to the higher proportions of cross-reactive antibodies against the pandemic strain found in this group (144). Overall, results showed that as antigenic distance between the prior and infecting strains increased, the weaker the ability of sera to inhibit the infecting strain.

While the focus has largely been directed towards antibody responses against drifting strains, the overall dynamics of the strain-specific B cell response in the context of antigenic drift still remains unclear, particularly in the light of the large degree of activation of B cells observed in the last chapter in response to heterosubtypic infection. In this chapter, the overall and strain-specific B cell response against an H3N2 influenza strain were investigated in the context of prior exposure to previously isolated H3N2 strains as a method to examine the effect of antigenic drift. Cross-reactivity of sera from C57BL/6 mice infected with different H3N2 strains was also assessed.

RESULTS

Serum antibodies show cross-reactivity between H3N2 strains up to 3 years apart in C57BL/6 mice.

To commence investigation of the B cell response against antigenically drifted strains of viruses in the context of exposure to prior strains in the murine model, a selection of available human H3N2 viruses were chosen based on antigenic distance as determined from ferret data (Figure 1.2) as well as their ability to infect mice, as later human H3N2 strains are unable to efficiently establish infection in mice due to loss of appropriate receptor specificity.

Although the antigenic properties of ferret antisera would be anticipated to be similar in our B6 mouse model, it was pertinent to characterize the antigenic properties of murine antisera against the chosen strains of influenza using a hemagglutinin inhibition assay. Mice were infected with $10^{4.5}$ pfu of either A/Udorn/307/1972 (Ud72), A/Victoria/3/1975 (Vic75), A/Bangkok/1/1979 (BK79), A/Philippines/2/1982 (Ph82) (all H3N2) or 30 pfu of A/Puerto Rico/8/1934 (H1N1) and serum was harvested at 7 weeks post infection to measure antibody levels at the time of reinfection to be used in the subsequent study. Samples were tested against these same strains in a hemagglutination inhibition assay.

The inhibitory profiles of sera raised against each strain are shown in Table 4.1. As expected, sera raised against the H1N1 virus PR8 was able to inhibit PR8 virus but unable to inhibit any H3N2 strains. The H3N2 viruses fell into two distinct antigenic clusters; antibodies to Vic75 reacted only to Vic75 and to the earlier isolate Ud72 but not with later strains, whereas antibodies to Ph82 reacted only to Ph82 and BK79 but not earlier strains. In addition, the data clearly show that antibody cross-reactivity to earlier strains is much stronger than to future strains. For example, despite only 3 years difference, sera raised against Ud72 was not able to inhibit Vic75 while the reverse was not true. Similarly, mice infected with BK79 virus showed titres near undetectable against Ph82 despite the strains falling within 3 years of each other.

It was hoped that these data would allow generation of an antigenic map similar to Fonville *et al*. (34). However, due to very limited cross-reactivity and small number of strains it was not possible to mathematically derive relationships between viruses and sera, meaning that

antigenic distances could not be mapped. Nonetheless, results aligned with the trends seen in other ferret antisera studies with more comprehensive viral strain panels (129).

Table 4.1. HI titres of mouse sera raised against H3N2 viruses and H1N1 PR8 virus[a].

			H1N1	H3N2			
		Virus	**PR8**	**Ud72**	**Vic75**	**BK79**	**Ph82**
Sera raised against	**RPMI**	**-**	<10[b]	<10	<10	<10	<10
	H3N2	**Ud72**	<10	88 ± 44	<10	<10	<10
		Vic75	<10	57 ± 34	64 ± 22	<10	<10
		BK79	<10	<10	<10	80 ± 0	19 ± 13
		Ph82	<10	<10	<10	9[c] ± 7	80 ± 49
	H1N1	**PR8**	145 ± 117	<10	<10	<10	<10

[a] HI titres were calculated as the average HI titre and standard deviations raised against specific strains from 5 mice per group (n=5).

[b] Detection limit of the assay was 10 HI units.

[c] Samples with undetectable titres were denoted as 5 HI units for the purpose of this calculation.

Antigenically distinct H3N2 strains differ in their ability to infect mouse lungs.

As a part of the multiple infection schedule established in Chapter 3 (Figure 3.4A), mice would be infected with a low dose of virus followed by a higher dose 6-8 weeks later. To characterize the replicative capacity of the chosen H3N2 strains – Ud72, Vic75, BK79 and Ph82 – within the mouse model, B6 mice were infected with 100 pfu for Ud72 and 500 pfu for all other viruses. Lungs were extracted at one hour post infection as an indicator of infectious virus in the inoculum that can be recovered prior to replication, and then again at 1, 2, 3, 5 and 7 days post infection. Lungs were homogenized and viral titres quantified by plaque assay. The H3N2 strain A/Texas/77 was also tested at 500 pfu for possible inclusion in subsequent experiments as a

potential bridge between the Vic75 and BK79 “antigenic clusters” as discussed in Smith *et al*. (28) and displayed in Figure 1.2.

As shown in Figure 4.1, almost all H3N2 strains were able to replicate in mouse lungs. Earlier strains such as Ud72 and Vic75 appeared to replicate most efficiently, reaching a plateau of approximately 10^5 pfu at around 3-5 dpi before being cleared by 7 dpi. Although Ph82 virus peaked at around 10^4 pfu in the lungs by 2 dpi, the virus persisted at lower titres of 10^3 pfu from 3-5 dpi before resolving by 7 dpi, suggestive of a milder infection. In comparison, BK79, despite its antigenic similarities to Ph82, did not establish a consistent infection in the mouse lungs over time, and TX77 replicated in only a proportion of the mice infected with virus.

Overall, the results indicate that earlier H3N2 strains such as Ud72 and Vic75 can replicate in B6 mouse lungs to high titres while the more recent strains including TX77 and BK79 have difficulty establishing a productive infection as corroborated by a study by Reading *et al.* (145). This is due in part to their susceptibility to the innate inhibitor SP-D which can bind to the highly glycosylated head domain of the HA of these strains (145-147). Although the aforementioned study found that Ph82 is similarly unable to replicate efficiently in mice, our lab stock of Ph82 was selected for resistance to these mouse innate inhibitors. Given the inability for TX77 virus to adequately and consistently infect mice at 500 pfu, this strain was not used in further experiments. While BK79 showed comparatively limited replication in the lungs at lower doses, the strain was included due to its antigenic similarity to Ph82.

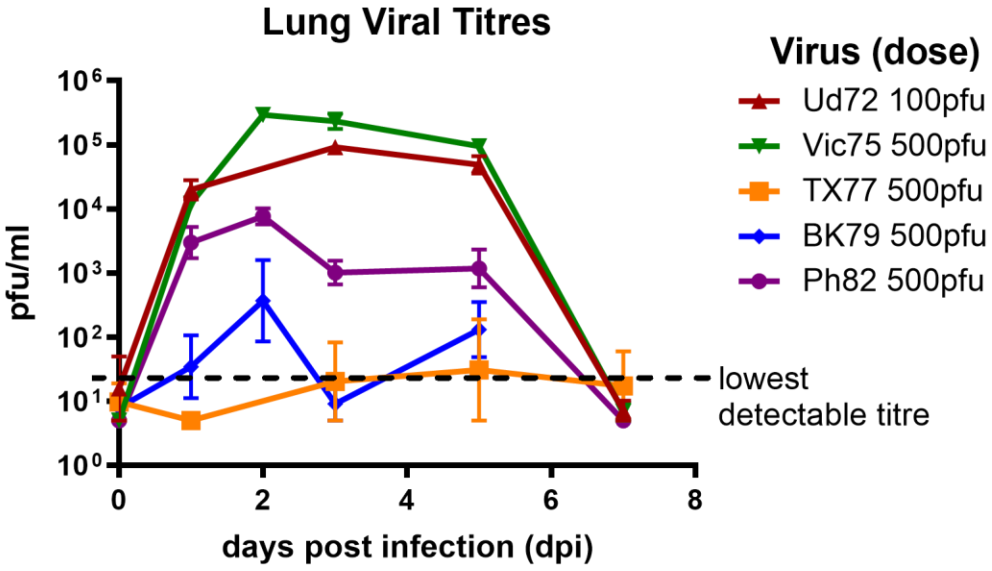

Figure 4.1. Viral replication kinetics of H3N2 viruses during primary, low-dose infection in B6 mice.

Six to eight week old C57BL/6 mice (n= 5) were infected with 500 pfu Vic75, TX77, BK79, Ph82 or 100pfu Ud72 virus by total respiratory tract (TRT) infection. At 1 hour post infection and 1, 2, 3, 5 and 7 dpi, lungs were collected and homogenized for quantification of viral titre by plaque assay. Dotted line shows the lowest detectable titre for this assay.

Primary B cell responses against different strains of H3N2 influenza virus infection appear to be similar in magnitude and kinetics.

Considering the differences in replication of the H3N2 viruses in our panel it was necessary to establish the impact of this on the primary B cell response kinetics and magnitude for each virus strain. B6 mice were infected with $10^{4.5}$ pfu of either Ud72, Vic75, BK79 or Ph82 virus and spleen, MLN and lungs were harvested on days 3, 5 and 7 pi. MLN and spleen cells were stained and analysed by flow cytometry to enumerate B cells and replication of each virus was determined by plaque assay of lung homogenates. Lung viral titres determined by plaque assay (Figure 4.2) confirmed the earlier viral replication hierarchy. At an dose of $10^{4.5}$ pfu, BK79 showed lower initial titres compared to Ud72 and Vic75 at 3 dpi ($p<0.05$ by two-way ANOVA). However, all strains replicated to moderate or high titres by 5 dpi and were not significantly

different to the well-established model H3N2 virus Ud72. As expected, all viruses were declining in titre by 7 dpi.

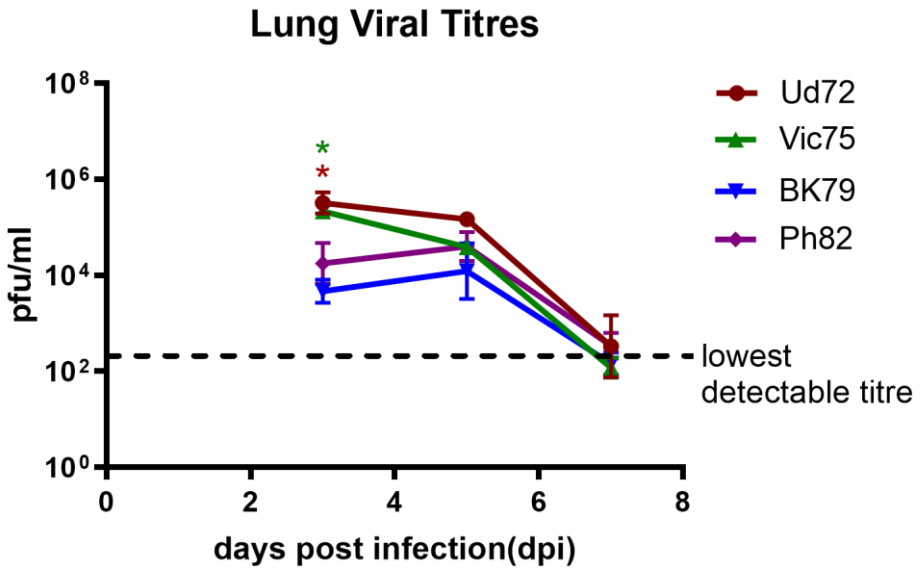

Figure 4.2. Kinetics of viral replication during primary H3N2 IAV infection.

C57BL/6 mice (n=3-4) were infected with $10^{4.5}$pfu of Ud72, PC73, Vic75, BK79, Ph82 or mock RPMI. On days 3, 5, and 7 post infection (dpi), lung, spleen and MLN were collected and processed. Lung viral titres were determined by plaque assay on MDCK cells. Symbols represent *$p<0.05$ for comparisons between BK79 versus the group corresponding to the colour of the symbol by two-way ANOVA with Tukey's multiple comparisons.

Flow cytometry analysis (gated as shown in Figure 4.3) revealed that total cellular and B cell responses in MLN and spleen were not significantly different between the different virus strains (Figure 4.4). The only exception was a small but statistical difference in MLN B cell responses between BK79 and Ud72 at 7 dpi ($p<0.05$), but given the magnitude of this difference (less than half a log), it may not be biologically relevant. Overall, total cellular and overall B cell responses appeared to be maintained at relatively uniform levels throughout the course of infection in both the MLN and spleen. This appeared to be the case for splenic responses even within subsets such as plasmablasts and GC B cells (Figures 4.5 and 4.6), likely a reflection of the spleen's location distal from the site of infection compared to the MLN. In contrast, both

plasmablasts and GC B cell responses in the MLN appeared to rise several log-fold from 3 to 7 dpi, for all the virus strains. The kinetics of this rise was not significantly different between virus strains (two-way ANOVA) with the exception of BK79 versus Ud72 at 7 dpi in the GC B cell subset ($p<0.05$). Similarly, IgA/G$^+$ responses in plasmablasts and GC B cells of the MLN seemed to reflect the overall totals of each subtype in trend. Notably, MLN IgA/G$^+$ plasmablasts appeared to undergo a 10^{3-4}-fold increase in number depending on strain over the course of 3 to 7 dpi while IgA/G$^+$ GC B cells increased from 10^{2-3}-fold, likely a reflection of the developing class-switched response over the course of infection.

An additional time point at 10 dpi may further distinguish the viral kinetics of each virus, but data showed that all selected H3N2 viruses were capable of replicating in C57BL/6 mice and displayed similar B cell response kinetics during primary infection. This suggested that these viruses would provide an adequate immune response for future experiments involving primary and secondary challenge.

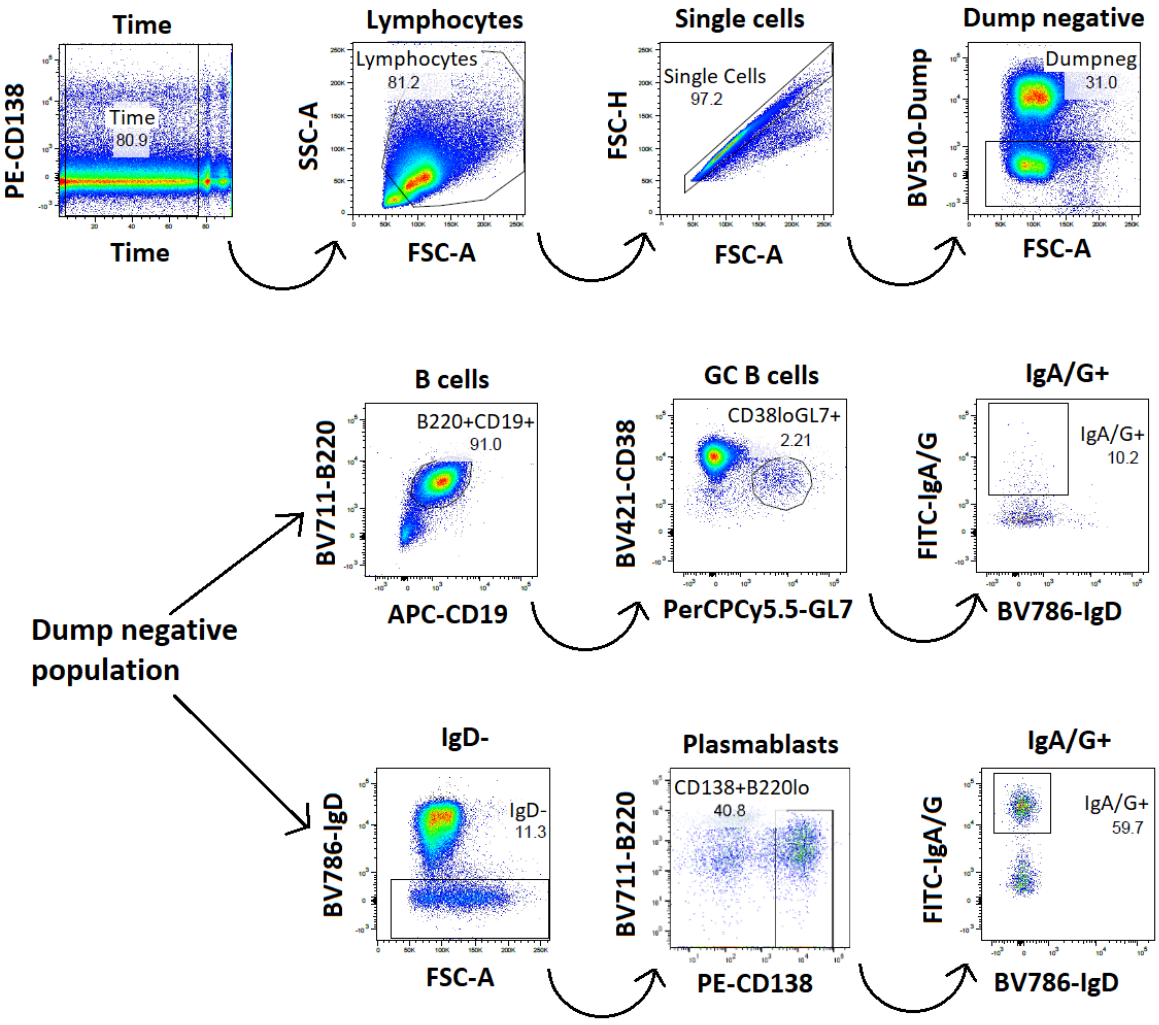

Figure 4.3. Gating scheme for B cell subsets during primary H3N2 IAV infection using flow cytometry.

C57BL/6 mice (n=3-4) were infected as described in Figure 4.2. On days 3, 5, and 7 post infection (dpi), spleen and MLN were collected and processed for flow cytometry. The gating scheme used to delineate cellular events is shown.

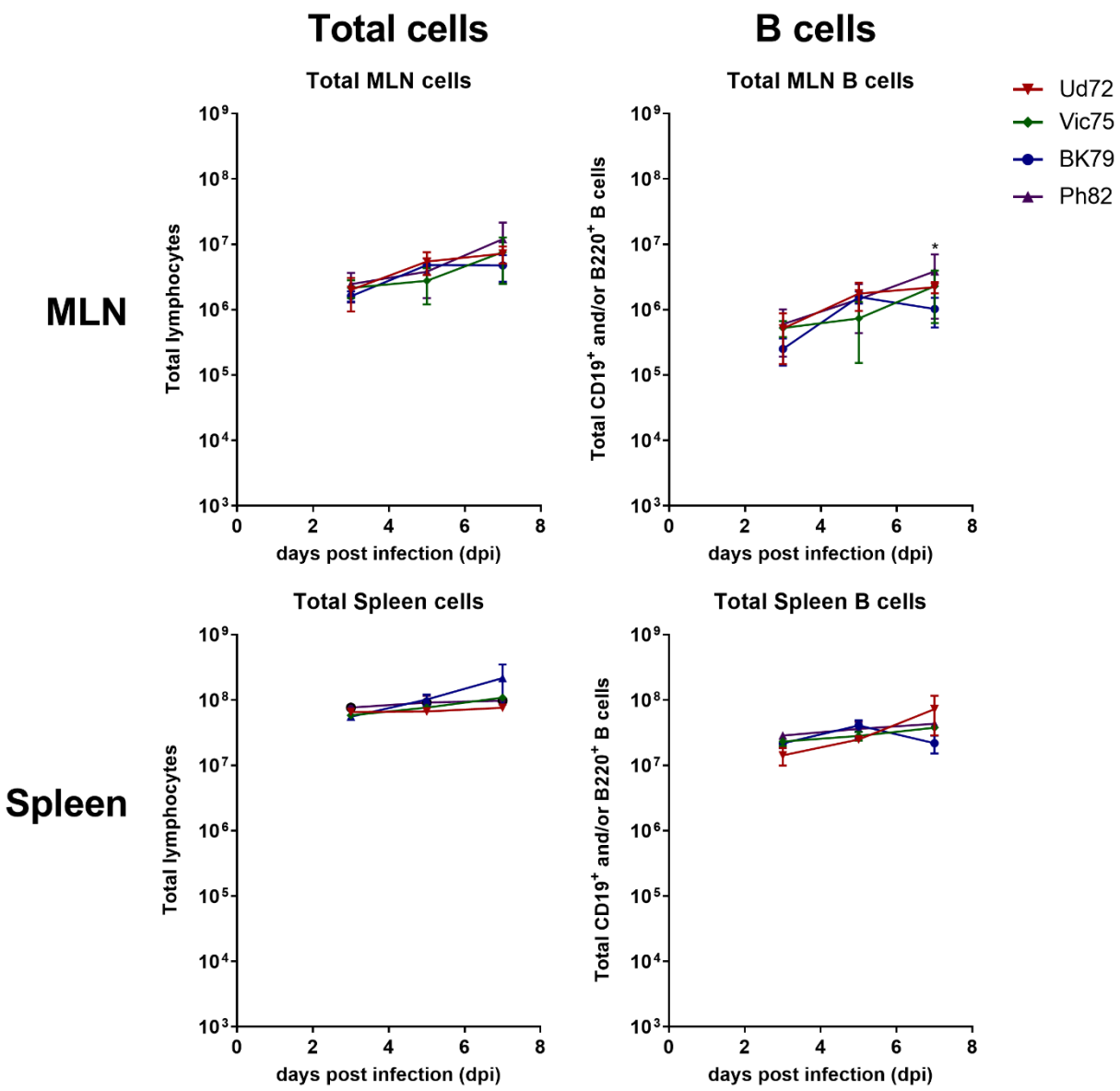

Figure 4.4. Kinetics of total lymphocytes and B cells during primary H3N2 IAV infection.

C57BL/6 mice (n=3-4) were infected as described in Figure 4.2 and processed in Figure 4.3. Total numbers of cells and overall $CD19^{+}B220^{+}$ B cells are shown. Symbol represents *$p<0.05$ between BK79 and Ud72 by two-way ANOVA with Tukey's multiple comparisons.

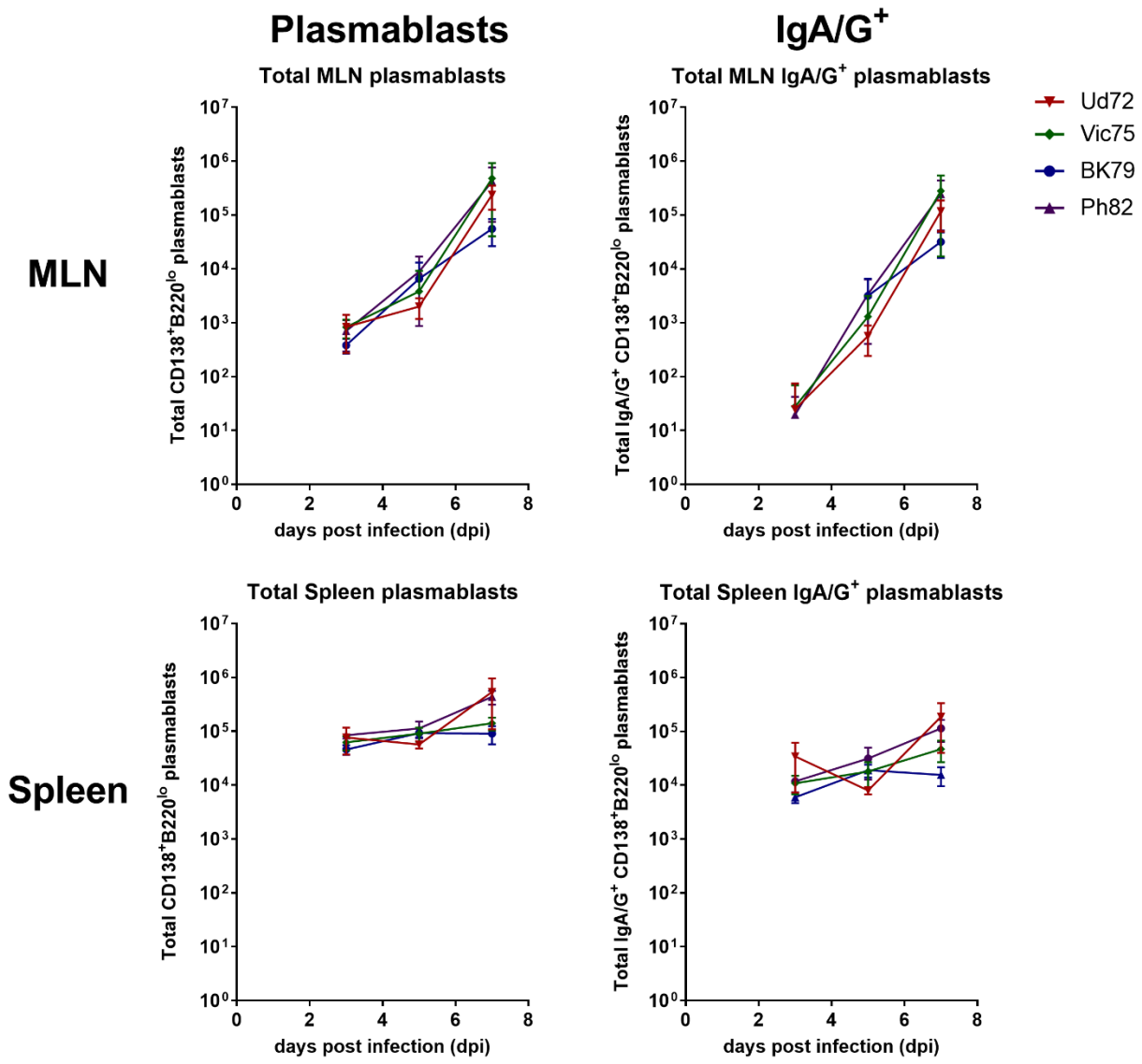

Figure 4.5. Kinetics of total overall and IgA/G+ plasmablasts during primary H3N2 IAV infection.

C57BL/6 mice (n=3-4) were infected as described in Figure 4.2 and processed in Figure 4.3. Total numbers of overall and IgA/G$^+$ CD138$^+$B220^{lo} B cells are shown.

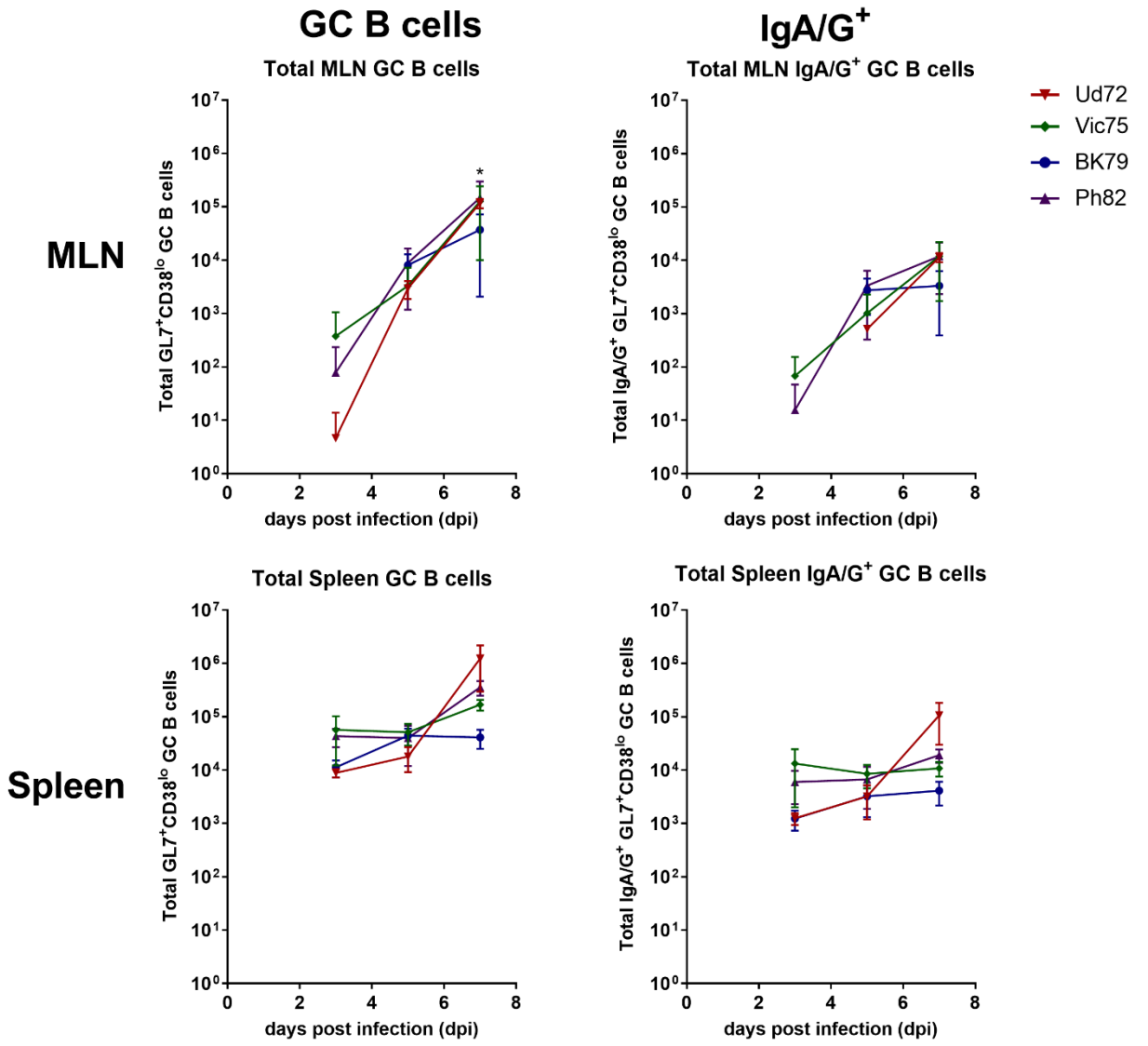

Figure 4.6. Kinetics of viral replication and B cell subsets during primary H3N2 IAV infection.

C57BL/6 mice (n=3-4) were infected as described in Figure 4.2 and processed in Figure 4.3. Total numbers of overall and IgA/G$^+$ GL7$^+$CD38^{lo} B cells are shown. Symbol represents *$p<0.05$ between Ud72 versus BK79 by two-way ANOVA with Tukey's multiple comparisons.

Establishment of a protocol for the investigation of B cell responses in the context of antigenic drift.

Upon characterization of infection of the chosen H3N2 viral strains in B6 mice, a model was established to investigate the kinetics of the B cell response to drifted H3N2 strains in the context of pre-existing memory against prior strains. Based upon the model previously used to examine B cell responses in the context of antigenic shift, the experimental design is shown in Figure 4.7.

Figure 4.7 describes three separate experiments that compare primary and secondary responses against Ph82 virus infection to prior infection with different drift variants (one per experiment). Homologous secondary infection groups designated as 'sPhil' were infected with 500 pfu of Ph82, while primary groups, 'pPhil', received an initial mock infection of RPMI, before both groups were infected with 10^5 pfu of Ph82 6-8 weeks later. Experimental groups were infected with 500 pfu of an earlier strain of either Ud72, Vic75 or BK79 before infection with 10^5 pfu Ph82 6-8 weeks later, designated 'UdPhil', 'VicPhil' and 'BKPhil' accordingly. A group of RPMI mock infection at both timepoints was also included as a negative control.

Experimental groups represent differing scenarios of host infection by drifted strains of H3N2 with increasing antigenic difference from Ph82. The BKPhil group represents minimal drift at 3 years apart, VicPhil represents 7 years of drift while UdPhil represents a total of 10 years of antigenic drift between first and second infecting strains. Each experimental group was examined with the same protocol in separate studies before results were collated for collective analyses.

Upon days 3, 5, 7 and 10 post infection, mice were sacrificed and spleen and MLN harvested for processing and analysis of B cell responses by flow cytometry and anti-Ph82 specific ASC responses by ELISPOT. Lungs were also harvested and homogenized samples used to determine lung viral titres during infection by plaque assay on MDCK cells.

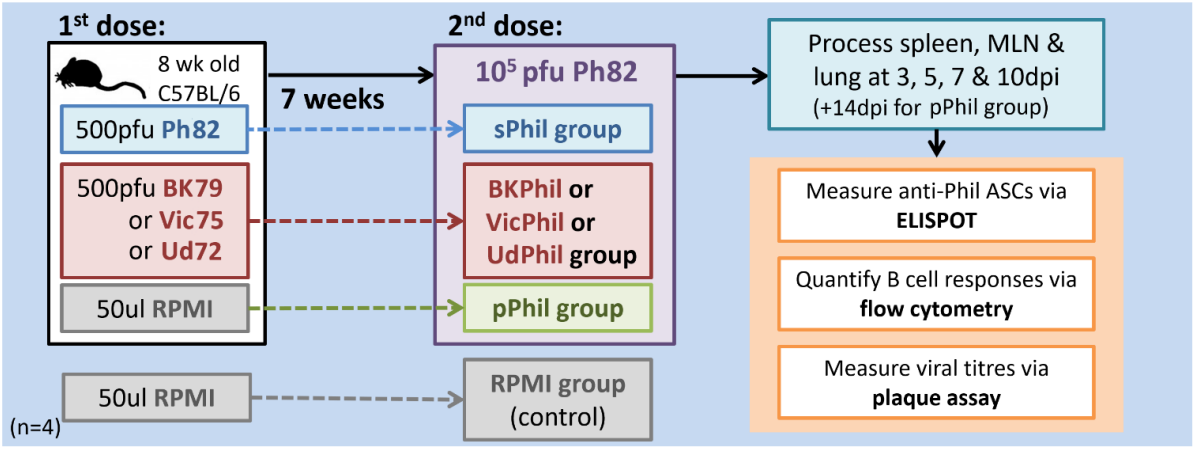

Figure 4.7. Experimental plan to investigate the kinetics of the B cell response against Ph82 infection in the presence of prior exposure to Ph82, BK79, Vic75, Ud72 or mock infection.

Eight to ten week-old C57BL/6 mice (n= 4) were infected with Ph82, mock RPMI or in three separate experiments either 100 pfu Ud72, 500 pfu BK79 or Vic75. Mice were then infected with 10^5 pfu of Ph82 virus 6-8 weeks post infection in groups as shown. On days 3, 5, 7 and 10 post infection (dpi), spleen, MLN, and lungs were collected and processed for ELISPOT, flow cytometry and plaque assay respectively.

The secondary-like pattern of recall B cell responses after sequential infection with antigenically distant strains is confirmed by analysis of the total responding B cell populations.

To dissect the B cell response into its effector subsets in the scenario of antigenic drift, the samples from the experiments above were processed and analysed by flow cytometry as indicated in Figure 4.7. Individual experiments using the same protocol were then collated for analysis as shown in Figure 4.8-10. Total numbers of mice in each group are indicated. Differences in the number of experimental repeats for the respective groups account for the different group sizes and the fact that pPhil and sPhil are included in every experiment.

The magnitude and kinetics of both the primary (pPhil) and secondary (sPhil) responses were used to assess whether experimental group kinetics were more ‘primary-like’or ‘secondary-like’, guided by statistical analysis. The spleen from RPMI-treated animals was used to

determine the baseline (steady-state) response. As indicated previously, MLN are not visible for detection without infectious stimuli so no RPMI control was available for MLN responses, although the assumption is that the number of B cells would be very low prior to visible expansion of these tissues.

As shown in Figure 4.8, total numbers of MLN and splenic lymphocytes were quite similar in magnitude between groups throughout the course of infection with only some minor differences detected. The same findings were reflected in the B cell populations but differences were more marked in the MLN with pPhil and sPhil showing more prominent differences at days 3, 5 and 10 dpi ($p<0.01$). In comparison, primary and secondary plasmablast responses (Fig. 4.9) in the MLN showed consistent differences in trends throughout the course of infection (at least $p<0.05$ for all time points), with an earlier response in sPhil which appeared to peak around 5 dpi compared to a later peak response at 7 dpi in pPhil. Of the experimental groups, both VicPhil and UdPhil responses were significantly different to pPhil from 5-10 dpi ($p<0.05$), suggestive of a more secondary-like response. Although BKPhil appeared to be visually different from pPhil in kinetics, this was only significant at days 7-10 dpi ($p<0.01$). These trends appear to extend to the class-switched IgA/G$^+$ responses. While the pPhil response peaks at 7 dpi, the IgA/G$^+$ plasmablast responses of all other groups either approach or reach their peak earlier at 5 dpi, with sPhil, UdPhil and VicPhil all showing significantly higher numbers at this timepoint compared to pPhil (at least $p<0.05$). This suggests groups with any prior H3N2 strain exposure are either able to class-switch more rapidly or that pre-existing class-switched cells can be quickly recruited to respond to the infection. Differences between IgM$^+$ responses were less pronounced at early time points, but sPhil, UdPhil and VicPhil groups showed significant differences with pPhil at 7 dpi (at least $p<0.05$) and at 10 dpi. All groups showed a lower magnitude response compared to pPhil (at least $p<0.05$). This is in line with the idea of a more directed class-switched response against the pathogen near the site of infection.

Similar to splenic B cells, splenic plasmablast populations did not appear to vary significantly from the control RPMI response, with the exception of pPhil at 7 dpi ($p<0.0001$, pPhil vs. RPMI). The number of splenic plasmablasts in the pPhil group was also found to be significantly higher in number than sPhil and VicPhil at 10 dpi (at least $p<0.05$). Taken together with the difference observed in VicPhil compared to pPhil at 7dpi ($p<0.05$), this may provide

stronger evidence of a more secondary-like response for VicPhil than for other groups in this instance. However, the overall trends also suggest that all other responses are likely to be more secondary-like in nature given that the splenic plasmablast response was not statistically different to RPMI. Despite an elevated initial response at 3 dpi by BKPhil and a significantly elevated response at 7 dpi compared to pPhil, IgM^+ plasmablast responses in the spleen largely appeared to remain within baseline levels, showing no differences to RPMI. While there may be some elevation of responses at 7 dpi compared to RPMI and all other groups apart from BKPhil for IgA/G^+ plasmablast responses, the kinetics between primary and secondary responses up to that timepoint were too similar to draw any solid conclusions from this data. Statistically significant differences were also noted at 10 dpi with numbers of pPhil IgA/G^+ plasmablasts in the spleen significantly higher than those in sPhil, BKPhil, VicPhil and RPMI groups which may suggest more secondary-like responses in these experimental groups. As a whole, for both MLN and spleen, the IgA/G^+ plasmablast responses were lower on day 10 for the recalled responses compared to the primary response, possibly due to contraction after earlier infection resolution in these groups.

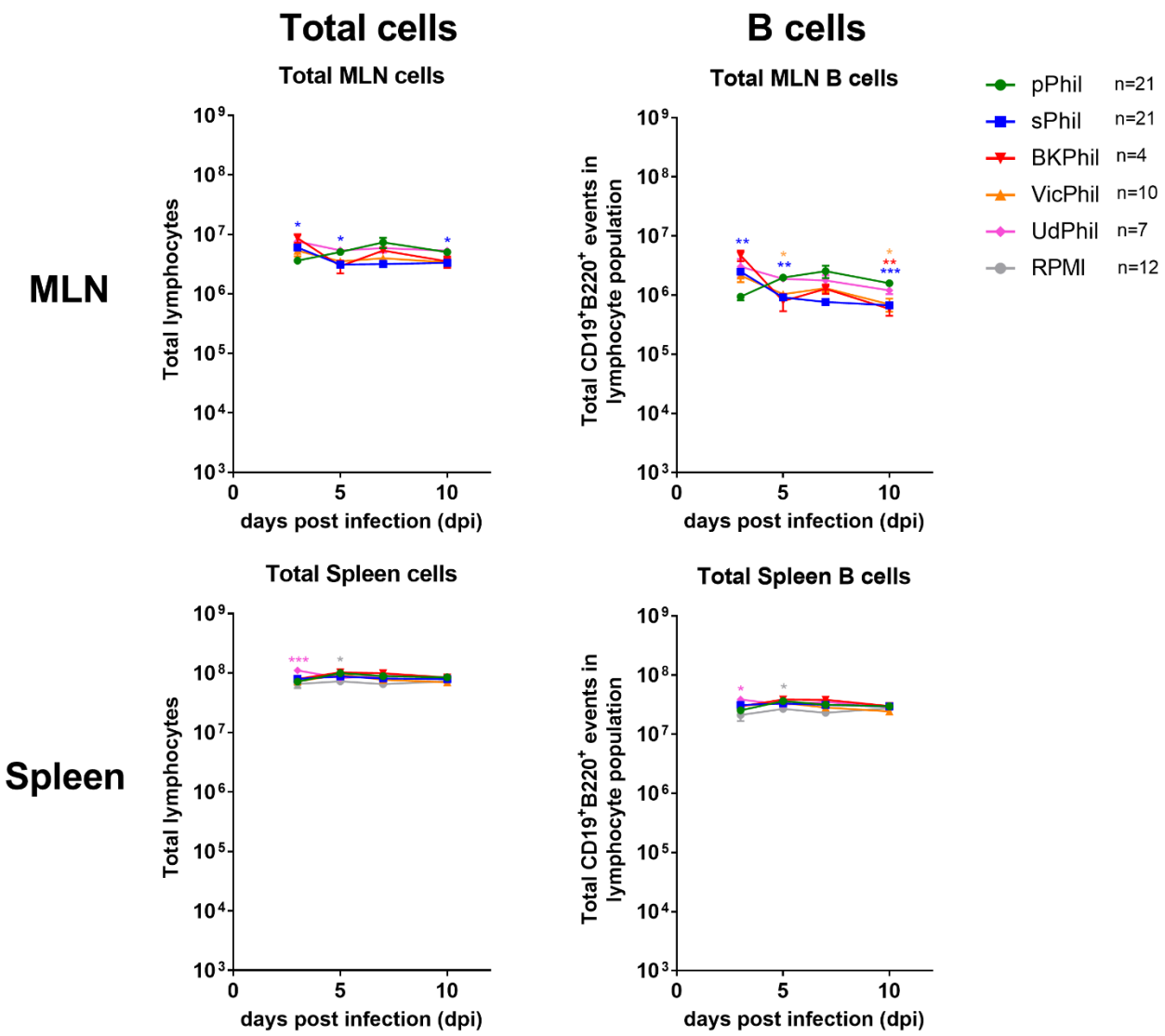

Figure 4.8. Kinetics of the total cellular and B cell response against Phil/82 infection in the presence of prior exposure to Ph82, BK79, Vic75, Ud72 or mock infection.

C57BL/6 mice (n=4) were infected as outlined in Figure 4.7. Total numbers of cells and overall $CD19^+$ $B220^+$ B cells in the MLN and spleen are shown. Symbols above timepoints indicative of statistical significance by two-way ANOVA – comparisons were made between pUd and the group of the same colour as the symbol as indicated by the key. Number of symbols indicative of level of significance: * $p<0.05$, ** $p<0.01$, *** $p<0.001$, **** $p<0.0001$.

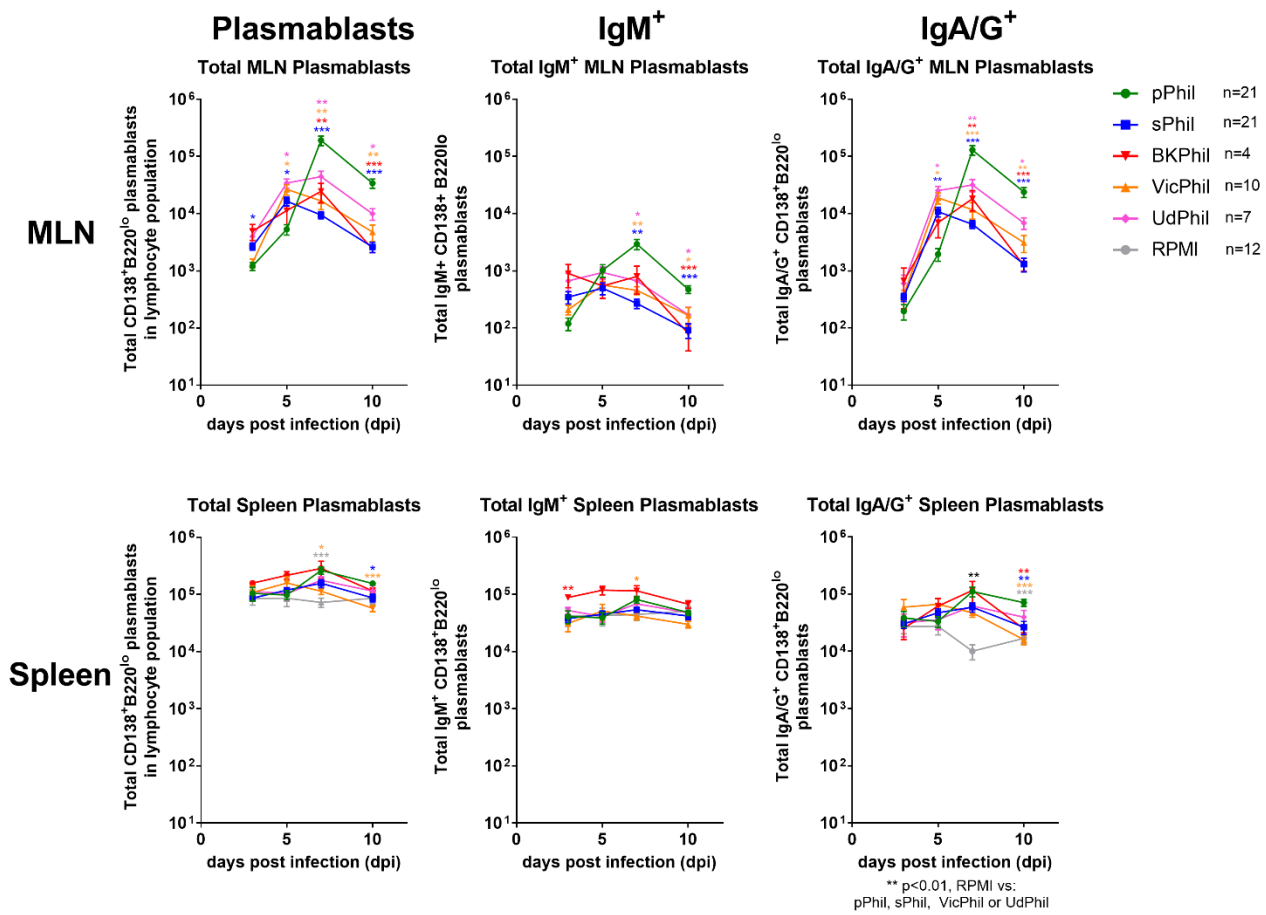

Figure 4.9. Kinetics of the plasmablast response against Ph82 infection in the presence of prior exposure to Ph82, BK79, Vic75, Ud72 or mock infection.

C57BL/6 mice (n=4) were infected as outlined in Figure 4.7. Total numbers of overall, IgM^+ and IgA/G^+ $CD19^+$ $B220^{lo}$ plasmablasts in the MLN and spleen are shown. Symbols above timepoints indicative of statistical significance by two-way ANOVA – comparisons were made between pUd and the group of the same colour as the symbol as indicated by the key. Comparisons in black are indicated by the notes below each graph. Number of symbols indicative of level of significance: * $p<0.05$, ** $p<0.01$, *** $p<0.001$, **** $p<0.0001$.

As seen in Figure 4.10, primary GC B cell responses in the MLN have a clearly distinguishable kinetic profile compared to other groups during the course of infection which increases over 100-fold from around 10^3 to 10^5 cells from 3 to 10 dpi. This was markedly different to sPhil at early time points with >1 log-fold higher response seen at 3 dpi for sPhil, a peak at 5 dpi followed by a slow decline from this point onwards ($p<0.001$, pPhil vs sPhil at 3, 5 and 10 dpi). These contrasting profiles enabled a clearer differentiation of responses in the experimental groups into primary- or secondary-like. VicPhil showed significantly different trends to pPhil by two-way ANOVA ($p<0.05$, pPhil vs. VicPhil at 3, 5 and 10 dpi) while almost overlapping sPhil in kinetics and magnitude, suggestive of a similar recall response. While BKPhil and UdPhil showed similar kinetics to sPhil, significant differences to pPhil were only noted at 10 dpi for these two groups ($p<0.01$ for pPhil vs. UdPhil and $p<0.001$ for pPhil vs. BKPhil) perhaps in part due to smaller sample sizes and larger variability for these groups. As previously seen, these trends seemed to be reflected in the IgA/G^+ GC B cell responses. In particular, UdPhil appears to show elevated levels of IgA/G^+ GC B cells at 5 dpi compared to pPhil ($p<0.05$) before descending to levels below pPhil by 10 dpi ($p<0.05$) which may be suggestive of a more secondary-like response in the group with high magnitudes early during infection before declining by 10 dpi. Overall, all groups apart from pPhil declined in response by 10 dpi while numbers of IgA/G^+ GC B cells in the MLN continued on an incline in pPhil.

Overall, splenic GC B cell responses across all groups were not significantly different to the RPMI control until 7 dpi, where responses in the pPhil group rose to plateau between 7 to 10 dpi. Paradoxically, mice infected with more distant strains prior to Phil such as UdPhil and VicPhil were found to be more secondary-like by their difference with pPhil on both 7 and 10 dpi ($p<0.001$) while BKPhil appeared to differ from primary responses only on 10 dpi ($p<0.01$). This, however, may be the effect of a smaller sample size and thus higher variability in response. Taken with the IgA/G^+ GC B cell response in the spleen that echoed these trends, results suggest that all groups with prior H3N2 exposure responded in a secondary-like manner in this subset.

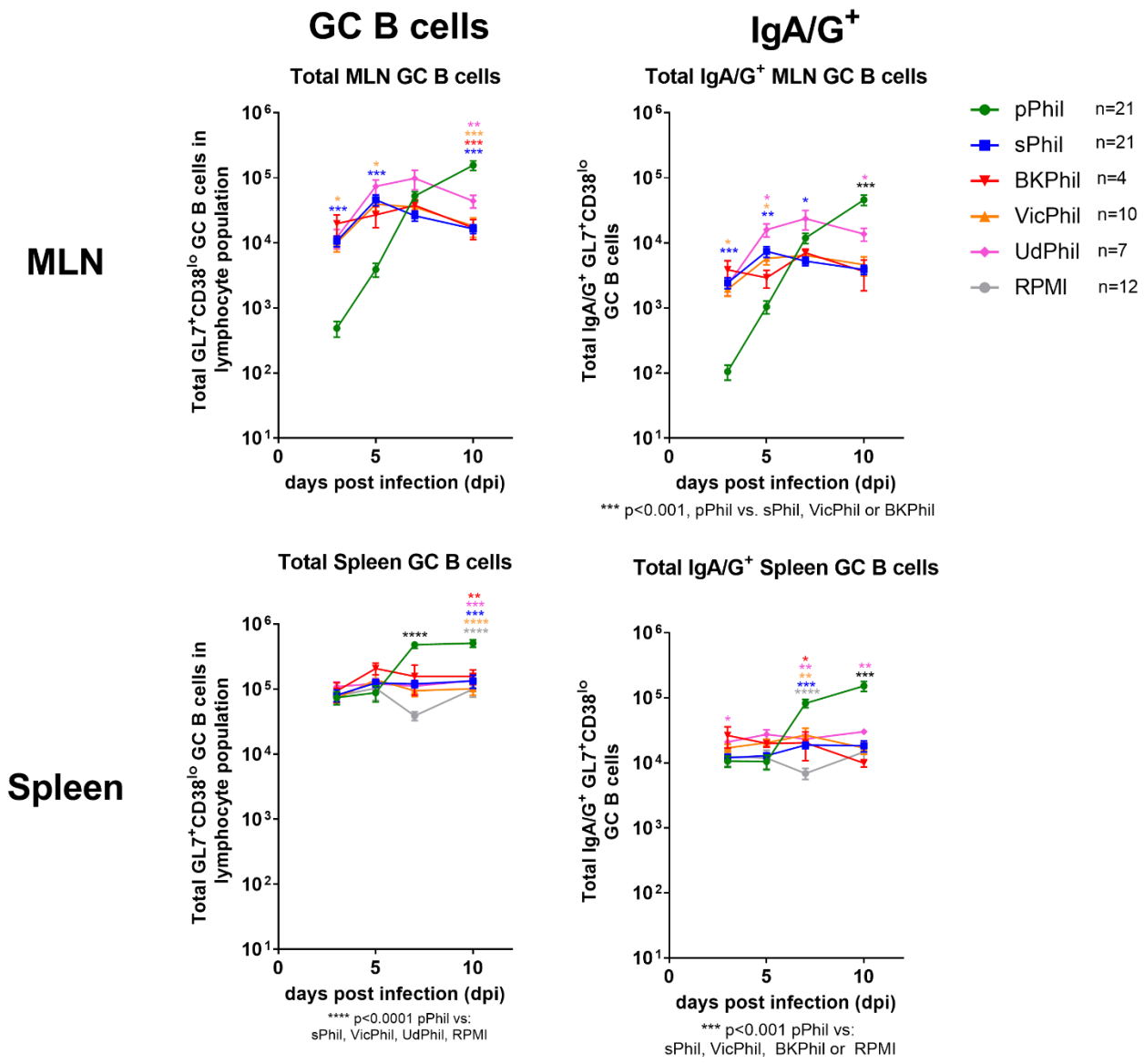

Figure 4.10. Kinetics of the GC B cell response against Ph82 infection in the presence of prior exposure to Ph82, BK79, Vic75, Ud72 or mock infection.

C57BL/6 mice (n=4) were infected as outlined in Figure 4.7. Total numbers of overall and IgA/G$^+$ GL7$^+$CD38^{lo} germinal centre (GC) B cells in the MLN and spleen are shown. Symbols above timepoints indicative of statistical significance by two-way ANOVA – comparisons were made between pUd and the group of the same colour as the symbol as indicated by the key. Comparisons in black are indicated by the notes below each graph. Number of symbols indicative of level of significance: * p<0.05, ** p<0.01, *** p<0.001, **** p<0.0001.

Prior infection with H3N2 strains induces an early secondary-like Ph82-specific antibody secreting cell response even when strains differ by 10 years of antigenic drift.

ELISPOT data from the experiments outlined in Figure 4.7 were collated into Figure 4.11 to investigate the correlations between prior infection of H3N2 strains of varying antigenic distance on the kinetics of Ph82-specific ASC responses upon Ph82 infection. As in the flow cytometry data, total numbers of mice in each group are indicated and differences in the number of experimental repeats account for the different group sizes.

Primary responses were similar to prior experiments with Ud72 and PR8 as expected (Figure 3.4), in that more prominent IgM^+ responses were observed in the spleen while IgA/G^+ ASC responses dominated in the MLN (note the difference in scale between IgM^+ and IgA/G^+). As for sUd in earlier experiments, the sPhil group showed fewer ASCs at the peak of the response in the MLN than was evident in pPhil, likely due to reduced antigen stimulus through neutralization of the inoculum, and for those MLN ASCs producing IgA/G antibodies, the response peaked at day 5 rather than day 7 for the primary response.

In the MLN, IgM^+ ASC responses of the sPhil and pPhil groups were significantly different from days 5 to 10 post infection ($p<0.001$ by two-way ANOVA), with a minimal response in sPhil mice while pPhil showed a distinguishable level of ASC responses over the course of infection. The responses of the BKPhil group, representing sequential infection by two closely related viruses, also showed a pattern of minimal response like sPhil ($p<0.001$ at 5 and 7 dpi). The response of the VicPhil group was found to be similar to BKPhil, with significant differences to pPhil on days 5 ($p<0.01$), 7 ($p<0.05$) and 10 ($p<0.01$) post infection and no signficant differences to sPhil for all time points. Although the UdPhil group had less power to distinguish differences due to less replicates, it could be seen that responses reached a similar magnitude to pPhil at 5 dpi, but declined to minimal levels by 10 dpi, distinguishing the response from pPhil ($p<0.01$). In terms of the class-switched IgA/G^+ responses in the MLN, BKPhil and VicPhil showed a significantly greater response at the day 5 time point than did pPhil ($p<0.01$ for BKPhil, $p<0.05$ for VicPhil), which was the same trend observed for sPhil and UdPhil. However, unlike sPhil, the UdPhil group continued to increase, trending towards a peak at day 7

as observed for pPhil. Taking both non-class switched and class switched responses together, the data suggest that the pattern of responses of BKPhil and VicPhil more closely resembled that of sPhil, while those of UdPhil displayed characteristics of both pPhil and sPhil, with secondary-like early IgA/G$^+$ ASC responses but a delayed peak. This may suggest that perhaps the larger antigenic difference between Udorn and Phil viruses may mean less of the antibody produced is neutralising so antigen stimulus is greater and B cells continue to respond. However, a greater number of mice in the UdPhil group is necessary to confirm these findings. Overall, the results are suggestive of a bolstered class-switched ASC response in mice with prior exposure to H3N2 strains differing across 10 years of drift as a result of some form of immune memory.

In the spleen, IgM$^+$ responses appeared to be minimal across all groups with the exception of pPhil. No groups were significantly different to the baseline RPMI control apart from pPhil at 7 dpi ($p<0.0001$) and 10 dpi ($p<0.01$). Splenic IgA/G$^+$ ASC responses likewise supported a secondary-like response in all experimental groups, with significantly higher responses than pPhil on day 3 and 5 observed with sPhil ($p<0.0001$ both days) and BKPhil ($p<0.05$ at 3 dpi, $p<0.0001$ at 5 dpi) and the same trend for VicPhil and UdPhil. The UdPhil response appeared to be the largest, as in the MLN, however again this observation did not reach significance due to a smaller sample size.

Overall, these data indicate that prior infection with H3N2 strains followed by infection with a more recent strain, separated by up to 10 years of antigenic drift, induce secondary-like virus-specific ASC responses in the mouse, with earlier class switching in both the MLN and spleen and minimal IgM$^+$ responses in the spleen. From the data shown, antigenic distance appears to only impact the kinetics and magnitude of ASC responses in the MLN with UdPhil potentially having somewhat different response profile than pairs with less antigenic distance.

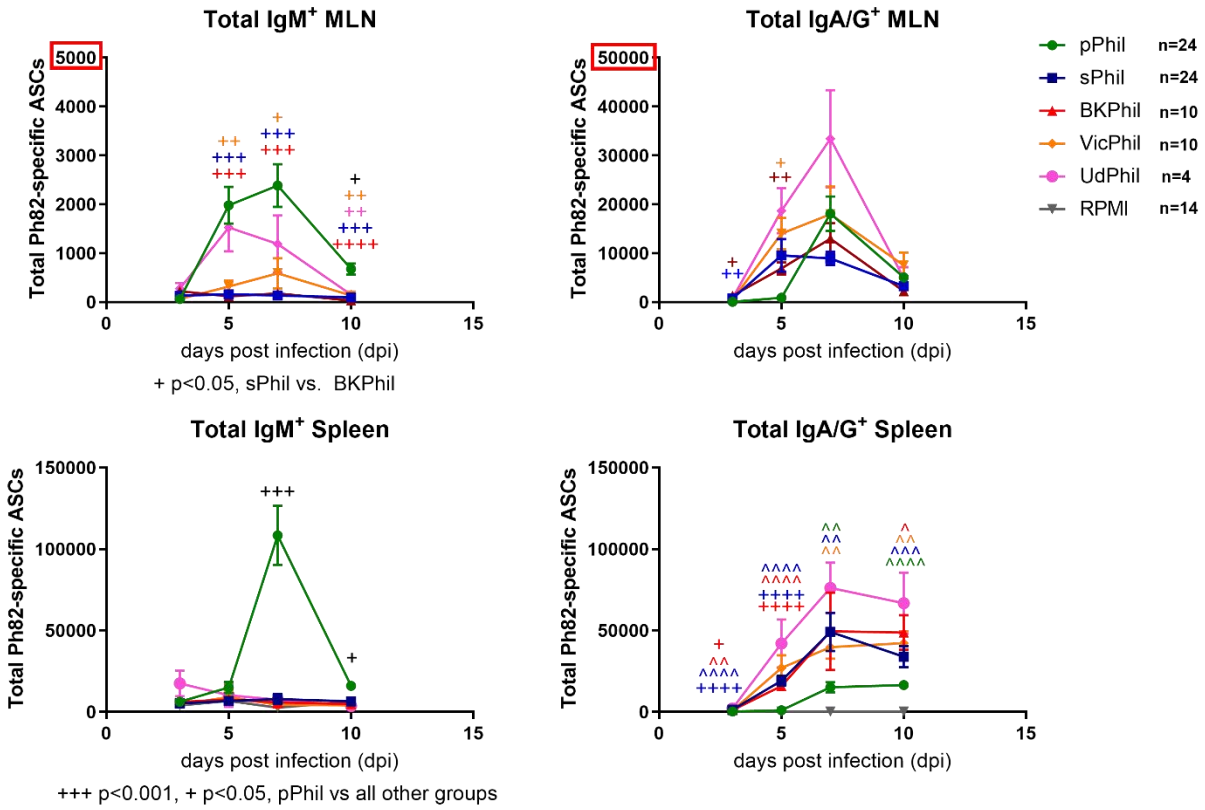

Figure 4.11. Kinetics of the MLN and Spleen Phil-specific ASC response against Ph82 infection in the presence of prior exposure to selected H3N2 strains or mock infection.

C57BL/6 mice (n=4) were infected with H3N2 viruses as per Figure 4.7. Spleen and MLN were collected on days 3, 5, 7 and 10 post infection and processed into single cell suspensions to be overlaid onto purified Ph82 virus coated plates to detect Ph82-specific antibody secreting cells by ELISPOT. Groups with different infection models with the number of IgM^+ and IgA/G^+ ASCs per million cells in the MLN and spleen for each experiment are shown. Symbols above timepoints indicative of statistical significance by two-way ANOVA. Colors represent comparisons between the group of the same colour in the key versus pPhil (+ symbols) or versus RPMI (^ symbols). Number of symbols indicative of level of significance: + $p<0.05$, ++ $p<0.01$, +++ $p<0.001$, ++++ $p<0.0001$.

In accord with a secondary-like response in the experimental groups, lung viral titres of sPhil, VicPhil and BKPhil (Figure 4.12) dropped to below the limit of detection by day 3 and were thus significantly lower in comparison to pPhil even at early timepoints ($p<0.05$, two-way ANOVA, Tukey post-hoc), suggesting early clearance before the infection took hold. Lung viral titres of UdPhil were not measured at 1 dpi but at 3-10 dpi, titres remained below the detection limit, also indicative of enhanced viral clearance. Overall, titres appeared to align with the observations from ELISPOT and flow cytometry data, suggesting that these secondary-like responses resulted in faster clearance of infection.

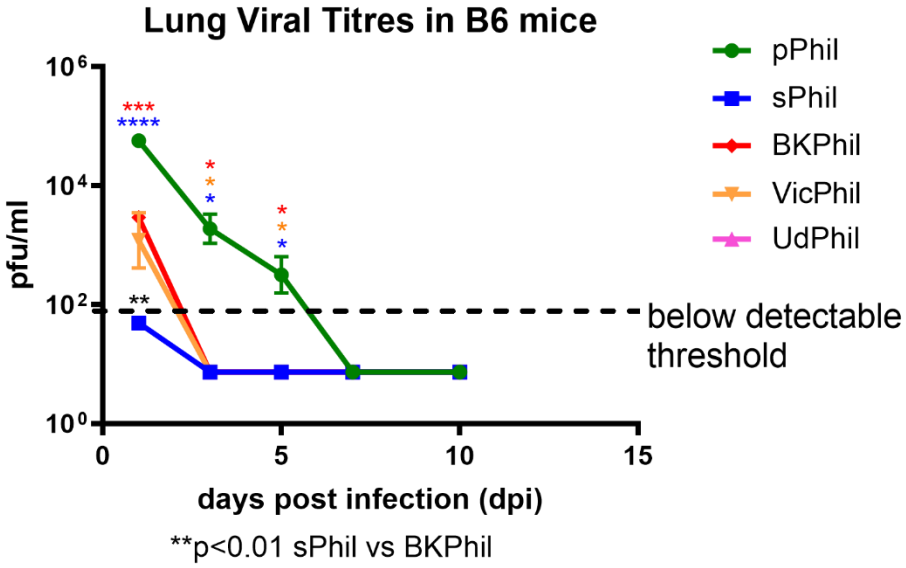

Figure 4.12. Kinetics of the B cell response against Ph82 infection in the presence of prior exposure to Ph82, BK79, Vic75, Ud72 or mock infection.

C57BL/6 mice (n=4) were infected as outlined in Figure 4.3. The viral titres of lungs from infected mice is shown. Symbols above timepoints indicative of statistical significance by two-way ANOVA – comparisons were made between pUd and the group of the same colour as the symbol as indicated by the key. Comparison in black represents significance between sPhil versus BKPhil. Number of symbols indicative of level of significance: * $p<0.05$, ** $p<0.01$, *** $p<0.001$, **** $p<0.0001$. Due to overlapping data, UdPhil is not visible, but titres of UdPhil were below detectable threshold from 3 to 10dpi. No data was obtained for 1 hpi for UdPhil.

Overall, the results from both Ph82-specific ASCs and B cell subsets indicate a more secondary-like response in all experimental groups, from 3 years of antigenic drift between BK79 and Ph82 to 10 years between Ud72 and Ph82. Further studies would be necessary to confirm this phenomenon, but this suggests that prior infection with H3N2 strains representing up to 10 years of antigenic drift may still induce some capacity to respond in a secondary-like fashion against infection of a drifted strain.

Primary infection by H3N2 strains in B6 mice appear to induce B cell responses that are largely unable to cross-react to drifted strains.

Results from the above experiments suggested secondary-like responses were possible in influenza experienced mice exposed to newer strains, despite 10 years of antigenic drift, yet the lack of cross-reactivity of serum raised against differing strains in response to Ph82 virus as seen in the HI assay shown in Table 4.1 appeared to contradict this assertion. To further investigate this apparent disparity between B cells and the antibodies produced against H3N2 infection, the Ud72 HA probe, described in the previous chapter, was used to investigate the cross-reactivity of B cells by flow cytometry. Ideally the experiment would have also used a probe specific for the Phil HA but several attempts to make such a probe proved unsuccessful.

B6 mice were infected with $10^{4.5}$ pfu of either Ud72, Vic75, BK79, Ph82 or mock infected with RPMI. MLN and spleen were harvested on 14 dpi, processed and analysed by flow cytometry, using the panel of antibodies shown in Supplementary Table 1 and gated as shown in Figure 4.13. Figures 4.14 show the total number of cells in each compartment as well as the percentage and total number of B cells, plasmablasts and GC B cells in the cellular population. A broad gating strategy was used for gating lymphocytes to capture larger plasmablasts. All of these responses were of a similar magnitude for each strain in both the MLN and spleen as seen previously (ns, $p>0.05$ by two-way ANOVA), although Ud72 B cell subsets were slightly elevated showing an incremental increase in both cell number and percentage for each subset.

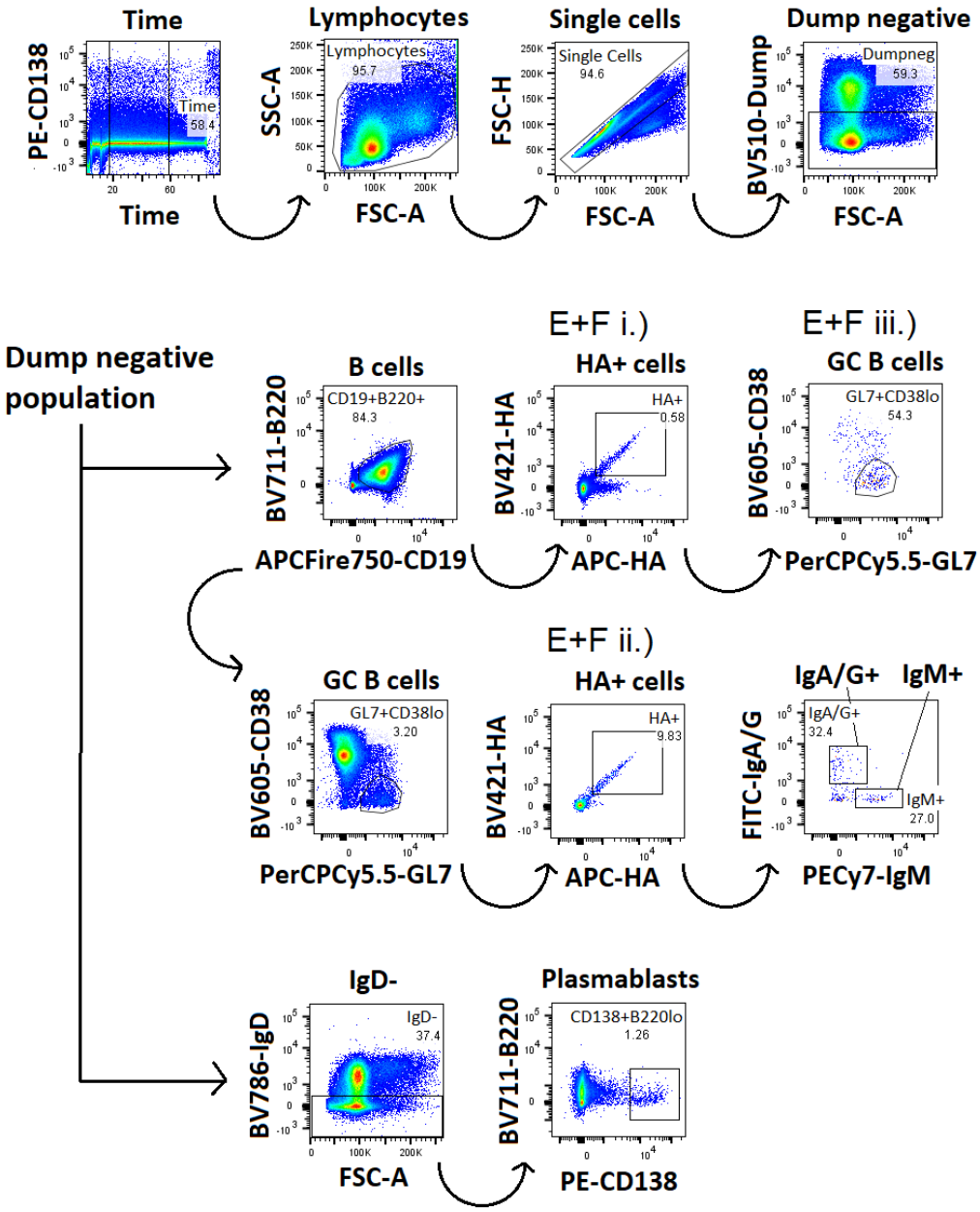

Figure 4.13. Gating scheme in the analysis of Ud72 HA+ B cell subsets during primary H3N2 infection.

Six to eight week-old C57BL/6 mice (n= 5) were infected with $10^{4.5}$ pfu of Ud72, Vic75, BK79 or Ph82 virus. At 14 days post infection (dpi), mediastinal lymph nodes (MLN) were collected and processed for analysis by flow cytometry. The number of cells in each sample was determined using a Beckman Coulter Counter. The gating scheme used to delineate cellular events is shown.

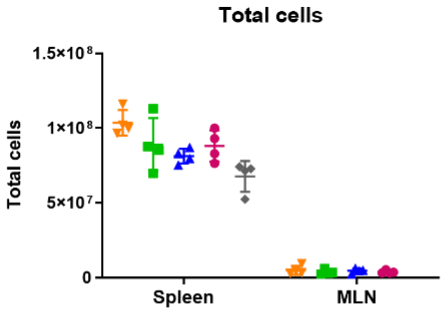

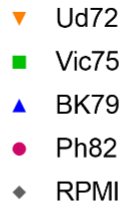

% in lymphocyte population

Total populations

B cells

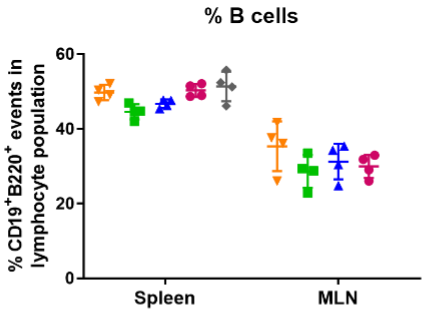

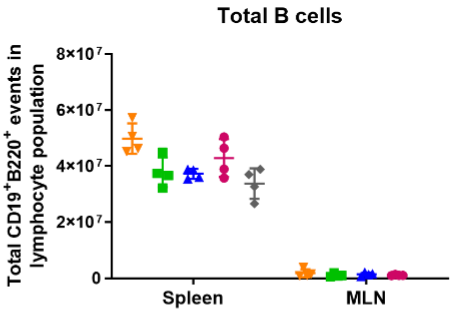

Plasmablasts

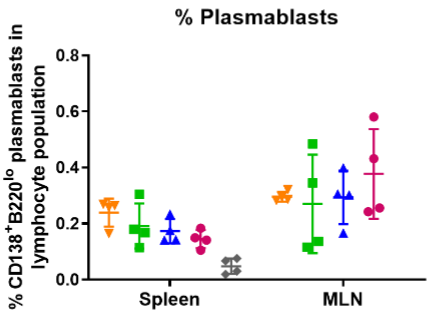

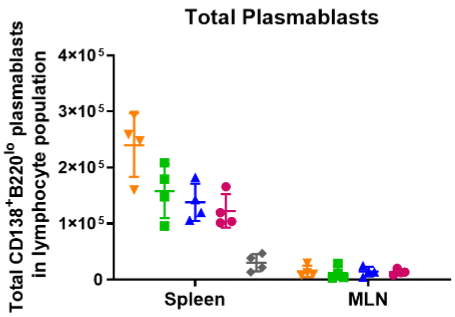

GC B cells

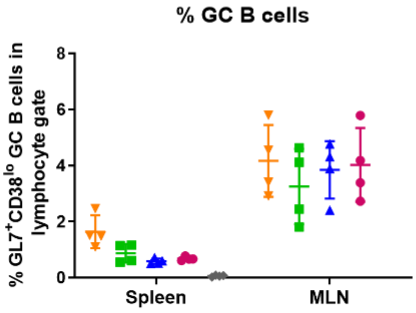

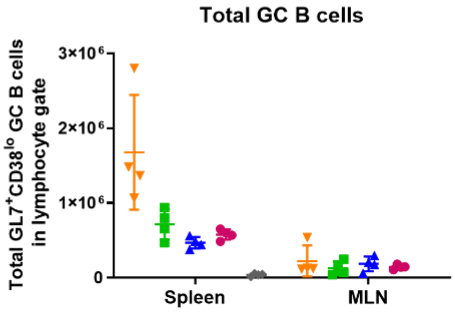

Figure 4.14. Proportions and total numbers of B cells and their subsets during primary H3N2 infection at 14 dpi.

Six to eight-week-old C57BL/6 mice (n= 5) were infected and processed as outlined in Figure 4.13. Total number of cells per sample, percentage of and total numbers of the B cell subsets in the overall lymphocyte population, including $CD19^+$ $B220^+$ B cells, $CD38^{lo}GL7^+$ GC B cells and $CD138^+B220^{lo}$ plasmablasts are shown.

Ud72 HA^+ cells in the overall B cell population, Ud72 HA^+ cells in the GC B cell population and GC B cells in the Ud72 HA^+ B cell population were all examined to further elucidate the proportions and subsets involved in the Ud72 HA^+ B cell response (Fig. 4.15). In analyses of both Ud HA^+ B cell and GC B cell populations, mice infected with Ud72 responded with the highest proportions ($p<0.05$) and numbers ($p<0.0001$) of Ud72 HA^+ B cells and GC B cells in the spleen as expected. Although proportions of Ud72 HA^+ cells were significantly higher than other groups in the MLN, a contraction in total cells in the MLN (as seen in Figure 4.6B) after the resolution of infection (14 dpi) likely accounts for the minimal total MLN responses. Mice infected with Vic75 showed mildly elevated numbers of Ud72 HA^+ cells – especially in the total B cell and GC B cell populations in the spleen – but this was not statistically significant. B cells or GC B cells in groups infected with BK79 and Ph82 appeared to be unable to bind to the Ud72 probe beyond baseline levels.

Notably, of the Ud72 HA^+ B cell population in Ud72 and Vic75 infected mice, a sizable proportion of these B cells in the MLN were GC B cells as identified by the markers CD38 and GL7 as outlined in Figure 4.13. This suggests a significant proportion of these responding B cells mature in germinal centres to hone their responses against reinfection with similar strains, despite their numbers in Vic75-infected mice and the contracting numbers of cells in the MLN. The minimal proportion and numbers of GC B cells in the Ud72 HA^+ B cell population for BK79, Ph82 and RPMI groups reflects the minimal responses against Ud72 HA^+ in the B cell population.

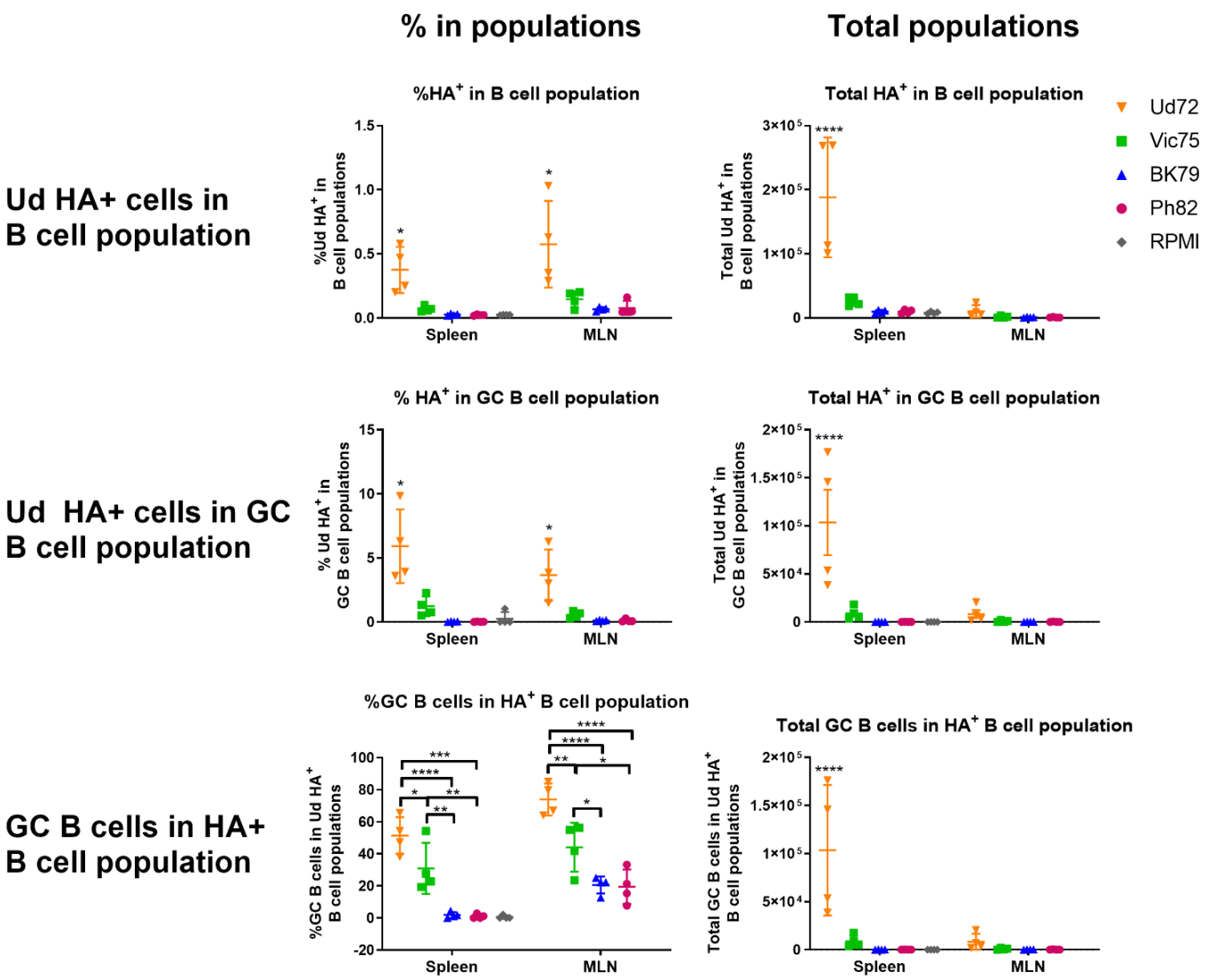

Figure 4.15. The proportion and total number of Ud72 HA+ B cells in the GC B cell and B cell populations.

Six to eight-week-old C57BL/6 mice (n= 5) were infected and processed as outlined in Figure 4.13. Percentages and total numbers of Ud HA^+ cells in the $CD19^+$ $B220^+$ B cell population, Ud HA^+ cells in the $CD38^{lo}GL7^+$ GC B cell population and GC B cells in the Ud HA^+ B cell population are shown. Symbols represent *p<0.05, **p<0.01, ***p<0.001 and **** p<0.0001 by ordinary two-way ANOVA with Tukey's multiple comparisons.

Taken together, results suggest that only mice infected with the Ud72 strain corresponding to virus with a matched HA, or mice infected with the relatively antigenically similar Vic75 strain (observed by cross-reactive neutralization of Ud72 virus by Vic75 sera measured by HI assay) will induce any level of B cells recognizing Ud72 HA. Although the response of the antigenically similar virus Vic75 was much lower in magnitude, it was nevertheless significant compared to other strains in terms of the percentage of germinal centre B cells that could bind to the Ud HA. Further investigation using these probes will be of great interest, especially with regards to the effects of recall of these cross-reactive B cells during subsequent infections.

CHAPTER 5 – DISCUSSION

In this thesis, the kinetics of B cell responses during influenza infection in the context of primary and secondary homologous, heterosubtypic and drifted strain infection have been studied using the B6 mouse model. It was hypothesized that, as HA is reported to be the immunodominant antigen in the response to influenza infection in the mouse (29), that the expansion of B cells during secondary infection would be determined by the antigenic relationship of the virus to that previously encountered during the primary infection.

The primary response against influenza infection was first characterised in the B6 mouse model to establish the pattern of B cell expansion during infection in naïve hosts. In prior studies involving primary PR8 infection of BALB/c mice, plasmablasts in the mediastinal lymph node (MLN) appeared to respond a few days earlier at 10 dpi followed by a peak GC B cell response at 15 dpi (132). An earlier response was also observed in our model, where MLN plasmablast populations peaked at around 7 dpi while GC B cells peaked at 10 dpi. Such differences in timing could be the effect of the different mouse strains given that the susceptibility and degree of inflammatory responses against influenza virus differs between BALB/c and C57BL/6 strains (148) and also the strain of virus, as much lower doses of PR8 are used to infect mice than are needed to establish primary infection with the Udorn virus used here. Although it is known that influenza-specific GC B cell responses continue to mature until as long as 14 – 21 dpi in B6 mice (149), data obtained from the Ud72-specific ELISPOT assay (Figure 3.5) indicated that the primary antibody secreting response against Ud72 virus peaked sharply at 7 dpi in the MLN suggesting that further B cell differentiation to effector cells in the MLN did not occur once the infection had been cleared. Such results are also in line with studies of peripheral blood effector B cell responses after influenza vaccination, where IgA^+ and IgG^+ influenza-specific effector B cells were largely detected from 7-11 days post vaccination in human participants before declining and reaching undetectable levels by day 21 (114). Overall, initial studies established important groundwork about the kinetic trends of primary B cell responses to Udorn virus, especially with regards to its differentiated subsets.

To examine B cell responses in the context of secondary infection, it was first necessary to determine whether primary and secondary homologous infections could be distinguished in

our model. Initial experiments characterized GC B cell and plasmablast responses during primary and homologous secondary Udorn influenza infection in the MLN, where most of the B cell expansion occurred, and also the spleen. Consistently differentiating the overall kinetic curves of primary and homologous secondary B cell responses measured by flow cytometry using two-way ANOVA was not possible as statistically significant differences were not always observed (Figure 3.9-11). The small sample size (n=4) and variation within these initial experiments undoubtedly played a role in this. However, given that the secondary (sUd) responses were initially 2 logs higher in magnitude compared to pUd at 3 dpi (Figure 3.11) for GC B cells in the MLN, the Mann-Whitney test was used to further analyse the earlier timepoints. Consequently, sUd was found to be significantly elevated in comparison to pUd by Mann-Whitney test at 3 dpi for total MLN GC B cells ($p<0.05$, Figure 3.11). In comparison, days 5 to 10 dpi showed no significant differences between primary and secondary responses in same subset. While the dogma of adaptive immune responses dictates that secondary responses would be expected to reach a higher magnitude compared to the primary response, this was not seen in these results. However, the viral load in the sUd group was below the detectable threshold throughout the course of infection, likely due to pre-existing antibodies and recall of memory cytotoxic T cell responses. These responses, which allowed rapid control of viral replication in comparison to the pUd mice (Figure 3.13) meant that the overall effective antigenic stimulus in the secondary response was much less despite the mice receiving a higher virus inoculum dose. The initial spike of GC B cells in the MLN at 3 dpi followed by responses that are non-significant from pUd from 5 dpi onwards was hence likely a result of the rapid decline in viral antigen availability as secondary and protective adaptive responses (including aforementioned B cell responses) were mobilised. This may also account for the non-significantly different MLN plasmablast responses between sUd and pUd. Although the subsets trended towards a similar response as GC B cells, the initial 3 dpi ‘spike’ in response was not prominent in the sUd group, possibly reflective of the absence of sufficient antigen stimuli.

To investigate B cell responses recalled by a heterosubtypic infection, the antigenically distinct H1N1 PR8 virus was used to initially infect mice followed by a secondary infection with H3N2 Udorn virus and the responses examined for their similarity to pUd or sUd. If the original hypothesis is correct, in this scenario it would be expected that the B cells would respond in a primary-like manner due to the antigenic differences between the surface antigens of PR8 and

Udorn viruses. However, when analysed by flow cytometry, significant differences were typically identified between the PR8Ud and pUd groups during earlier time points at 3 dpi within MLN GC B cells and both 3 and 5 dpi for MLN plasmablasts (Figure 3.10+11), with a single point of significant difference between PR8Ud and sUd found at 7 dpi in total and IgA/G$^+$ MLN GC B cells ($p<0.01$, Figure 3.11). Hence, heterosubtypic responses against influenza displayed early responses at higher magnitudes similar to a secondary response despite later elevated responses at 7 dpi. Through the use of the ELISPOT assay, the class-switched IgA/G$^+$ Ud-specific ASC responses in the MLN and to a lesser extent in the spleen, were shown to be elevated in the PR8Ud group compared to both pUd and sUd, especially early during the infection in the MLN ($p<0.05$, Mann-Whitney test for PR8Ud vs. pUd, PR8Ud vs. sUd at both 3 and 5 dpi). While the IgM$^+$ response in the MLN of the PR8Ud group appeared to differ from sUd from 3 to 7 dpi, the overall magnitudes of all groups were relatively low in comparison to the class-switched IgA/G$^+$ responses which may suggest they are not as biologically significant. These results appear to indicate that despite prior immunity against an antigenically unrelated strain – H1N1 PR8 virus – the PR8Ud mouse group was able to induce an elevated and more rapid class-switched secondary-like ASC response against the heterosubtypic H3N2 Udorn strain.

Given the importance of T cell help in the production of class-switched, affinity matured antibody-secreting cells (150), CD4$^+$ T cell memory likely plays a key role in this boosted response in early differentiated subsets and class-switching despite an assumed lack of antigenic recognition of the Ud HA and NA by memory B cells. Memory CD4$^+$ T cells originally primed against PR8 virus may be cross-reactive with conserved internal protein epitopes also found in Ud72, stimulating a more rapid and higher magnitude B cell response against subsequent influenza infection. Evidence for this boosting effect of CD4$^+$ T cell memory on B cells during influenza infection was shown by the higher magnitude of responses seen in mice with NP-specific memory CD4$^+$ T cells as a result of NP-peptide immunization. These mice displayed higher levels of antibody secreting cells, GC B cells and T follicular helper cells upon influenza infection compared to mice primed with an unrelated protein (151). Interestingly, the specificity of the CD4$^+$ T cells also appeared to shape the specificity of the B cells that were boosted by these cells – HA-specific T cells boosted HA-specific antibody responses, while NP-specific T cells boosted NP-specific responses - which may imply a higher prevalence of internal protein-

specific B cells in the case of heterologous infection where cross-reactivity would be restricted to mostly non-surface antigens. While the study by Alam *et al.* investigated NP and HA-specific ASCs in particular, the present study used ELISPOT plates coated with whole lysed virus, which would be expected to capture all influenza protein-specific ASC responses including those to the internal proteins such as NP, so does not provide any definition of the ASC specificity. In addition to $CD4^+$ T cell memory, the antiviral effect of cross-reactive cytotoxic T cells in the case of heterologous infection has been well-established and may have contributed to the more rapid clearance as well as potential effects on B cell responses (152, 153). In studies where mice were primed with seasonal H3N2 (sH3N2) followed by a pandemic H1N1 virus or the same strains in reverse order, $CD8^+$ T cell populations were found to correlate with protection despite some variation in PA and NP epitopes between the viruses. In addition, adoptive transfer of T cells from mice infected with sH3N2 provided protection against pH1N1 infection of the recipient mouse, but only when both $CD4^+$ and $CD8^+$ T cells were transferred from the donor (153). Such phenomena may explain the reduction in viral titre observed in PR8Ud-infected mice lungs compared to primary infection despite a lack of cross-reactive hemagglutination-inhibiting antibodies as seen by results in Table 3.2.

It is also likely that cross-reactive virus-specific B cell responses directed towards non-HA epitopes may have been boosted upon Ud72 infection and contributed to virus control. Although HA-specific B cell and antibody responses are immunodominant for protection (88), studies have shown that internal protein-specific B cells may also play a role in combatting infection. In a study by LaMere *et al.* (97), it has been shown that anti-NP IgG antibodies aided in viral clearance in the case of heterosubtypic infection through engaging FcR-dependant mechanisms. Furthermore, injection of NP-specific IgG, in conjunction with enhanced CD8+ T cell numbers, was able to rescue poor viral clearance in B cell deficient mice during heterosubtypic infection (97).

Studies have also shown that in cases where pre-existing neutralizing antibodies to the head of HA do not react with the novel virus, such as in heterosubtypic infection, antibodies that target the stem of the HA can play an important role in assisting with controlling the infection. Such was the case during pandemic H1N1 infection or avian H5N1 influenza vaccination where broadly cross-reactive antibodies were found to be produced against the stem of the HA in the

absence of cross-reactive head epitopes (154, 155). Furthermore, investigation of the antibodies produced against the pandemic H1N1 vaccine in healthy adults showed that a substantial proportion of B cells secreting broadly cross-reactive antibodies were specific for the HA stem and derived from a memory pool as evidenced by high levels of somatic hypermutation (156, 157). This suggests that in the absence of epitopes on the HA head that memory B cells can recognise, the remaining memory B cell repertoire against more conserved regions are boosted in response to the novel strain, some of which may have anti-viral function. Taking this into consideration, these responses may have contributed to the secondary-like results seen in mice previously infected with H1N1 PR8 followed by H3N2 Udorn.

Prior studies of serum antibody responses against strains of H3N2 influenza virus have shown that antigenic drift occurs in a staggered, punctuated manner with 'clusters' of drift occurring every 3 to 8 years (30). While antigenic distance between strains has been typically measured with ferret antisera (28, 34), it has been shown that different mammalian models result in differing antigenic maps between strains evident in a comparison of human with ferret antisera against cell-grown and egg-grown H3 viruses (158). In the present study, antisera from B6 mice were measured in HI assays to characterize antigenic relatedness of the strains under study. Results obtained showed similar trends found previously with ferret antisera against H3N2 strains, where sera were most likely to show some level of inhibition against strains that were within 3 years of isolation of the virus sera were raised against (Table 4.1). Although the intention was to form an antigenic map using the resultant HI data, the lack of detectable cross-reactivity interconnecting the samples prevented production of a viable data set for a map to be constructed. This may result from suboptimal generation of robust antibody responses against the H3N2 strains in mice or simply not having enough strains to provide sufficient empirical data to enable the relationship between antisera and strain-specific inhibition to be mathematically calculated to construct a map. Viral replication data from low dose infection (500 pfu) of mice shown in Figure 4.1 suggests less robust viral replication for later H3N2 strains (BK79 and TX77) which may have in turn led to a more focused antibody response with subdominant cross-reactive antibodies under-represented. However, this dose was 60-fold lower than that used to infect mice to generate the antisera. Data from Figure 4.2 where mice were infected with the same high dose ($10^{4.5}$ pfu) used to generate antisera suggested similar viral loads and kinetics between all strains as well as B cell responses of similar magnitude and kinetics, suggesting the

magnitude of the response between H3N2 strains does not vary significantly at higher doses. It therefore appears likely that a wider coverage of strains would be necessary to compute an antigenic map of seasonal H3N2 strains in mice at a resolution beyond the scope of this study.

As discussed previously, it is known that seasonal H3N2 strains have shown gradual reduction of receptor specificity towards avian sialic acid receptors over the course of their adaptation to and circulation in human populations (159). This phenomenon has been noted such that by the 1990s, strains circulating in humans were shown to have reduced ability to agglutinate chicken red blood cells containing the α2-3-linked sialic acid receptors of avian species (160). As mouse lungs have been shown to contain only avian-like sialic acid receptors (161), this loss of receptor specificity in more recent H3N2 strains affects their ability to infect mice (159, 162). However, some historical strains of H3N2 viruses have also been shown to have a lowered capacity to infect mice due to another mechanism involving glycosylation sites. As shown by Reading *et al.* (145), H3N2 strains from ’77 to ’92 have reduced capacity to infect mice due to an increased number of glycosylation sites on the HA and a resultant increase in sensitivity to the innate lung surfactant SP-D. For all H3N2 virus strains selected here to study drift, the virus could be isolated from the lungs over the course of several days (Figure 4.1). However, the efficiency of replication differed, with older strains such as Ud72 and Vic75 showing the highest levels of replication. TX77 proved to be inconsistent, with only one in five mice showing any virus in the lungs by plaque assay, likely as a result of inhibition by SP-D as discussed and was excluded from further study. While BK79 also showed reduced replication in mice, this strain was used for further studies due to its antigenic closeness to Ph82 and ability to consistently induce immune responses in mice as seen in experiments shown in Figure 4.2. Overall trends appeared to align with Reading’s study (145) that showed a reduction in infection and replication in mice as H3N2 strains acquired more glycosylation sites, with earlier strains such as Vic75 and Ud72 able to efficiently replicate while later more glycosylated strains such as TX77 and BK79 were less efficient. In this respect, Ph82 appears to defy this trend in its ability to replicate to similar magnitudes to Ud72 and Vic75. While previous studies have shown that inoculation of mice with wild-type Ph82 does not lead to productive infection, the strain of Ph82 used here to infect mice was a β-inhibitor resistant variant of this virus (130). This variant contained a mutation at residue 165 of the HA enabling resistance to mannose binding lectin (MBL), allowing more efficient infection of mice. Previously, the Ph82 variant was found to

replicate to 1000-fold higher titres in mouse lung than the parent Ph82 and had acquired lethality for mice. However, in the present study, mice appeared to show little to no clinical signs at the dose of $10^{4.5}$ pfu used. While it is acknowledged that the mutation at residue 165 in the HA may alter the antigenic properties of this strain compared to wild-type Ph82, the focus of this study was not to analyse the strains themselves but rather how the differences between strains over time impact the B cell response. In this context and from the data presented, it is apparent that the strain used was sufficient to analyse the phenomenon of drift on B cell responses.

As the variable of primary interest in Chapter 4 is the effect of antigenic distance between two strains on the B cell response of a host, a possible confounding factor would be differences in the immunogenicity of the strains involved. To address this, mice challenged with the selected strains were analysed for their B cell responses as shown in Figure 4.4-4.6. It was apparent that there was minimal variation between strains in terms of B cell responsiveness, with similar numbers of total B cells, GC B cells and plasmablasts in the MLN and spleen. This shows that the strains analysed in this study induced similar humoral responses to the model H3N2 Ud72 strain, ruling out the possibility of differences in consequent secondary responses stemming from discrepancies in the immune response to various strains.

In the context of secondary infection, it is expected that the host would respond more rapidly and efficiently against reinfection of the same pathogen as a result of adaptive immunity. However, influenza virus subverts the adaptive response through the process of antigenic drift, whereby the selective pressure of host immunity causes escape mutants which alter the antigenic properties of its surface antigens. As drift is a staggered but linear process (30), prior exposure to influenza strains followed by infection of a drifted strain would be expected to yield fewer protective responses with increasing antigenic distance as the antibodies and underlying memory B cells against the prior strain gradually become less able to recognize and react to the surface antigens of drifted strains. This can be seen in the previously discussed study by O'Donnell, where it was found that priming with earlier strains of H1N1 viruses were more likely to reduce lung viral titres of ferrets subsequently infected with the pandemic 2009 H1N1 strain (CA/09) as earlier seasonal H1N1 strains showed more antigenic similarities towards CA/09 (129). In comparison, our study of the effect of antigenic drift on the underlying B cell responses during influenza infection proved to be less clear cut. Upon infection of Ph82 in the context of prior

infection with Ud72, Vic75 or BK79, the numbers of Ph82-specific ASCs from all groups appeared secondary-like in terms of its kinetics and magnitude – trending towards an elevated IgA/G+ ASC response as early as 5 dpi in both MLN and spleen – with only minor variations. While there were some apparent differences in the IgM^+ ASC responses in the MLN between pPhil and other groups including BKPhil, VicPhil and sPhil, the numbers of these cells were far outnumbered by populations of class-switched IgA/G^+ ASCs in the same compartment – around a 10-fold difference – suggesting they were not as biologically relevant to the overall response. Hence a robust, secondary-like IgA/G^+ ASC response in both the MLN and spleen for all experimental groups would suggest that strains up to 10 years apart and separated by 3 antigenic clusters can still be recognized by the adaptive immune response and induce a secondary-like B cell response against the drifted strain.

When results from this drift experiment were compared to responses seen in the heterologous infection model used in Figure 3.8 involving PR8 and Ud72 viruses, responses appeared surprisingly similar, especially when considering the vast antigenic differences from drifted strains of the same lineage versus heterologous infections of entirely different subtypes. Statistical analysis showed that heterologous infection – first of PR8 followed by Ud72 7 weeks later – induced responses that appeared more secondary-like than expected between strains of completely different subtypes. Similarly, infection of strains from the same subtype but varying antigenic distance appeared to induce more consistent secondary-like responses throughout the course of infection. Hence, both shift and drift models tested in this thesis appeared to provide evidence against the hypothesis that the degree and nature of B cell responses and B cell cross-reactivity during secondary influenza infection would reflect the antigenic relationships of the HA between viruses shown through antibody reactivity.

Factors that may contribute to the results observed may include recall of underlying cross-reactive T cell memory responses that boost B cells reacting towards the second strain and/or B cell memory against conserved components or epitopes between strains such as the NP or HA stem respectively as mentioned previously. Another potential factor to account for is the effect of serum antibodies against the initial infecting strain (Ud72, Vic75 or BK79) on the infecting dose of Ph82. As replication of the second virus was greatly reduced, the presence of any cross-reactive pre-existing antibodies against the infecting strain may neutralize the second

dose of virus and cause a similar secondary-like trend. However as shown in Table 4.1, cross reactivity would only be expected of the BK79 strain, which induced some level of HI response against Ph82, a correlate of virus neutralizing antibody (163) against Ph82 virus.

The anti-Ph82 ASC responses in the context of prior exposure to earlier H3N2 strains as seen in Figure 4.11 suggest that measurement of antibody responses by HI assay alone – which measures the capacity of serum to inhibit hemagglutination of RBCs by virus, mediated by binding of HA to sialic acid on RBCs - does not account for the full breadth of the immune response against drifted strains in the context of prior influenza infection. The data obtained from flow cytometry within the same experiments (Figure 4.8-10) also support the secondary-like trends observed by ELISPOT assays. While the splenic data proved largely inconclusive or similar to baseline responses depending on subset – likely as a result of its biological distance from the site of infection, the results obtained from the MLN trended towards a largely secondary-like response in mice with exposure to any H3N2 strain prior to Ph82 infection for both plasmablasts and GC B cells in line with the ELISPOT data. Although the markers used in these studies did not allow for the identification of memory B cells, the marked elevation of class-switched IgA/G$^+$ MLN GC B cells at 3 dpi in all mouse groups with prior exposure to H3N2 virus compared to the primary response may hint at some recognition of Ph82 by cross-reactive memory B cells and/or a boosting and acceleration of class switching by memory T cells.

As postulated in the theory behind the concept of original antigenic sin (164), it is possible that the memory B cells from which these ASCs may have originated have a higher capacity to recognize and bind strains that contain epitopes drifted from its target antigen due to the higher avidity and valency of B cell receptors compared to secreted antibodies. This may contribute to observed secondary-like responses either in conjunction with or instead of other memory T cell or B cell mechanisms discussed earlier. From the doctrine of original antigenic sin, antigenic seniority and the changes in antibody landscape over an individual's lifetime, the effect of prior immunity against older strains on protection and clearance of newer strains in the context of antigenic drift have been a topic of ongoing discussion (109, 112-114, 116, 165) (refs). The results from our studies suggest a secondary-like response in mouse groups with any prior exposure to H3N2 viruses upon infection by a drifted strain of the same subtype. Aligning

with this data, viral replication within mouse lungs (Figure 4.12) indicated that mice infected with any H3N2 strain prior to Ph82 exposure had minimal titres and next to no clinical signs upon infection. This suggests that the observed secondary-like B cell responses and other virus-specific concomitant immunity induced by prior infection were likely protective and aided in viral clearance. As the antibody responses against both prior and drifted strains were not tested, it cannot be definitively proven that the data fully contradicts the concept of original antigenic sin as described by Davenport (113), but in contrast to observations and predictions of memory responses hindering responses against drifted strains, this data suggest that pre-existing secondary-like immunity to prior H3N2 strains enabled mice to clear Ph82 infection much more rapidly than a primary infection irrespective of any diminished capacity to produce antibody to the second strain. These results appear to be in line with those seen by Wrammert *et al.* (109) and Fonville *et al.* (34) whereby infection or vaccination with a drifted strain produces the maximal response against the newer strain rather than the older ones despite evidence of immunological memory. However, further studies beyond the scope of this project would be necessary to provide more insight into the phenomenon of original antigenic sin, such as the investigation of the antibody responses before and after secondary infection as well as comparisons of the prior strain-specific ASCs with anti-Ph82 ASCs post-Ph82 infection. Furthermore, as shown by previous studies (122), prior infection as compared with vaccination has a tendency to induce a more effective response against subsequent infection or vaccination, so care must be taken to avoid over-generalization of any data presented through a single means of virus exposure.

As shown in Figures 4.8-10, 4.11 and Table 4.1, the sera from mice did not appear to cross-react with strains beyond 3 years of the infecting strain by HI assay, yet upon infection with the drifted Ph82 strain, both Ph82-specific ASCs and B cell subsets including plasmablasts and GC B cells appeared to respond in a secondary-like manner. While ideally, the use of recombinant Ph82 HA to probe Ph82 HA-specific B cell responses with flow cytometry would have provided a wealth of information as to the specificity of B cells against antigenically drifted strains, the recombinant Ph82 HA that was generated for this project was unable to bind to Ph82-specific B cells despite thorough troubleshooting. Hence to further investigate the HA cross-reactivity of the underlying B cell response, mice were infected with the chosen H3N2 strains at $10^{4.5}$ pfu. At 14 dpi, MLN and spleen were harvested and processed for staining with a modified marker for Ud72 HA before samples were analysed by flow cytometry as shown in Figure 4.13.

Although results observed in Figures 4.8-11 suggested the responding B cell populations as a whole appeared to be more cross-reactive than the antibodies produced, the use of a Ud72 HA marker appears to suggest HA-specific B cells react similarly to its virus-specific serum antibodies – that is, potential cross-reactivity observed up to three years of drift – in terms of cross-reactivity with other H3N2 strains.

Taking this experiment together with the secondary-like Ph82 virus-specific responses against Ph82 in the context of prior infection by prior strains, the data appears to further refute the hypothesis that recall of virus-specific B cells would reflect the antigenic relatedness of the HA between the first and second infecting strains. While the antibody response against influenza has been thought to be immunodominant against the HA, our experiments appear to indicate that the pool of available virus-specific B cell responses against influenza infection in the context of prior exposure may be more diverse than expected. If the cross-reactivity of HA-specific B cells against other influenza strains was the sole or main determinant of secondary-like and/or cross-reactive responses against infections of newer strains, then the prior experiments involving paired H3N2 strains of varying antigenic distance as well as the heterosubtypic model involving PR8 and Udorn would be expected to show more primary-like trends rather than the secondary-like responses seen throughout these studies.

However, there are several factors to be considered about these studies prior to making any solid conclusions. Firstly, experiments involving the measurement of cross-reactivity both in sera and in B cells were both conducted in conditions of primary infection when the infection had largely or completely resolved, whereas the experiments that contribute to the investigation of the effect of antigenic drift on B cell kinetics was conducted during a secondary infection 6-8 weeks post initial infection. The consistent secondary-like responses in mice infected with strains of increasing antigenic distance would suggest an underlying, pre-existing immunity against the drifted strain rather than an arising cross-reactive response, but it is possible that the ongoing infection may have stimulated the immune response and inflammation so as to promote secondary-like reactivity against the infecting strain. It would hence be of great interest to study whether the specificity of B cell responses may diversify as a result of secondary infection before further conclusions are made. Finally, while experiments from Figures 4.8-11 produced a wealth of data on the kinetics and magnitudes of the B cell responses and Ph82-specific ASC responses,

little can be said of the specificity of the B cell subsets measured by flow cytometry. In order to thoroughly investigate the potential cross-reactive response of HA-specific B cells against drifted strains, investigation of serum and HA-specific B cell responses against both the initial and drifted strains in a similar model involving sequential infection of drifted H3N2 strains as described in Figure 4.7 would be necessary.

Furthermore, it would be of great interest to further study the component specificity of the non-HA head virus-specific B cells – whether through purification of specific viral proteins to coat in ELISPOT assays or generation of further recombinant viral proteins as probes to look at specific responses. In particular, the recent approach of Tan *et al.* (166), who used recombinant NP to probe the NP-specific B cell responses, would provide much insight as to the potential cross-reactive responses in the context of secondary influenza infections. This would be especially pertinent as it was found that NP-specific GC B cells were present in high frequencies at 35 days post infection in the lungs, MLN and spleen, even higher in percentage compared to HA-specific GC B cell responses. This corroborates our results which also suggest a large quantity of virus-specific B cell responses recalled during secondary infection may not be HA-specific. Another factor that would expect to contribute to secondary B cell responses is that of T cell memory in contexts of both drift and shift. Further studies involving the use of T cell markers in flow cytometry experiments and further HA strain-specific markers would be necessary to confirm this and further elucidate whether the 'boost' from recall of a pre-existing memory helper T cell population translates to an earlier secondary strain-specific B cell response or even a more cross-reactive response.

Contrary to our initial hypothesis that the B cell response during infection of an antigenically related strain would reflect the antigenic relatedness between the HA of the first and second infecting strains, this study points to a previously unidentified high degree of cross-reactivity in the response to antigenically diverse influenza strains at the level of B cells. Whether these responding B cells can induce antibodies or other factors that might aid in curtailing a secondary infection of an antigenically distinct strain or are functionally irrelevant and place an drain on the hosts reserves to fight infection remains unclear and difficult to address in the context of a recalled cross-reactive cytotoxic response that itself would limit a secondary infection. Further studies to investigate the specificity of the responding B cells, determine

whether they are primary or memory B cells and determine the relevance of the antibodies that they produce would be highly informative and provide much needed data on the breadth and nature of these observed secondary-like responses in the context of prior influenza exposure.

REFERENCES

1. **Mahony JB, Petrich A, Smieja M.** 2011. Molecular diagnosis of respiratory virus infections. Crit Rev Clin Lab Sci **48:**217-249.
2. **Kuiken T, Riteau B, Fouchier RA, Rimmelzwaan GF.** 2012. Pathogenesis of influenza virus infections: the good, the bad and the ugly. Curr Opin Virol **2:**276-286.
3. **W.H.O.** January 2018 2018. Influenza (Seasonal). http://www.who.int/mediacentre/factsheets/fs211/en/. Accessed 15th February.
4. **Couch RB.** 1996. Orthomyxoviruses. *In* th, Baron S (ed), Medical Microbiology, Galveston (TX).
5. **Tong S, Zhu X, Li Y, Shi M, Zhang J, Bourgeois M, Yang H, Chen X, Recuenco S, Gomez J, Chen LM, Johnson A, Tao Y, Dreyfus C, Yu W, McBride R, Carney PJ, Gilbert AT, Chang J, Guo Z, Davis CT, Paulson JC, Stevens J, Rupprecht CE, Holmes EC, Wilson IA, Donis RO.** 2013. New world bats harbor diverse influenza A viruses. PLoS Pathog **9:**e1003657.
6. **Samji T.** 2009. Influenza A: understanding the viral life cycle. Yale J Biol Med **82:**153-159.
7. **Nayak DP, Balogun RA, Yamada H, Zhou ZH, Barman S.** 2009. Influenza virus morphogenesis and budding. Virus Res **143:**147-161.
8. **Byrd-Leotis L, Cummings RD, Steinhauer DA.** 2017. The Interplay between the Host Receptor and Influenza Virus Hemagglutinin and Neuraminidase. Int J Mol Sci **18**.
9. **Rogers GN, Paulson JC.** 1983. Receptor determinants of human and animal influenza virus isolates: differences in receptor specificity of the H3 hemagglutinin based on species of origin. Virology **127:**361-373.
10. **Imai M, Kawaoka Y.** 2012. The role of receptor binding specificity in interspecies transmission of influenza viruses. Curr Opin Virol **2:**160-167.
11. **de Graaf M, Fouchier RA.** 2014. Role of receptor binding specificity in influenza A virus transmission and pathogenesis. EMBO J **33:**823-841.
12. **Bouvier NM, Palese P.** 2008. The biology of influenza viruses. Vaccine **26 Suppl 4:**D49-53.
13. **Chen W, Calvo PA, Malide D, Gibbs J, Schubert U, Bacik I, Basta S, O'Neill R, Schickli J, Palese P, Henklein P, Bennink JR, Yewdell JW.** 2001. A novel influenza A virus mitochondrial protein that induces cell death. Nat Med **7:**1306-1312.
14. **Gong Y-N, Chen G-W, Chen C-J, Kuo R-L, Shih S-R.** 2014. Computational Analysis and Mapping of Novel Open Reading Frames in Influenza A Viruses. PLOS ONE **9:**e115016.
15. **O'Donnell CD, Subbarao K.** 2011. The contribution of animal models to the understanding of the host range and virulence of influenza A viruses. Microbes and Infection **13:**502-515.
16. **Chou YY, Vafabakhsh R, Doganay S, Gao Q, Ha T, Palese P.** 2012. One influenza virus particle packages eight unique viral RNAs as shown by FISH analysis. Proc Natl Acad Sci U S A **109:**9101-9106.
17. **Gilbertson B, Zheng T, Gerber M, Printz-Schweigert A, Ong C, Marquet R, Isel C, Rockman S, Brown L.** 2016. Influenza NA and PB1 Gene Segments Interact during the Formation of Viral Progeny: Localization of the Binding Region within the PB1 Gene. Viruses **8**.
18. **Matrosovich MN, Matrosovich TY, Gray T, Roberts NA, Klenk HD.** 2004. Neuraminidase is important for the initiation of influenza virus infection in human airway epithelium. J Virol **78:**12665-12667.
19. **Flint SJ, Racaniello VR, Rall GF, Skalka AM, Enquist LW.** 2015. Principles of virology, 4th Edition. ed. ASM Press.
20. **Dias A, Bouvier D, Crepin T, McCarthy AA, Hart DJ, Baudin F, Cusack S, Ruigrok RW.** 2009. The cap-snatching endonuclease of influenza virus polymerase resides in the PA subunit. Nature **458:**914-918.

21. **Klemm C, Boergeling Y, Ludwig S, Ehrhardt C.** 2018. Immunomodulatory Nonstructural Proteins of Influenza A Viruses. Trends Microbiol doi:10.1016/j.tim.2017.12.006.
22. **Paterson D, Fodor E.** 2012. Emerging Roles for the Influenza A Virus Nuclear Export Protein (NEP). PLOS Pathogens **8:**e1003019.
23. **Rambaut A, Pybus OG, Nelson MI, Viboud C, Taubenberger JK, Holmes EC.** 2008. The genomic and epidemiological dynamics of human influenza A virus. Nature **453:**615-619.
24. **Boni MF.** 2008. Vaccination and antigenic drift in influenza. Vaccine **26 Suppl 3:**C8-14.
25. **Kim H, Webster RG, Webby RJ.** 2018. Influenza Virus: Dealing with a Drifting and Shifting Pathogen. Viral Immunol doi:10.1089/vim.2017.0141.
26. **Landolt GA, Olsen CW.** 2007. Up to new tricks - a review of cross-species transmission of influenza A viruses. Anim Health Res Rev **8:**1-21.
27. **Ferguson NM, Galvani AP, Bush RM.** 2003. Ecological and immunological determinants of influenza evolution. Nature **422:**428-433.
28. **Smith DJ, Lapedes AS, de Jong JC, Bestebroer TM, Rimmelzwaan GF, Osterhaus AD, Fouchier RA.** 2004. Mapping the antigenic and genetic evolution of influenza virus. Science **305:**371-376.
29. **Altman MO, Angeletti D, Yewdell JW.** 2018. Antibody Immunodominance: The Key to Understanding Influenza Virus Antigenic Drift. Viral Immunol **31:**142-149.
30. **Russell CA, Jones TC, Barr IG, Cox NJ, Garten RJ, Gregory V, Gust ID, Hampson AW, Hay AJ, Hurt AC, de Jong JC, Kelso A, Klimov AI, Kageyama T, Komadina N, Lapedes AS, Lin YP, Mosterin A, Obuchi M, Odagiri T, Osterhaus AD, Rimmelzwaan GF, Shaw MW, Skepner E, Stohr K, Tashiro M, Fouchier RA, Smith DJ.** 2008. The global circulation of seasonal influenza A (H3N2) viruses. Science **320:**340-346.
31. **Koel BF, Burke DF, Bestebroer TM, van der Vliet S, Zondag GC, Vervaet G, Skepner E, Lewis NS, Spronken MI, Russell CA, Eropkin MY, Hurt AC, Barr IG, de Jong JC, Rimmelzwaan GF, Osterhaus AD, Fouchier RA, Smith DJ.** 2013. Substitutions near the receptor binding site determine major antigenic change during influenza virus evolution. Science **342:**976-979.
32. **Wilson IA, Cox NJ.** 1990. Structural basis of immune recognition of influenza virus hemagglutinin. Annu Rev Immunol **8:**737-771.
33. **Bedford T, Riley S, Barr IG, Broor S, Chadha M, Cox NJ, Daniels RS, Gunasekaran CP, Hurt AC, Kelso A, Klimov A, Lewis NS, Li X, McCauley JW, Odagiri T, Potdar V, Rambaut A, Shu Y, Skepner E, Smith DJ, Suchard MA, Tashiro M, Wang D, Xu X, Lemey P, Russell CA.** 2015. Global circulation patterns of seasonal influenza viruses vary with antigenic drift. Nature **523:**217-220.
34. **Fonville JM, Wilks SH, James SL, Fox A, Ventresca M, Aban M, Xue L, Jones TC, Le NMH, Pham QT, Tran ND, Wong Y, Mosterin A, Katzelnick LC, Labonte D, Le TT, van der Net G, Skepner E, Russell CA, Kaplan TD, Rimmelzwaan GF, Masurel N, de Jong JC, Palache A, Beyer WEP, Le QM, Nguyen TH, Wertheim HFL, Hurt AC, Osterhaus A, Barr IG, Fouchier RAM, Horby PW, Smith DJ.** 2014. Antibody landscapes after influenza virus infection or vaccination. Science **346:**996-1000.
35. **Webster RG, Laver WG, Air GM, Schild GC.** 1982. Molecular mechanisms of variation in influenza viruses. Nature **296:**115-121.
36. **Ito T, Couceiro JN, Kelm S, Baum LG, Krauss S, Castrucci MR, Donatelli I, Kida H, Paulson JC, Webster RG, Kawaoka Y.** 1998. Molecular basis for the generation in pigs of influenza A viruses with pandemic potential. J Virol **72:**7367-7373.
37. **Neumann G, Noda T, Kawaoka Y.** 2009. Emergence and pandemic potential of swine-origin H1N1 influenza virus. Nature **459:**931-939.
38. **Hemmink JD, Whittaker CJ, Shelton HA.** 2018. Animal Models in Influenza Research. Methods Mol Biol **1836:**401-430.

39. **Groves HT, McDonald JU, Langat P, Kinnear E, Kellam P, McCauley J, Ellis J, Thompson C, Elderfield R, Parker L, Barclay W, Tregoning JS.** 2018. Mouse Models of Influenza Infection with Circulating Strains to Test Seasonal Vaccine Efficacy. Front Immunol **9:**126.
40. **Sanders CJ, Doherty PC, Thomas PG.** 2011. Respiratory epithelial cells in innate immunity to influenza virus infection. Cell and Tissue Research **343:**13-21.
41. **Loo Y-M, Gale M.** 2011. Immune signaling by RIG-I-like receptors. Immunity **34:**680-692.
42. **Kawai T, Akira S.** 2011. Toll-like Receptors and Their Crosstalk with Other Innate Receptors in Infection and Immunity. Immunity **34:**637-650.
43. **McAuley JL, Tate MD, MacKenzie-Kludas CJ, Pinar A, Zeng W, Stutz A, Latz E, Brown LE, Mansell A.** 2013. Activation of the NLRP3 inflammasome by IAV virulence protein PB1-F2 contributes to severe pathophysiology and disease. PLoS Pathog **9:**e1003392.
44. **Goraya MU, Wang S, Munir M, Chen JL.** 2015. Induction of innate immunity and its perturbation by influenza viruses. Protein Cell **6:**712-721.
45. **van de Sandt CE, Kreijtz JH, Rimmelzwaan GF.** 2012. Evasion of influenza A viruses from innate and adaptive immune responses. Viruses **4:**1438-1476.
46. **Lin KL, Suzuki Y, Nakano H, Ramsburg E, Gunn MD.** 2008. CCR2+ monocyte-derived dendritic cells and exudate macrophages produce influenza-induced pulmonary immune pathology and mortality. J Immunol **180:**2562-2572.
47. **Hashimoto G, Wright PF, Karzon DT.** 1983. Antibody-dependent cell-mediated cytotoxicity against influenza virus-infected cells. J Infect Dis **148:**785-794.
48. **Chen X, Liu S, Goraya MU, Maarouf M, Huang S, Chen JL.** 2018. Host Immune Response to Influenza A Virus Infection. Front Immunol **9:**320.
49. **McGill J, Heusel JW, Legge KL.** 2009. Innate immune control and regulation of influenza virus infections. J Leukoc Biol **86:**803-812.
50. **van Domselaar R, Bovenschen N.** 2011. Cell death-independent functions of granzymes: hit viruses where it hurts. Rev Med Virol **21:**301-314.
51. **Jameson J, Cruz J, Ennis FA.** 1998. Human cytotoxic T-lymphocyte repertoire to influenza A viruses. J Virol **72:**8682-8689.
52. **Assarsson E, Bui HH, Sidney J, Zhang Q, Glenn J, Oseroff C, Mbawuike IN, Alexander J, Newman MJ, Grey H, Sette A.** 2008. Immunomic analysis of the repertoire of T-cell specificities for influenza A virus in humans. J Virol **82:**12241-12251.
53. **Kreijtz JH, de Mutsert G, van Baalen CA, Fouchier RA, Osterhaus AD, Rimmelzwaan GF.** 2008. Cross-recognition of avian H5N1 influenza virus by human cytotoxic T-lymphocyte populations directed to human influenza A virus. J Virol **82:**5161-5166.
54. **Zhu J, Paul WE.** 2010. Peripheral CD4+ T-cell differentiation regulated by networks of cytokines and transcription factors. Immunol Rev **238:**247-262.
55. **Zhu J, Paul WE.** 2010. Heterogeneity and plasticity of T helper cells. Cell Res **20:**4-12.
56. **Belz GT, Wodarz D, Diaz G, Nowak MA, Doherty PC.** 2002. Compromised influenza virus-specific CD8(+)-T-cell memory in CD4(+)-T-cell-deficient mice. J Virol **76:**12388-12393.
57. **Chiu C, Ellebedy AH, Wrammert J, Ahmed R.** 2015. B cell responses to influenza infection and vaccination. Curr Top Microbiol Immunol **386:**381-398.
58. **Monto AS, Kendal AP.** 1973. Effect of neuraminidase antibody on Hong Kong influenza. Lancet **1:**623-625.
59. **Angeletti D, Yewdell JW.** 2018. Is It Possible to Develop a "Universal" Influenza Virus Vaccine? Outflanking Antibody Immunodominance on the Road to Universal Influenza Vaccination. Cold Spring Harb Perspect Biol **10**.

60. **de Jong JC, Beyer WE, Palache AM, Rimmelzwaan GF, Osterhaus AD.** 2000. Mismatch between the 1997/1998 influenza vaccine and the major epidemic A(H3N2) virus strain as the cause of an inadequate vaccine-induced antibody response to this strain in the elderly. J Med Virol **61:**94-99.
61. **Lamere MW, Moquin A, Lee FE, Misra RS, Blair PJ, Haynes L, Randall TD, Lund FE, Kaminski DA.** 2011. Regulation of antinucleoprotein IgG by systemic vaccination and its effect on influenza virus clearance. J Virol **85:**5027-5035.
62. **Mozdzanowska K, Maiese K, Furchner M, Gerhard W.** 1999. Treatment of influenza virus-infected SCID mice with nonneutralizing antibodies specific for the transmembrane proteins matrix 2 and neuraminidase reduces the pulmonary virus titer but fails to clear the infection. Virology **254:**138-146.
63. **Treanor JJ, Tierney EL, Zebedee SL, Lamb RA, Murphy BR.** 1990. Passively transferred monoclonal antibody to the M2 protein inhibits influenza A virus replication in mice. J Virol **64:**1375-1377.
64. **Rimmelzwaan GF, Baars M, van Beek R, van Amerongen G, Lovgren-Bengtsson K, Claas EC, Osterhaus AD.** 1997. Induction of protective immunity against influenza virus in a macaque model: comparison of conventional and iscom vaccines. J Gen Virol **78 (Pt 4):**757-765.
65. **Skountzou I, Satyabhama L, Stavropoulou A, Ashraf Z, Esser ES, Vassilieva E, Koutsonanos D, Compans R, Jacob J.** 2014. Influenza virus-specific neutralizing IgM antibodies persist for a lifetime. Clin Vaccine Immunol **21:**1481-1489.
66. **Mazanec MB, Coudret CL, Fletcher DR.** 1995. Intracellular neutralization of influenza virus by immunoglobulin A anti-hemagglutinin monoclonal antibodies. J Virol **69:**1339-1343.
67. **Seibert CW, Rahmat S, Krause JC, Eggink D, Albrecht RA, Goff PH, Krammer F, Duty JA, Bouvier NM, Garcia-Sastre A, Palese P.** 2013. Recombinant IgA is sufficient to prevent influenza virus transmission in guinea pigs. J Virol **87:**7793-7804.
68. **van Riet E, Ainai A, Suzuki T, Hasegawa H.** 2012. Mucosal IgA responses in influenza virus infections; thoughts for vaccine design. Vaccine **30:**5893-5900.
69. **Jones PD, Ada GL.** 1987. Persistence of influenza virus-specific antibody-secreting cells and B-cell memory after primary murine influenza virus infection. Cell Immunol **109:**53-64.
70. **Martin SW, Goodnow CC.** 2002. Burst-enhancing role of the IgG membrane tail as a molecular determinant of memory. Nat Immunol **3:**182-188.
71. **Shaffer AL, Lin KI, Kuo TC, Yu X, Hurt EM, Rosenwald A, Giltnane JM, Yang L, Zhao H, Calame K, Staudt LM.** 2002. Blimp-1 orchestrates plasma cell differentiation by extinguishing the mature B cell gene expression program. Immunity **17:**51-62.
72. **Baumgarth N.** 2013. How specific is too specific? B-cell responses to viral infections reveal the importance of breadth over depth. Immunol Rev **255:**82-94.
73. **Tarlinton DM, Smith KG.** 2000. Dissecting affinity maturation: a model explaining selection of antibody-forming cells and memory B cells in the germinal centre. Immunol Today **21:**436-441.
74. **MacLennan IC.** 1994. Germinal centers. Annu Rev Immunol **12:**117-139.
75. **Victora GD, Nussenzweig MC.** 2012. Germinal centers. Annu Rev Immunol **30:**429-457.
76. **Pieper K, Grimbacher B, Eibel H.** 2013. B-cell biology and development. J Allergy Clin Immunol **131:**959-971.
77. **Yu X, Tsibane T, McGraw PA, House FS, Keefer CJ, Hicar MD, Tumpey TM, Pappas C, Perrone LA, Martinez O, Stevens J, Wilson IA, Aguilar PV, Altschuler EL, Basler CF, Crowe JE, Jr.** 2008. Neutralizing antibodies derived from the B cells of 1918 influenza pandemic survivors. Nature **455:**532-536.
78. **Baumgarth N, Herman OC, Jager GC, Brown LE, Herzenberg LA, Chen J.** 2000. B-1 and B-2 cell-derived immunoglobulin M antibodies are nonredundant components of the protective response to influenza virus infection. J Exp Med **192:**271-280.

79. **Lam JH, Baumgarth N.** 2019. The Multifaceted B Cell Response to Influenza Virus. J Immunol **202:**351-359.
80. **Wiley DC, Wilson IA, Skehel JJ.** 1981. Structural identification of the antibody-binding sites of Hong Kong influenza haemagglutinin and their involvement in antigenic variation. Nature **289:**373-378.
81. **Wilson IA, Skehel JJ, Wiley DC.** 1981. Structure of the haemagglutinin membrane glycoprotein of influenza virus at 3 A resolution. Nature **289:**366-373.
82. **Angeletti D, Gibbs JS, Angel M, Kosik I, Hickman HD, Frank GM, Das SR, Wheatley AK, Prabhakaran M, Leggat DJ, McDermott AB, Yewdell JW.** 2017. Defining B cell immunodominance to viruses. Nat Immunol **18:**456-463.
83. **Broecker F, Liu STH, Sun W, Krammer F, Simon V, Palese P.** 2018. Immunodominance of Antigenic Site B in the Hemagglutinin of the Current H3N2 Influenza Virus in Humans and Mice. J Virol **92**.
84. **Victora GD, Wilson PC.** 2015. Germinal center selection and the antibody response to influenza. Cell **163:**545-548.
85. **Lee PS, Wilson IA.** 2015. Structural characterization of viral epitopes recognized by broadly cross-reactive antibodies. Curr Top Microbiol Immunol **386:**323-341.
86. **Woodruff MC, Kim EH, Luo W, Pulendran B.** 2018. B Cell Competition for Restricted T Cell Help Suppresses Rare-Epitope Responses. Cell Rep **25:**321-327 e323.
87. **Altman MO, Bennink JR, Yewdell JW, Herrin BR.** 2015. Lamprey VLRB response to influenza virus supports universal rules of immunogenicity and antigenicity. Elife **4**.
88. **Epstein SL, Misplon JA, Lawson CM, Subbarao EK, Connors M, Murphy BR.** 1993. Beta 2-microglobulin-deficient mice can be protected against influenza A infection by vaccination with vaccinia-influenza recombinants expressing hemagglutinin and neuraminidase. J Immunol **150:**5484-5493.
89. **Johansson BE, Grajower B, Kilbourne ED.** 1993. Infection-permissive immunization with influenza virus neuraminidase prevents weight loss in infected mice. Vaccine **11:**1037-1039.
90. **Johansson BE, Bucher DJ, Kilbourne ED.** 1989. Purified influenza virus hemagglutinin and neuraminidase are equivalent in stimulation of antibody response but induce contrasting types of immunity to infection. J Virol **63:**1239-1246.
91. **Sandbulte MR, Jimenez GS, Boon AC, Smith LR, Treanor JJ, Webby RJ.** 2007. Cross-reactive neuraminidase antibodies afford partial protection against H5N1 in mice and are present in unexposed humans. PLoS Med **4:**e59.
92. **Murphy BR, Kasel JA, Chanock RM.** 1972. Association of serum anti-neuraminidase antibody with resistance to influenza in man. N Engl J Med **286:**1329-1332.
93. **Walz L, Kays SK, Zimmer G, von Messling V.** 2018. Neuraminidase-Inhibiting Antibody Titers Correlate with Protection from Heterologous Influenza Virus Strains of the Same Neuraminidase Subtype. J Virol **92**.
94. **Sandbulte MR, Westgeest KB, Gao J, Xu X, Klimov AI, Russell CA, Burke DF, Smith DJ, Fouchier RA, Eichelberger MC.** 2011. Discordant antigenic drift of neuraminidase and hemagglutinin in H1N1 and H3N2 influenza viruses. Proc Natl Acad Sci U S A **108:**20748-20753.
95. **Fox A, Quinn KM, Subbarao K.** 2018. Extending the Breadth of Influenza Vaccines: Status and Prospects for a Universal Vaccine. Drugs **78:**1297-1308.
96. **Fujimoto Y, Tomioka Y, Takakuwa H, Uechi G, Yabuta T, Ozaki K, Suyama H, Yamamoto S, Morimatsu M, Mai le Q, Yamashiro T, Ito T, Otsuki K, Ono E.** 2016. Cross-protective potential of anti-nucleoprotein human monoclonal antibodies against lethal influenza A virus infection. J Gen Virol **97:**2104-2116.

97. **LaMere MW, Lam HT, Moquin A, Haynes L, Lund FE, Randall TD, Kaminski DA.** 2011. Contributions of antinucleoprotein IgG to heterosubtypic immunity against influenza virus. J Immunol **186:**4331-4339.
98. **Liu W, Zou P, Chen YH.** 2004. Monoclonal antibodies recognizing EVETPIRN epitope of influenza A virus M2 protein could protect mice from lethal influenza A virus challenge. Immunol Lett **93:**131-136.
99. **Kreijtz JH, Fouchier RA, Rimmelzwaan GF.** 2011. Immune responses to influenza virus infection. Virus Res **162:**19-30.
100. **Hutchinson EC, Charles PD, Hester SS, Thomas B, Trudgian D, Martinez-Alonso M, Fodor E.** 2014. Conserved and host-specific features of influenza virion architecture. Nat Commun **5:**4816.
101. **Houser K, Subbarao K.** 2015. Influenza vaccines: challenges and solutions. Cell Host Microbe **17:**295-300.
102. **Paules C, Subbarao K.** 2017. Influenza. Lancet **390:**697-708.
103. **Caspard H, Mallory RM, Yu J, Ambrose CS.** 2017. Live-Attenuated Influenza Vaccine Effectiveness in Children From 2009 to 2015-2016: A Systematic Review and Meta-Analysis. Open Forum Infect Dis **4:**ofx111.
104. **Gaglani M, Pruszynski J, Murthy K, Clipper L, Robertson A, Reis M, Chung JR, Piedra PA, Avadhanula V, Nowalk MP, Zimmerman RK, Jackson ML, Jackson LA, Petrie JG, Ohmit SE, Monto AS, McLean HQ, Belongia EA, Fry AM, Flannery B.** 2016. Influenza Vaccine Effectiveness Against 2009 Pandemic Influenza A(H1N1) Virus Differed by Vaccine Type During 2013-2014 in the United States. J Infect Dis **213:**1546-1556.
105. **CDC.** 2018. Recommended Immunization Schedule for Children and Adolescents Aged 18 Years or Younger, United States, 2018. https://www.cdc.gov/vaccines/schedules/hcp/child-adolescent.html. Accessed 24 October.
106. **Krammer F, Smith GJD, Fouchier RAM, Peiris M, Kedzierska K, Doherty PC, Palese P, Shaw ML, Treanor J, Webster RG, Garcia-Sastre A.** 2018. Influenza. Nat Rev Dis Primers **4:**3.
107. **(CDC) CfDCaP.** September 4, 2018 2018. Selecting Viruses for the Seasonal Influenza Vaccine, *on* Centers for Disease Control and Prevention (CDC). https://www.cdc.gov/flu/about/season/vaccine-selection.htm. Accessed 17 Dec.
108. **Zost SJ, Parkhouse K, Gumina ME, Kim K, Diaz Perez S, Wilson PC, Treanor JJ, Sant AJ, Cobey S, Hensley SE.** 2017. Contemporary H3N2 influenza viruses have a glycosylation site that alters binding of antibodies elicited by egg-adapted vaccine strains. Proc Natl Acad Sci U S A **114:**12578-12583.
109. **Wrammert J, Smith K, Miller J, Langley WA, Kokko K, Larsen C, Zheng NY, Mays I, Garman L, Helms C, James J, Air GM, Capra JD, Ahmed R, Wilson PC.** 2008. Rapid cloning of high-affinity human monoclonal antibodies against influenza virus. Nature **453:**667-671.
110. **Sasaki S, Jaimes MC, Holmes TH, Dekker CL, Mahmood K, Kemble GW, Arvin AM, Greenberg HB.** 2007. Comparison of the influenza virus-specific effector and memory B-cell responses to immunization of children and adults with live attenuated or inactivated influenza virus vaccines. J Virol **81:**215-228.
111. **Petrie JG, Ohmit SE, Johnson E, Truscon R, Monto AS.** 2015. Persistence of Antibodies to Influenza Hemagglutinin and Neuraminidase Following One or Two Years of Influenza Vaccination. J Infect Dis **212:**1914-1922.
112. **Francis T.** 1960. On the doctrine of original antigenic sin. Proceedings of the American Philosophical Society **104:**572-578.
113. **Davenport FM, Hennessy AV.** 1956. A serologic recapitulation of past experiences with influenza A; antibody response to monovalent vaccine. J Exp Med **104:**85-97.

114. **Sasaki S, He XS, Holmes TH, Dekker CL, Kemble GW, Arvin AM, Greenberg HB.** 2008. Influence of prior influenza vaccination on antibody and B-cell responses. PLoS One **3:**e2975.
115. **Ellebedy AH.** 2018. Immunizing the Immune: Can We Overcome Influenza's Most Formidable Challenge? Vaccines (Basel) **6**.
116. **Andrews SF, Huang Y, Kaur K, Popova LI, Ho IY, Pauli NT, Henry Dunand CJ, Taylor WM, Lim S, Huang M, Qu X, Lee JH, Salgado-Ferrer M, Krammer F, Palese P, Wrammert J, Ahmed R, Wilson PC.** 2015. Immune history profoundly affects broadly protective B cell responses to influenza. Sci Transl Med **7:**316ra192.
117. **Lessler J, Riley S, Read JM, Wang S, Zhu H, Smith GJ, Guan Y, Jiang CQ, Cummings DA.** 2012. Evidence for antigenic seniority in influenza A (H3N2) antibody responses in southern China. PLoS Pathog **8:**e1002802.
118. **Kucharski AJ, Lessler J, Read JM, Zhu H, Jiang CQ, Guan Y, Cummings DA, Riley S.** 2015. Estimating the life course of influenza A(H3N2) antibody responses from cross-sectional data. PLoS Biol **13:**e1002082.
119. **Henry C, Palm AE, Krammer F, Wilson PC.** 2018. From Original Antigenic Sin to the Universal Influenza Virus Vaccine. Trends Immunol **39:**70-79.
120. **O'Donnell CD, Wright A, Vogel L, Boonnak K, Treanor JJ, Subbarao K.** 2014. Humans and ferrets with prior H1N1 influenza virus infections do not exhibit evidence of original antigenic sin after infection or vaccination with the 2009 pandemic H1N1 influenza virus. Clin Vaccine Immunol **21:**737-746.
121. **Andrews SF, Kaur K, Pauli NT, Huang M, Huang Y, Wilson PC.** 2015. High preexisting serological antibody levels correlate with diversification of the influenza vaccine response. J Virol **89:**3308-3317.
122. **Kim JH, Liepkalns J, Reber AJ, Lu X, Music N, Jacob J, Sambhara S.** 2016. Prior infection with influenza virus but not vaccination leaves a long-term immunological imprint that intensifies the protective efficacy of antigenically drifted vaccine strains. Vaccine **34:**495-502.
123. **Smith DJ, Forrest S, Ackley DH, Perelson AS.** 1999. Variable efficacy of repeated annual influenza vaccination. Proc Natl Acad Sci U S A **96:**14001-14006.
124. **Hoskins TW, Davies JR, Smith AJ, Miller CL, Allchin A.** 1979. Assessment of inactivated influenza-A vaccine after three outbreaks of influenza A at Christ's Hospital. Lancet **1:**33-35.
125. **Keitel WA, Cate TR, Couch RB, Huggins LL, Hess KR.** 1997. Efficacy of repeated annual immunization with inactivated influenza virus vaccines over a five year period. Vaccine **15:**1114-1122.
126. **Skowronski DM, Chambers C, De Serres G, Sabaiduc S, Winter AL, Dickinson JA, Gubbay JB, Fonseca K, Drews SJ, Charest H, Martineau C, Krajden M, Petric M, Bastien N, Li Y, Smith DJ.** 2017. Serial Vaccination and the Antigenic Distance Hypothesis: Effects on Influenza Vaccine Effectiveness During A(H3N2) Epidemics in Canada, 2010-2011 to 2014-2015. J Infect Dis **215:**1059-1099.
127. **Linderman SL, Hensley SE.** 2016. Antibodies with 'Original Antigenic Sin' Properties Are Valuable Components of Secondary Immune Responses to Influenza Viruses. PLoS Pathog **12:**e1005806.
128. **van der Most RG, Roman FP, Innis B, Hanon E, Vaughn DW, Gillard P, Walravens K, Wettendorff M.** 2014. Seeking help: B cells adapting to flu variability. Sci Transl Med **6:**246ps248.
129. **O'Donnell CD, Wright A, Vogel LN, Wei CJ, Nabel GJ, Subbarao K.** 2012. Effect of priming with H1N1 influenza viruses of variable antigenic distances on challenge with 2009 pandemic H1N1 virus. J Virol **86:**8625-8633.
130. **Hartley CA, Reading PC, Ward AC, Anders EM.** 1997. Changes in the hemagglutinin molecule of influenza type A (H3N2) virus associated with increased virulence for mice. Arch Virol **142:**75-88.

131. **Whittle JR, Wheatley AK, Wu L, Lingwood D, Kanekiyo M, Ma SS, Narpala SR, Yassine HM, Frank GM, Yewdell JW, Ledgerwood JE, Wei CJ, McDermott AB, Graham BS, Koup RA, Nabel GJ.** 2014. Flow cytometry reveals that H5N1 vaccination elicits cross-reactive stem-directed antibodies from multiple Ig heavy-chain lineages. J Virol **88:**4047-4057.
132. **Wolf AI, Strauman MC, Mozdzanowska K, Whittle JR, Williams KL, Sharpe AH, Weiser JN, Caton AJ, Hensley SE, Erikson J.** 2014. Coinfection with Streptococcus pneumoniae modulates the B cell response to influenza virus. J Virol **88:**11995-12005.
133. **He XS, Sasaki S, Narvaez CF, Zhang C, Liu H, Woo JC, Kemble GW, Dekker CL, Davis MM, Greenberg HB.** 2011. Plasmablast-derived polyclonal antibody response after influenza vaccination. J Immunol Methods **365:**67-75.
134. **Huang KY, Li CK, Clutterbuck E, Chui C, Wilkinson T, Gilbert A, Oxford J, Lambkin-Williams R, Lin TY, McMichael AJ, Xu XN.** 2014. Virus-specific antibody secreting cell, memory B-cell, and sero-antibody responses in the human influenza challenge model. J Infect Dis **209:**1354-1361.
135. **Sze DM, Toellner KM, Garcia de Vinuesa C, Taylor DR, MacLennan IC.** 2000. Intrinsic constraint on plasmablast growth and extrinsic limits of plasma cell survival. J Exp Med **192:**813-821.
136. **Corti D, Voss J, Gamblin SJ, Codoni G, Macagno A, Jarrossay D, Vachieri SG, Pinna D, Minola A, Vanzetta F, Silacci C, Fernandez-Rodriguez BM, Agatic G, Bianchi S, Giacchetto-Sasselli I, Calder L, Sallusto F, Collins P, Haire LF, Temperton N, Langedijk JP, Skehel JJ, Lanzavecchia A.** 2011. A neutralizing antibody selected from plasma cells that binds to group 1 and group 2 influenza A hemagglutinins. Science **333:**850-856.
137. **Nakamura G, Chai N, Park S, Chiang N, Lin Z, Chiu H, Fong R, Yan D, Kim J, Zhang J, Lee WP, Estevez A, Coons M, Xu M, Lupardus P, Balazs M, Swem LR.** 2013. An in vivo human-plasmablast enrichment technique allows rapid identification of therapeutic influenza A antibodies. Cell Host Microbe **14:**93-103.
138. **McCarthy KR, Watanabe A, Kuraoka M, Do KT, McGee CE, Sempowski GD, Kepler TB, Schmidt AG, Kelsoe G, Harrison SC.** 2018. Memory B Cells that Cross-React with Group 1 and Group 2 Influenza A Viruses Are Abundant in Adult Human Repertoires. Immunity **48:**174-184 e179.
139. **Murphy K, Travers P, Walport M, Janeway C.** 2012. Janeway's immunobiology, 8th ed. ed. Garland Science.
140. **Wang Z, Chua BY, Ramos JV, Parra SM, Fairmaid E, Brown LE, Jackson DC, Kedzierska K.** 2015. Establishment of functional influenza virus-specific CD8(+) T cell memory pools after intramuscular immunization. Vaccine **33:**5148-5154.
141. **Wang Z, Kedzierski L, Nuessing S, Chua BYL, Quinones-Parra SM, Huber VC, Jackson DC, Thomas PG, Kedzierska K.** 2016. Establishment of memory CD8+ T cells with live attenuated influenza virus across different vaccination doses. J Gen Virol **97:**3205-3214.
142. **Kucharski AJ, Lessler J, Cummings DAT, Riley S.** 2018. Timescales of influenza A/H3N2 antibody dynamics. PLoS Biol **16:**e2004974.
143. **Manicassamy B, Medina RA, Hai R, Tsibane T, Stertz S, Nistal-Villan E, Palese P, Basler CF, Garcia-Sastre A.** 2010. Protection of mice against lethal challenge with 2009 H1N1 influenza A virus by 1918-like and classical swine H1N1 based vaccines. PLoS Pathog **6:**e1000745.
144. **Hancock K, Veguilla V, Lu X, Zhong W, Butler EN, Sun H, Liu F, Dong L, DeVos JR, Gargiullo PM, Brammer TL, Cox NJ, Tumpey TM, Katz JM.** 2009. Cross-reactive antibody responses to the 2009 pandemic H1N1 influenza virus. N Engl J Med **361:**1945-1952.
145. **Reading PC, Morey LS, Crouch EC, Anders EM.** 1997. Collectin-mediated antiviral host defense of the lung: evidence from influenza virus infection of mice. J Virol **71:**8204-8212.
146. **Anonymous.** !!! INVALID CITATION !!! {Hartley, 1997 #260;Reading, 1997 #364}.
147. **Reading PC, Tate MD, Pickett DL, Brooks AG.** 2007. Glycosylation as a target for recognition of influenza viruses by the innate immune system. Adv Exp Med Biol **598:**279-292.

148. **Bouvier NM, Lowen AC.** 2010. Animal Models for Influenza Virus Pathogenesis and Transmission. Viruses **2:**1530-1563.
149. **Frank GM, Angeletti D, Ince WL, Gibbs JS, Khurana S, Wheatley AK, Max EE, McDermott AB, Golding H, Stevens J, Bennink JR, Yewdell JW.** 2015. A Simple Flow-Cytometric Method Measuring B Cell Surface Immunoglobulin Avidity Enables Characterization of Affinity Maturation to Influenza A Virus. MBio **6:**e01156.
150. **Lee SK, Rigby RJ, Zotos D, Tsai LM, Kawamoto S, Marshall JL, Ramiscal RR, Chan TD, Gatto D, Brink R, Yu D, Fagarasan S, Tarlinton DM, Cunningham AF, Vinuesa CG.** 2011. B cell priming for extrafollicular antibody responses requires Bcl-6 expression by T cells. J Exp Med **208:**1377-1388.
151. **Alam S, Knowlden ZA, Sangster MY, Sant AJ.** 2014. CD4 T cell help is limiting and selective during the primary B cell response to influenza virus infection. J Virol **88:**314-324.
152. **Hillaire ML, Rimmelzwaan GF, Kreijtz JH.** 2013. Clearance of influenza virus infections by T cells: risk of collateral damage? Curr Opin Virol **3:**430-437.
153. **Hillaire ML, van Trierum SE, Kreijtz JH, Bodewes R, Geelhoed-Mieras MM, Nieuwkoop NJ, Fouchier RA, Kuiken T, Osterhaus AD, Rimmelzwaan GF.** 2011. Cross-protective immunity against influenza pH1N1 2009 viruses induced by seasonal influenza A (H3N2) virus is mediated by virus-specific T-cells. J Gen Virol **92:**2339-2349.
154. **Wrammert J, Koutsonanos D, Li GM, Edupuganti S, Sui J, Morrissey M, McCausland M, Skountzou I, Hornig M, Lipkin WI, Mehta A, Razavi B, Del Rio C, Zheng NY, Lee JH, Huang M, Ali Z, Kaur K, Andrews S, Amara RR, Wang Y, Das SR, O'Donnell CD, Yewdell JW, Subbarao K, Marasco WA, Mulligan MJ, Compans R, Ahmed R, Wilson PC.** 2011. Broadly cross-reactive antibodies dominate the human B cell response against 2009 pandemic H1N1 influenza virus infection. J Exp Med **208:**181-193.
155. **Ellebedy AH, Krammer F, Li GM, Miller MS, Chiu C, Wrammert J, Chang CY, Davis CW, McCausland M, Elbein R, Edupuganti S, Spearman P, Andrews SF, Wilson PC, Garcia-Sastre A, Mulligan MJ, Mehta AK, Palese P, Ahmed R.** 2014. Induction of broadly cross-reactive antibody responses to the influenza HA stem region following H5N1 vaccination in humans. Proc Natl Acad Sci U S A **111:**13133-13138.
156. **Li GM, Chiu C, Wrammert J, McCausland M, Andrews SF, Zheng NY, Lee JH, Huang M, Qu X, Edupuganti S, Mulligan M, Das SR, Yewdell JW, Mehta AK, Wilson PC, Ahmed R.** 2012. Pandemic H1N1 influenza vaccine induces a recall response in humans that favors broadly cross-reactive memory B cells. Proc Natl Acad Sci U S A **109:**9047-9052.
157. **Leach S, Shinnakasu R, Adachi Y, Momota M, Makino-Okamura C, Yamamoto T, Ishii KJ, Fukuyama H, Takahashi Y, Kurosaki T.** 2019. Requirement for memory B-cell activation in protection from heterologous influenza virus reinfection. Int Immunol **31:**771-779.
158. **Xie H, Wan XF, Ye Z, Plant EP, Zhao Y, Xu Y, Li X, Finch C, Zhao N, Kawano T, Zoueva O, Chiang MJ, Jing X, Lin Z, Zhang A, Zhu Y.** 2015. H3N2 Mismatch of 2014-15 Northern Hemisphere Influenza Vaccines and Head-to-head Comparison between Human and Ferret Antisera derived Antigenic Maps. Sci Rep **5:**15279.
159. **Lin YP, Xiong X, Wharton SA, Martin SR, Coombs PJ, Vachieri SG, Christodoulou E, Walker PA, Liu J, Skehel JJ, Gamblin SJ, Hay AJ, Daniels RS, McCauley JW.** 2012. Evolution of the receptor binding properties of the influenza A(H3N2) hemagglutinin. Proc Natl Acad Sci U S A **109:**21474-21479.
160. **Medeiros R, Escriou N, Naffakh N, Manuguerra JC, van der Werf S.** 2001. Hemagglutinin residues of recent human A(H3N2) influenza viruses that contribute to the inability to agglutinate chicken erythrocytes. Virology **289:**74-85.

161. **Ibricevic A, Pekosz A, Walter MJ, Newby C, Battaile JT, Brown EG, Holtzman MJ, Brody SL.** 2006. Influenza virus receptor specificity and cell tropism in mouse and human airway epithelial cells. J Virol **80:**7469-7480.
162. **Iwatsuki-Horimoto K, Nakajima N, Ichiko Y, Sakai-Tagawa Y, Noda T, Hasegawa H, Kawaoka Y.** 2018. Syrian Hamster as an Animal Model for the Study of Human Influenza Virus Infection. J Virol **92**.
163. **Potter CW, Oxford JS.** 1979. Determinants of immunity to influenza infection in man. Br Med Bull **35:**69-75.
164. **Fazekas de St G, Webster RG.** 1966. Disquisitions of Original Antigenic Sin. I. Evidence in man. J Exp Med **124:**331-345.
165. **Petrie JG, Cheng C, Malosh RE, VanWormer JJ, Flannery B, Zimmerman RK, Gaglani M, Jackson ML, King JP, Nowalk MP, Benoit J, Robertson A, Thaker SN, Monto AS, Ohmit SE.** 2016. Illness Severity and Work Productivity Loss Among Working Adults With Medically Attended Acute Respiratory Illnesses: US Influenza Vaccine Effectiveness Network 2012-2013. Clin Infect Dis **62:**448-455.
166. **Tan HX, Esterbauer R, Vanderven HA, Juno JA, Kent SJ, Wheatley AK.** 2019. Inducible Bronchus-Associated Lymphoid Tissues (iBALT) Serve as Sites of B Cell Selection and Maturation Following Influenza Infection in Mice. Front Immunol **10:**611.

APPENDICIES

A Blood

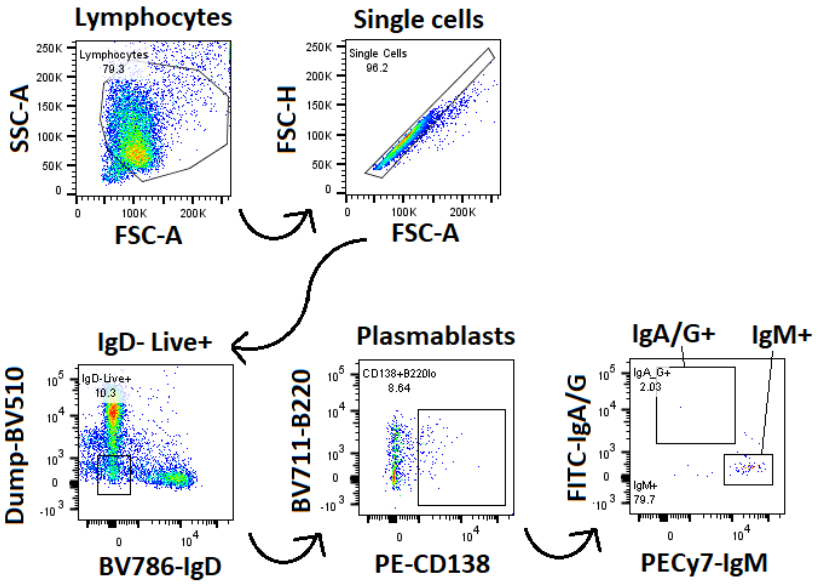

B Bone Marrow

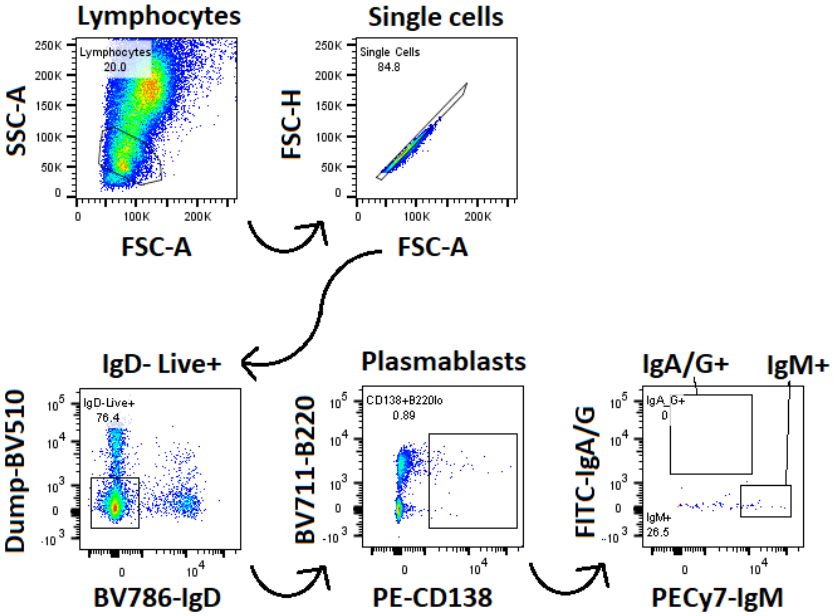

C MLN

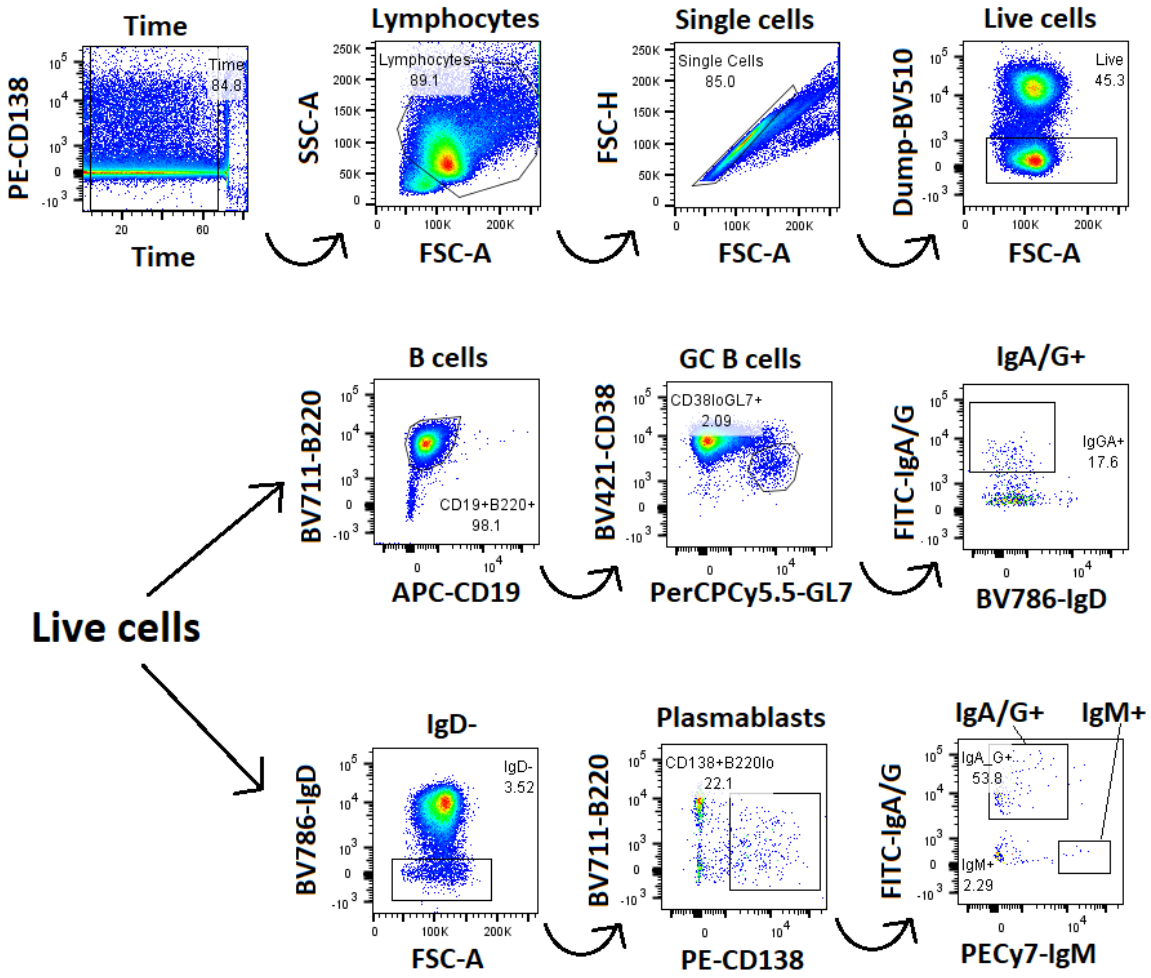
Time
PE-CD138
Time
Time
84.8
Lymphocytes
SSC-A
FSC-A
Lymphocytes
89.1
Single cells
FSC-H
FSC-A
Single Cells
85.0
Live cells
Dump-BV510
FSC-A
Live
45.3
Live cells
B cells
BV711-B220
APC-CD19
CD19+B220+
98.1
GC B cells
BV421-CD38
PerCPCy5.5-GL7
CD38loGL7+
2.09
IgA/G+
FITC-IgA/G
BV786-IgD
IgGA+
17.6
IgD-
BV786-IgD
FSC-A
IgD-
3.52
Plasmablasts
BV711-B220
PE-CD138
CD138+B220lo
22.1
IgA/G+
IgM+
FITC-IgA/G
PECy7-IgM
IgA_G+
53.8
IgM+
2.29

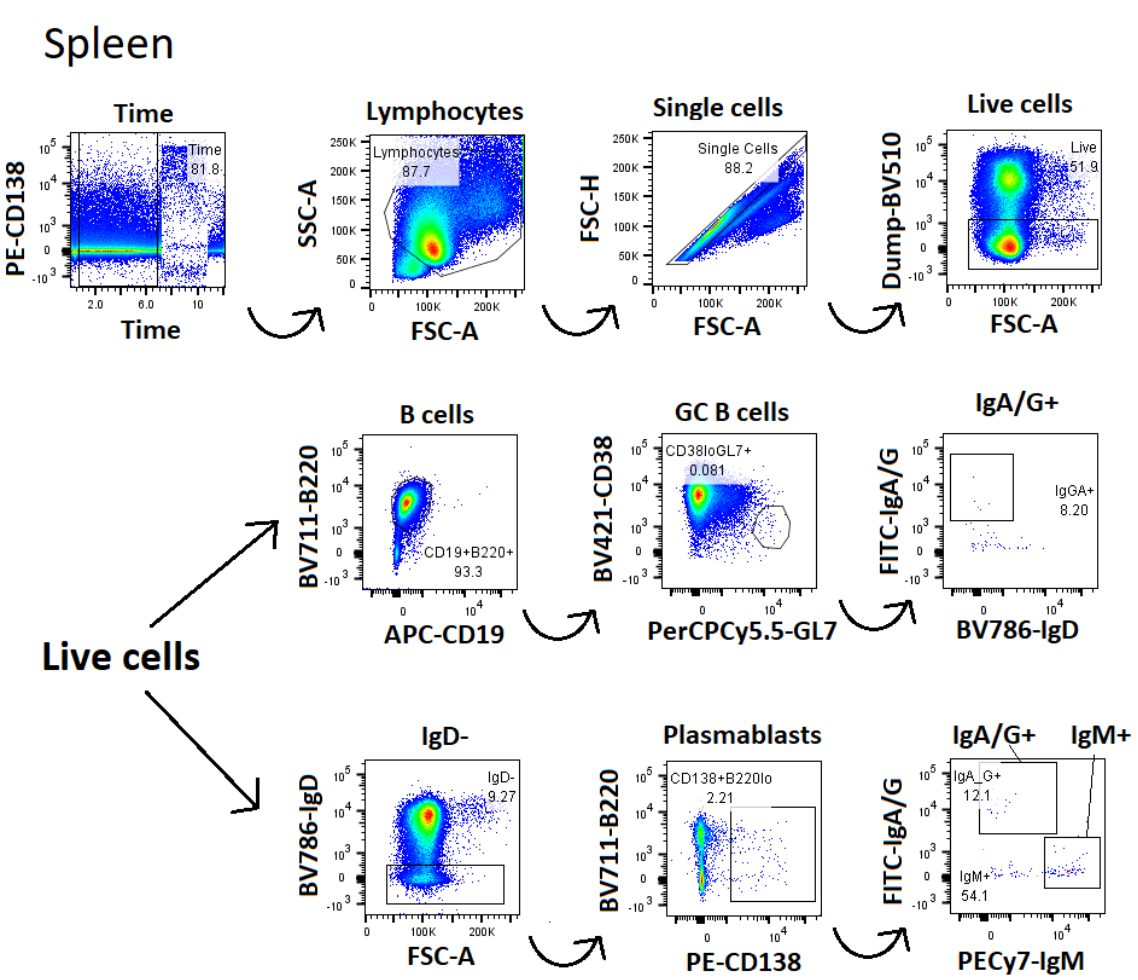

Supplementary Figure 1. Gating Strategy for Figure 3.1, Kinetics of B cells and their subsets in murine compartments during primary IAV infection by flow cytometry. 6-8 week old C57BL/6 mice (n= 5) were infected with $10^{4.5}$PFU of Ud72 virus. On days 5, 7, 10 and 14 post infection (dpi), spleen, mediastinal lymph nodes (MLN), bone marrow (BM) and peripheral blood were collected and processed for analysis by flow cytometry. Figure shows the gating scheme with the gated populations of each scatterplot for A) blood, B) bone marrow (BM), C) mediastinal lymph node (MLN) and D) spleen. Data obtained from a sample at 7 dpi and is representative of the gating strategy throughout the experiment.

Supplementary Table 1. Selection panel for flow cytometric analysis of B cell subsets with virus-specific HA probes as shown in Figure 4.6.

Specific Marker	Aids detection of	Fluorochrome
HA	Virus-specific HA^+ B cells	Brilliant Violet 421
Streptavidin (SA) + Live/Dead-Aqua	Non-B cells & dead cells for exclusion	Brilliant Violet 510
CD38	GC B cells	Brilliant Violet 605
B220	Pan B cell marker	Brilliant Violet 711
IgD	Non-class switched B cells	Brilliant Violet 786
HA	Virus-specific HA^+ B cells	APC
CD19	Pan B cell marker	APC Fire 750
IgA/G1/G2c/G3 (pooled)	Class-switched B cells	FITC
GL7	GC B cells	PerCP-Cy5.5
CD138	Plasmablasts & Plasma cells	PE
IgM	Non-class switched B cells	PE-Cy7
CD3	T cells	Biotin
CD5	B1 cells	(Dump channel via
F480	Macrophages	Brilliant Violet 510)
CD11c	Dendritic cells	
Gr-1	Granulocytes	